Rep. Prog. Phys., Vol. 43, 1980. Printed in Great Britain

Glassy metals

H S CHEN

Bell Laboratories, Murray Hill, New Jersey 07974, USA

Abstract

Glassy metals not only exhibit technologically interesting properties, e.g. high fracture strength, excellent soft magnetic behaviour and good corrosion resistance, they also constitute ideal materials for the studies of low-temperature transport, critical behaviour and electrical properties of disordered metals. During the past several years, there have been considerable efforts on the fundamental understanding of structure, atomic and electronic transport properties and low-temperature behaviour as well as further exploration of mechanical, magnetic and chemical properties. This review attempts to summarise past developments and to review comprehensively the present knowledge of structure and physical properties of glassy metals. The nature of the glassy state, various quenching techniques and glass-forming alloys are described first, followed by the discussion of structural models, experimental structural data and atomic transport properties including diffusivities and kinetics of structural relaxation, magnetic aging and crystallisation. The mechanical properties and magnetic behaviour are summarised, with emphasis laid on the influence of modification of these properties due to changes in structural and chemical disorder and states of magnetisation. Finally the electrical transport properties, spin wave excitations and critical behaviour, thermal and acoustic behaviour at very low temperatures, and chemical properties are presented.

This review was received in its present form in May 1979.

0034-4885/80/040353+83 $06.50

Contents

	Page
1. Introduction	355
2. Nature of the glassy state	356
2.1. Liquid–glass transition	357
2.2. Structural relaxation	360
2.3. Modes of crystallisation	361
3. Glass formation	362
3.1. Rapid quenching techniques	362
3.2. Kinetic criteria	365
3.3. Glass-forming alloys	367
3.4. Factors affecting glass formation	369
4. Structure	371
4.1. Various structural models	371
4.2. Amorphous metals	372
4.3. Glassy alloys	374
4.4. Structural and compositional homogeneity	379
5. Atomic transport and transformation kinetics	380
5.1. Viscosity	381
5.2. Glass transition temperature	383
5.3. Atomic diffusivities	384
5.4. Kinetics of structural relaxation	386
5.5. Crystallisation processes	388
6. Mechanical properties	389
6.1. Density and thermal expansion	389
6.2. Elastic constants	390
6.3. Anelasticity	391
6.4. Deformation and fracture	393
6.5. Strength, toughness and embrittlement	396
7. Magnetic properties	400
7.1. Magnetic moments and Curie temperature	401
7.2. Mictomagnet and spin glass	403
7.3. Magnetisation processes	403
7.4. Magnetostriction and induced magnetic anisotropy	405
7.5. Invar and Elinvar behaviour	406
7.6. Spin wave excitations and critical behaviour	407
8. Electrical properties, low-temperature behaviour and corrosion resistance	408
8.1. Electrical resistivity	408
8.2. Thermal properties at low temperatures	415
8.3. Corrosion behaviour	418
9. Conclusion	419
Acknowledgments	422
References	423

1. Introduction

Metal liquids usually crystallise when cooled at rates for which some non-metallic liquids form glasses. By drastic quenching methods such as vapour condensation, electrodeposition, chemical deposition and rapid liquid quenching, however, non-crystalline structure can be retained for many metals and alloys. Amorphous metals have been obtained as a nickel deposit via decomposition of a nickel hyperphosphide solution by Wurtz as early as 1845, although the amorphous nature of the film could not be confirmed until the discovery of the x-ray diffraction method. A number of amorphous alloys were prepared by vapour quenching or electrodeposition in the 1950s, while the first glassy metal obtained by quenching from a melt was reported by Klement *et al* (1960). Since the publication of the paper on an Au–Si glassy alloy, a number of papers and reviews have appeared on the subjects of structure, electrical and magnetic properties and thermodynamic characterisation of non-crystalline metals (e.g. Duwez 1967, Giessen and Wagner 1972, Jones 1973).

Since the development of continuous fabrication of uniform ribbons and the consequent discovery of technically interesting properties such as high strength (Chen and Wang 1970, Leamy *et al* 1972, Masumoto and Maddin 1971, Chen and Polk 1974), soft magnetic behaviour (Sherwood *et al* 1974, Egami *et al* 1974, Fujimori *et al* 1974), and excellent corrosion resistance (Naka *et al* 1974), glassy metals have drawn further attention from the material and scientific communities (e.g. Robinson 1973, Gilman 1975a, Masumoto *et al* 1975, Cahn 1976) and are currently the focus of intense technological and fundamental studies.

Glassy metals possess unique properties arising from the unique characteristic of the glassy state, namely the absence of translational periodicity and compositional homogeneity. Fe-based glassy alloys are found to have fracture strengths ~ 350 kg mm^{-2}, exceeding the values exhibited by heavily cold-rolled steel wire. Despite the high strength, glassy metal fracture proceeds by the formation of shear deformation which contrasts with the brittle fracture commonly observed in oxide glasses and high-strength steels. Fe-, Co- and Ni-based glasses are ferromagnets with excellent soft magnetic behaviour comparable to the best conventional permalloys. In addition, Cr-containing glasses and some metal–metal-alloy glasses are shown to exhibit excellent corrosion resistance to chloride and sulphate solutions.

Glassy metals may be considered as solids with a frozen-in liquid structure and are macroscopically isotropic in the domain range $\geqslant 20$Å. Thus they constitute ideal materials for low-temperature transport and critical behaviour studies and are best suited for a study of electrons in the non-crystalline state. During the past few years, there have emerged new efforts on the basic understanding of physical properties of glassy metals as well as further exploration of technically important mechanical, magnetic and chemical properties and glass-forming systems. Extensive collections of papers on glassy metals may be found in 1977 *Proceedings of the 2nd International Conference on Rapidly Quenched Metals* edited by N J Grant and B C Giessen, section I (Cambridge, Mass.: MIT Press) and section II, 1976 *Mater. Sci. Engng* **23**, *Rep. Sci. Res. Inst. Tohoku University Series A* **26** No 1 (1976), No 4–5 (1977), 1978 *Rapidly Quenched Metals III* edited by B Cantor (London: Metals Society), and 1978 *Metallic Glasses* edited by J J Gilman and H J Leamy (Metals Park, Ohio: ASM).

The last volume contains reviews of the formation, structure, transport behaviour, and mechanical, magnetic and electrical properties. There have been recent papers on a general review of glassy metals by Duwez (1976) and Chen (1976a, 1977a).

This paper reviews past developments and the present understanding of physical properties of glassy metals with emphasis laid on recent results obtained since 1975. Section 2 describes the characteristics of the glassy state including the liquid–glass transition, structural relaxation and the crystallisation processes. Section 3 presents various rapid quenching techniques, glass-forming alloys, and factors governing the glass-forming tendency. Section 4 reviews various structural models and discusses experimental data, with emphasis laid on more recent work, particularly on the partial radial distribution functions of metal–metalloid and metal–metal alloys. Structural variations induced during preparation, structural relaxation and deformation processes are also presented. Section 5 deals with the temperature and compositional dependence of viscosities and glass transition temperatures, and the influence of different structural states on diffusivities and on the kinetics of structural relaxation, stress relief, magnetic aging and crystallisation. Section 6 summarises mechanical properties with the presentation of density, thermal expansion, elastic and anelastic behaviour, fracture strength and toughness, and discusses various flow models, structure of deformation bands and causes of embrittlement. The influence of changes in the structure and the state of magnetisation on these properties is also described. Section 7 reviews experimental results on ferromagnetism in glassy metals, which include the effects of chemical and structural disorder on the magnetic moment, Curie temperature, magnetoelastic effects, induced magnetic anisotropies and recent observations on spin wave excitations and critical behaviour. Section 8 deals with subjects on fundamental understanding of transport properties, such as electrical resistivity, superconducting behaviour, electronic properties and low-temperature phenomena, and describes corrosion behaviour of Fe-based glasses and some metal–metal alloys. In conclusion, §9 attempts to assess the present knowledge of structure and physical properties and identify some outstanding problems for future work.

2. Nature of the glassy state

The expression 'glass', in its original sense, refers to an amorphous or non-crystalline solid formed by continuous cooling of a liquid, while a solid is defined as any body having a viscosity greater than a somewhat arbitrary 10^{14} P. A glass lacks three-dimensional atomic periodicity beyond a few atomic distances. It is characterised by a limited number of diffuse halos in x-ray, electron and neutron diffraction and no sharp diffraction contrast in high-resolution electron microscopy. Glasses have been found in every category of materials based on bond type: covalent, ionic, van der Waal's, hydrogen and metallic (e.g. Turnbull 1969). The glass-forming tendency varies widely. Some oxide mixtures form glass at normal slow cooling rates ~ 1 K min^{-1}, while monatomic metals with possible incorporation of impurities require rates of $\sim 10^{10}$ K s^{-1} (Davies *et al* 1973).

The expression 'glass' is sometimes also applied to amorphous solids produced by electrodeposition, vapour condensation, sputtering and ion implantation, based on the similarity in diffraction patterns and crystallisation behaviour between amorphous solids formed by atomic condensations and ones formed by liquid solidification (Bagley *et al* 1968). Non-crystalline solids produced by different procedures are

often indistinguishable in x-ray measurements, but their physical properties may differ drastically in as-prepared state, e.g. Ni–P glasses produced by liquid quenching are ductile while electrodeposited amorphous Ni–P alloys are very brittle (Staudinger and Nakahara 1977). Organic inclusions and voids are sometimes present in thin films obtained by atomic condensation processes. In this review, for clarity the expression 'metallic glass' or 'glassy metal' is reserved only for the non-crystalline metals produced by the cooling of a melt, and those obtained by atomic condensation are referred to as amorphous metals.

During the solidification there occurs no essential change in spatial atomic configuration. A liquid and a glass thus belong structurally and thermodynamically to the same phase. A glass may be considered as a solid with frozen-in liquid structure. A glass in general is not in an internal equilibrium state and thus relaxes structurally to a more stable equilibrium state whenever atoms attain an appreciable mobility. Alternatively, glass is metastable with respect to crystalline phase(s) and transforms to the latter through nucleation and growth. On heating, a glass would transform to the liquid phase provided that the rates of crystallisation are sluggish enough. In the following, the transformation from a glass to a liquid and the crystallisation behaviour of glassy metals will be described.

2.1. Liquid–glass transition

To illustrate the liquid–solid transformation the temperature dependence of viscosities of a glass-forming $Pd_{77}Cu_6Si_{17}$ alloy (Chen and Goldstein 1972) is shown schematically in figure 1. The logarithm of the viscosity η and structural relaxation time τ are plotted against the reciprocal of reduced temperature $T_r = T/T_m$, where T_m is the thermodynamic equilibrium melting temperature. τ is the average time for a rearrangement of atomic position in a liquid and is approximately related to η and the shear modulus μ of the liquid by

$$\tau \approx \eta/\mu. \tag{2.1}$$

Here $\mu \approx 10^{11}$ dyn cm^{-2} for liquid metals.

The viscosities of liquid metals above T_m are low, $\sim 10^{-2}$ P, and increase slowly on cooling with a relatively low activation energy $\approx 3kT_m$. Below the melting temperature, the viscosity of supercooled liquids is fairly well described by the empirical Fulcher's expression

$$\eta \sim \eta_0 \exp\,[B/(T - T_0)] \tag{2.2}$$

where T_0 is known as an ideal glass transition temperature and η_0 and B are constants depending on materials.

In simple liquids, such as liquid metals and organic liquids, B is small and a small fraction of the chemical bonding energy in the structure, while T_0 is a substantial fraction (e.g. $\sim \frac{1}{3}$ to $\frac{2}{3}$) of T_m. In network forming liquids, B values are large and of the order of the chemical bonding energy and T_0 is low. In pure silica or germania (GeO_2) the viscosities are quite well described by an Arrhenius equation, i.e. $T_0 \approx 0$ K (e.g. Angell 1968). η of these oxides is high (e.g. $\sim 10^7$ P) even above T_m and increases rapidly with decreasing temperature.

Upon cooling below the melting temperature T_m, a liquid either crystallises or forms a glass. On crystallisation η increases discontinuously then follows the path X with activation energy ~ 3 eV (figure 1). If crystallisation is bypassed, η increases

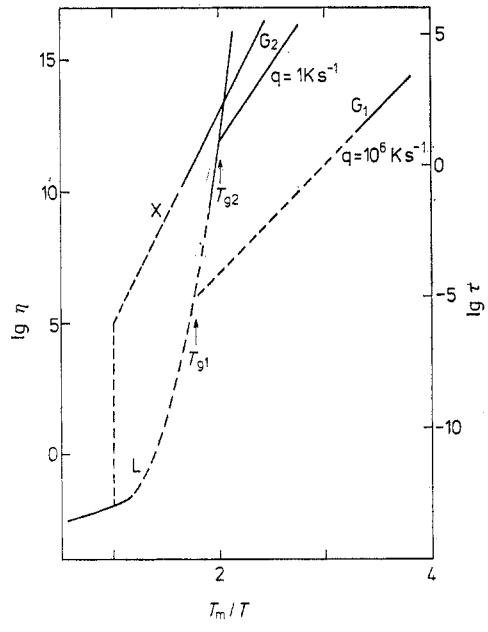

Figure 1. The temperature dependence of viscosity η and time constant τ for structural relaxation in a PdCuSi alloy.

continuously with decreasing temperature following the path L. The rate of increase in η and the time constant τ of the liquid increases with increasing undercooling. At sufficient undercooling, τ becomes comparable to or greater than the duration of experimental measurement. Below this temperature the atomic configuration remains virtually unaltered, thus giving rise to the discontinuity in the η against T relationship. η then is described by an Arrhenius equation with relatively low activation energy, ~ 1–2 eV (see §5). The temperatures, T_{g1} and T_{g2}, which correspond respectively to fast and slow cooling, and mark the transition from equilibrium to frozen-in non-equilibrium structure or iso-configurational structure, are known as glass transition temperatures T_g. Associated with the liquid–glass transition, the temperature coefficient of physical properties, e.g. thermal expansion, heat content and elastic constants, change rapidly but continuously from liquid-state values to the values near those for the crystalline state. At T_g, the structural relaxation time τ_g is related to the rates of cooling $q \equiv -\mathrm{d}T/\mathrm{d}t$ by (Chen 1978a)

$$\tau_g \approx (kT_g^2/Q)\, q^{-1} \tag{2.3}$$

where Q is the apparent activation energy of viscous flow, $\tau_g \propto \exp(Q/kT_g)$ and k is Boltzmann's constant. T_g increases with increasing q, and the rate of change in T_g with q is then

$$\mathrm{d}T_g/\mathrm{d}\ln q \approx kT_g^2/Q. \tag{2.4}$$

$kT_g^2/Q \approx 2$–10 K for metallic glasses. Equation (2.4) has also been derived by Kovacs (1963) for polymers based on the free volume model. Metallic glasses quenched at $q = 10^6$ K s^{-1} may have T_g higher by ~ 100 K than that obtained at the lower cooling rate $q = 1$ K s^{-1} as shown in figure 1.

At each cooling rate the glass freezes in a different state, e.g. G_1 and G_2. The glass has a lower viscosity or high diffusivity, and greater specific volume and internal

energy when produced at a faster cooling rate. Figure 2 illustrates the corresponding specific volume of a Pd–Cu–Si glass (Chen 1978b). G_1 and G_2 having been denoted by fictive glass transition temperatures T_{g1} and T_{g2}, correspond respectively to the glass state obtained upon cooling a liquid at 10^6 K s^{-1} and 1 K s^{-1}. The former exhibits a density lower by $\sim 0{\cdot}5\%$ than the latter. At extremely slow cooling rates, volume contraction occurs via path d. In practice, the length of the path d is limited by the increasing time constant τ required. Further extrapolation of the glassy volume would intersect the crystalline value ~ 200 K below T_g, corresponding approximately to the ideal glass temperature T_0. Controversy remains as to what may occur at T_0; however, for real systems, the observed glass transition is a purely kinetic phenomenon. The glass transition and associated property changes have been reviewed by

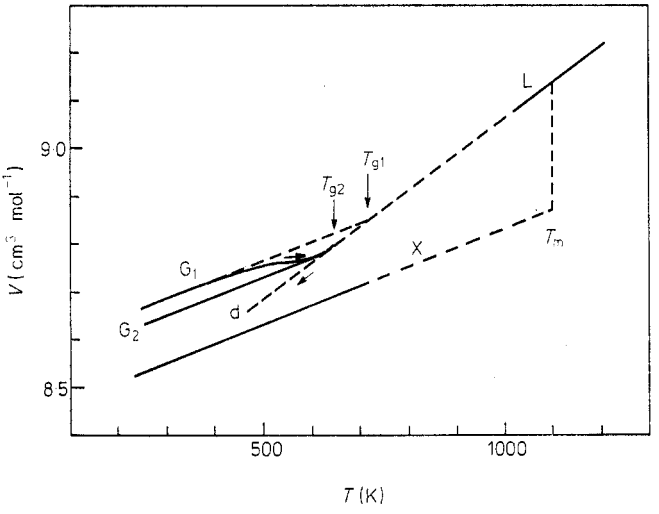

Figure 2. The specific volumes V of a PdCuSi alloy in various states. All notations are the same as in figure 1.

Kauzeman (1948), Gibbs and DiMarzio (1958), Turnbull and Cohen (1960) and Bagley (1974).

If the crystallisation of the glass is sluggish enough in the temperature range just above T_g, a reversible transition from the glass to the undercooled state may be demonstrated experimentally. Such a repeatable transition for a splat-quenched glassy metal was first manifested thermally for $Au_{77}Ge_{14}Si_9$ by Chen and Turnbull (1967). They found that the specific heat of the glass is only a little higher than the equilibrium crystalline mixture up to 295 K above which it rises sharply by ~ 5 cal mol^{-1} K^{-1} and levels off near 300 K which connects smoothly to the extrapolation of the high-temperature specific heat of the liquid alloy. This thermal behaviour could be repeated on the same sample after it had been carried through the transition and cooled again. Subsequent work (Chen and Turnbull 1968) showed the viscosity of the glass given by the form of equation (2.2) increases rapidly by four orders of magnitude from 10^9 P at 32°C to 10^{13} P at 12°C. These observations provide some of the strongest support for the view that the liquid-quenched non-crystalline metal is indeed a glass (Duwez 1967). The glass transition behaviour has been observed thermally for a number of glassy metals (Chen and Jackson 1978). However, in many other glassy

metals, the glass–liquid transition is unobservable at slow rates of measurement ~ 1 K s^{-1} because of the intervention of rapid crystallisation processes. Ideally the transition is observable at faster heating such that devitrification is bypassed.

2.2. Structural relaxation

Glasses, as ordinarily prepared, are thermodynamically 'unstable' relative to an internal equilibrium liquid state (as represented by L–d in figure 2), and relax structurally to the latter state at a rate depending on the previous thermal history and temperature. The glasses obtained at higher quenching rates which possess a greater frozen-in structural disorder and thus higher diffusivity would relax structurally at lower temperature. Many amorphous films produced by vapour deposition exhibit a highly disordered structure, and upon heating change structure just above the substrate condensation temperature.

Many physical properties (atomic diffusivity, mechanical ductility and magnetic anisotropy in particular) alter drastically associated with structural relaxation (§§ 5–7). As figures 1 and 2 show, the quenched Pd–Cu–Si glass denoted by G_1 attains an appreciable mobility (e.g. $\eta < 10^{12}$ P or $\tau < 10$ s) just above room temperature and undergoes volumetric contraction. Although the change in density associated with the structural relaxation in metallic glasses is small, $\sim 0{\cdot}5\%$, an appreciable increase was observed in many physical properties, e.g. Young's modulus by $\sim 7\%$ (Chen *et al* 1971, Chen 1978b, Soshiroda *et al* 1976, Berry and Pritchet 1973), internal energy by ~ 200 cal mol^{-1} (Chen and Coleman 1976), Curie temperature by as much as 35 K (Chen *et al* 1976), electrical resistivity by $\sim 5\%$ (H S Chen unpublished) and atomic diffusivity by many orders of magnitude (Chen *et al* 1978). Significantly, the rates of irreversible contraction are seen to exhibit two maxima at temperatures ≈ 200°C and ≈ 300°C. Similar behaviour was also found in the Young's modulus, internal energy and Curie temperature. The activation energy for the low-temperature relaxation is found to be low, of ~ 1–2 eV (Chen and Coleman 1976) compared with the activation energy ~ 5 eV for the viscous flow of glasses near T_g.

The occurrence of two modes of structural relaxation is further demonstrated by a different dependence of structure-sensitive properties on annealing temperature. Yeh (1976) reported that the resistivity ρ at liquid nitrogen temperature of an $Fe_{80}P_{13}C_7$ glass increases initially with increasing annealing temperature and peaks at ~ 200°C, far below the crystallisation temperature ~ 400°C. Further increase in annealing temperature causes ρ to decrease. The increase in ρ is small ($\sim 0{\cdot}2\%$) as compared with a several per cent increase in ρ associated with initial crystallisation of a number of metallic glasses (Chen and Turnbull 1968). Chen and Chuang (1977) reported the positron lifetime τ of a number of aged metallic glasses to increase from ~ 170 ps to ~ 175 ps following an anneal for ~ 30 min at 300 K, far below the glass transition temperature $T_g \approx 650$ K. With further annealing near T_g, τ decreases and approaches ~ 165 ps. The implication is that the structural relaxation at low temperature induces positron trapping sites which tend to disappear following high-temperature annealing. The trapping sites for the positron are thought to arise from local atomic structural rearrangement within a rigid glassy matrix which leads to atomic clusters somewhat similar to the initiation of the G–P zone in many alloys. The high-temperature relaxation, on the other hand, is thought to be associated with the glass transition commonly observed in a glassy state. The detailed atomic rearrangement and character of structural relaxation, however, are not clear.

2.3. Modes of crystallisation

Processes of crystallisation involve nucleation and growth of the crystalline phase. The rates of glass–crystal transformation are commonly dominated by the frequency of nucleation and therefore depend not only on diffusivity, as in the case of structural relaxation, but also strongly on thermodynamic parameters such as glass–crystal interfacial energy and the entropy of fusion. The heat of the glass–crystal transformation is one-half to one-third of the heat of fusion as a result of the difference in the specific heat between the supercooled liquid and the crystalline phase (Chen and Turnbull 1968). Detailed treatments on the kinetics of crystallisation will be discussed later (e.g. §5), and only a brief description of crystallisation processes is presented here.

Various crystallisation morphologies develop depending on annealing temperature and composition. Bagley and Turnbull (1970) observed a drastic change in the mode of crystallisation in vapour-deposited amorphous Ni–P films with phosphorus content. Upon heat treating a sample of Ni_3P composition at 175 °C for 2 min a few widely separated crystals nucleate and grow with a well-defined polyhedral shape into an amorphous matrix (figure 3(*a*) (plate)). There has been no apparent sharpening of the halos in the amorphous diffraction pattern, and the structure of the untransformed material appears not to change. The crystalline phase is identified as tetragonal Ni_3P intermetallic compound. The facet growth mode of crystallisation has been observed in amorphous films of $Cu_{30}Mg_{70}$ (Mader 1966), a liquid-quenched glass of $Pt_{77}Si_{23}$ (Duwez 1967) and electroless plated amorphous $Ni_{60}B_{40}$ (Watanabe and Tanabe 1976). Upon heat treating samples slightly richer in Ni than Ni_3P at 250 °C for 2 min dendritic crystallisation was observed as shown in figure 3(*b*) (plate). It was supposed that this morphology was due to the rejection of Ni by the crystalline Ni_3P phase. This dendritic crystallisation and spherulitic growth morphology were most commonly observed in amorphous solids, e.g. Fe_xSi_{1-x} with $x > 0{\cdot}5$ (Mangin *et al* 1977), Fe_xAu_{1-x} with $x > 0{\cdot}6$ (Marchal *et al* 1975), $Pd_{80}Si_{20}$ (Duwez 1967, Masumoto and Maddin 1971), $Fe_{75}P_{15}C_{10}$ (Rostogi 1973) and $Zr_{40}Cu_{60}$ (Vitek *et al* 1975). For compositions approximately Ni_4P annealed at 350 °C for 2 min, very fine-grained (~ 50 Å) crystallites appear and then coarsen uniformly, accompanied by continuous sharpening of the diffraction pattern (not shown). This mode of transformation was observed occasionally in vapour-deposited amorphous films such as Cu–Ag and Co–Au (Mader *et al* 1967) but has rarely been seen in liquid-quenched metallic glasses.

The facet and dendritic morphologies are the expected modes of crystallisation for a glass (or a liquid) with a continuous random type of structure, whereas a microcrystalline body might be expected to crystallise by grain growth process. However, an extremely fine-grained crystallite structure might arise from copious homogeneous nucleation of the crystal, followed by crystallite coarsening. Marchal *et al* (1975) noted a correlation between the mode of crystallisation and the resistance to crystallisation. They found in amorphous Fe_xAu_{1-x} films deposited at 80 K that the films with $x > 0{\cdot}60$ crystallised at relatively low temperature (< 200 K) by nucleation and growth process, while those with $x \leqslant 0{\cdot}60$ crystallisation occurred at a much higher temperature (≈ 500 K) into fine crystallites of the order of 100 Å. Vitek *et al* (1975) revealed by electron microscopy two non-crystalline structures in liquid-quenched glassy $Zr_{40}Cu_{60}$, an untransformed and a transformed phase. The transformed structure, which may be characterised by small oriented domains (10–15 Å) of crystallites in the sample annealed below the glass transition temperature, transforms to well-defined crystallites at temperatures higher by ~ 40 K than does the untransformed matrix. The relatively

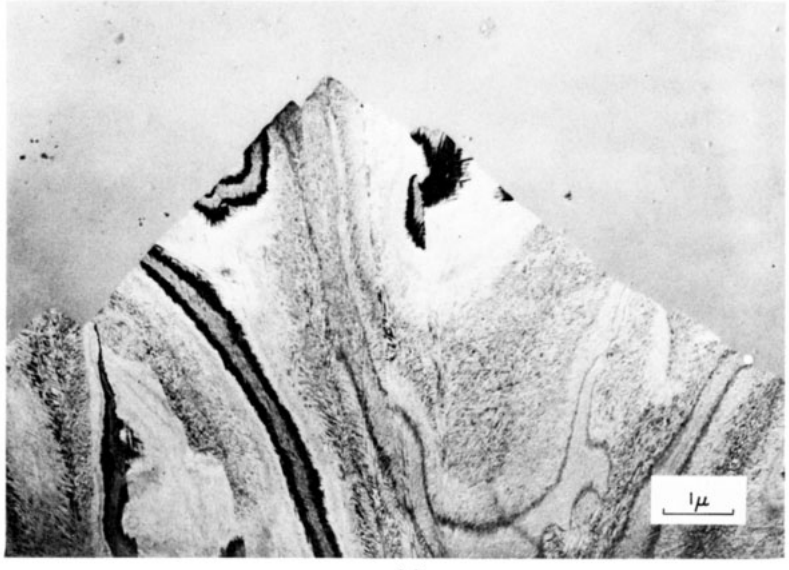

(*a*)

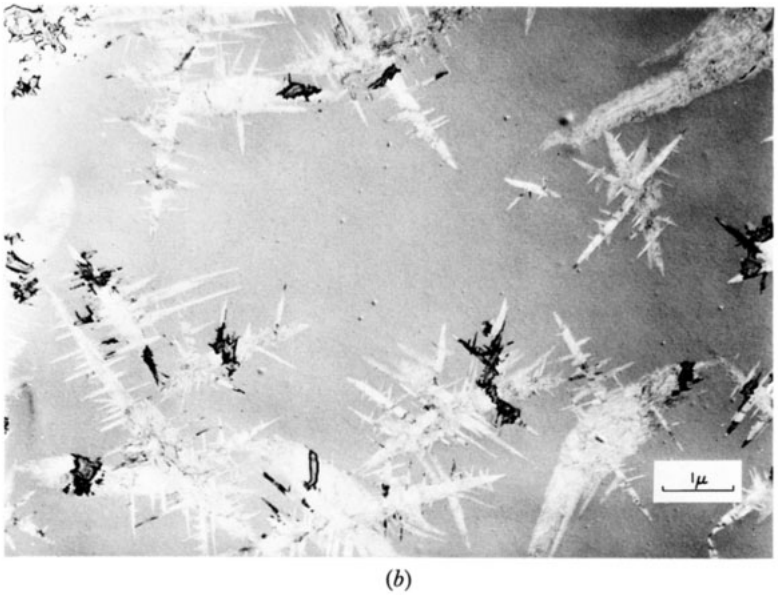

(*b*)

Figure 3. Crystallisation morphologies of amorphous Ni–P films. (a) Ni_3P composition, (*b*) composition slightly richer in Ni than Ni_3P.

high stability of amorphous films, which appear to transform by the grain coarsening mode, may arise from the low diffusivity of the films consisting of randomly oriented small crystallites.

An enhancement in thermal stability of amorphous films may also arise from completely different origins. Egami and Dahlgren (1978) observed a temperature of crystallisation ~ 50 K higher in a sputtered amorphous $Fe_{80}B_{20}$ as compared with a splat-cooled glassy sample of the same composition, which is probably due to the inclusion of krypton in the amorphous film. Kayano *et al* (1977) reported an improved thermal stability in a liquid-quenched $Pd_{80}Si_{20}$ glass by the introduction of a higher degree of structural disorder through neutron irradiation. Imura *et al* (1978) found that the thermal stability of $Fe_{80}P_{13}C_7$ and $Fe_{84}P_{16}$ was enhanced while that of $Ni_{75}B_{17}Si_5$ glass was reduced by electron irradiation. Elimination of ordered clusters or possible impurity incorporation may be responsible for the stabilisation of the irradiated samples.

Crystallisation processes of a metallic glass are rather complex. The glass transforms to the equilibrium stable phases through a sequence of progressively more stable phases upon annealing (Chen and Turnbull 1968, 1969, Masumoto and Maddin 1971, Masumoto and Kimura 1975a, Masumoto *et al* 1976b). Different crystallisation morphologies often appear simultaneously in the same sample (Yeh and Maddin 1976).

3. Glass formation

Two criteria for glass formation have been proposed: a structural criterion and a kinetic one. Structural criteria deal with geometrical atomic arrangement, bondings and atomic size effect and predict glass formation. Many of the structural theories have been reviewed by Rawson (1967) and Cahn (1970). The kinetic criterion developed mainly by Turnbull and Cohen (1960) and Turnbull (1969) considers the rate of cooling relative to the kinetics of crystallisation. Glass formation thus becomes a question of how fast a given liquid must be quenched in order that detectable crystallisation is prevented. The two criteria are complementary, since any criteria based on chemical bonding, coordination or chemical structure merely imply indirectly that particular structural characteristics inhibit nucleation or growth of the crystalline phase. In the following, the kinetic criteria which have been successfully employed to predict quantitatively the ease of glass formation, together with rapid quenching techniques developed for the production of metallic glasses, will be presented. It will be followed by a discussion of glass-forming alloys and factors governing the glass-forming tendency.

3.1. Rapid quenching techniques

Most metallic glasses, with the exception of the easy glass-forming alloys Pd–Cu–Si, Pd–Ni–P and Pt–Ni–P, are produced at a relatively high cooling rate of 10^5 K s^{-1} or higher. The high rates of cooling are achieved by spreading a thin layer of liquid in good contact with a highly conductive substrate, e.g. metals and sapphire. The rate of quenching is determined by the liquid–substrate heat transfer and the thickness and thermal conductivity of the liquid layer. The thickness of quenched metallic glasses is thus limited to ~ 50 μm. Alternatively, amorphous solids can be formed in which the

liquid state is bypassed completely. These processes, known as atomic (or molecular) deposition, involve growth from the vapour phase by thermal evaporation, sputtering, decomposition of gaseous compounds by radio frequency discharges, or from salt solution by electroless displacement of electrolysis. These techniques provide a very high effective quenching rate and yield amorphous solids which cannot be obtained as a glass by liquid quenching. Comprehensive reviews on liquid quenching techniques can be found in Jones (1973) and Kavesh (1978) and on atomic condensation methods in Chopra (1969) and Sinha *et al* (1976). Only those techniques commonly employed in the production of non-crystalline solids will be presented here.

3.1.1. Liquid quenching. Klement *et al* (1960) reported the first production of metallic glass $Au_{75}Si_{25}$ from a liquid by the so-called splat-quenching or gun technique. In this process, a small liquid globule was propelled into small droplets by means of a shock tube and the droplets were sprayed into thin foil on a copper substrate. Quenched samples produced were irregular in shape with varying thickness from about 1 μm to 10 μm. The edges of some individual droplets were very thin (~ 1000 Å) for direct transmission electron microscopy (Willens 1962).

The quenching rate attained was estimated experimentally and analytically to be at least 10^6 K s^{-1} and perhaps 10^{10} K s^{-1} (Predecki *et al* 1965b, Ruhl 1967). The maximum thickness y_m obtainable is determined by the thermal diffusivity of the melt D_t, and the critical quenching rate q_{cr} such that $y_m \approx (D_t T_m/q_{cr})^{1/2}$, where T_m is the melting temperature. For alloy liquids, $D_t \approx 0{\cdot}2$ cm^2 s^{-1} and $T_m \approx 1000$ K, then $y_m \approx 0{\cdot}1$ mm at $q_{cr} \approx 10^6$ K s^{-1}. The quenching rate q achieved varies with y^{-n} with $n = 1$–2 for Newtonian to ideal quenching, where y is the thickness. q varies within the foil due to varying thickness and thus results in structural inhomogeneities.

Pietrokowsky (1963) designed a piston and anvil technique in which the liquid globule is squeezed between a fast moving piston and a fixed anvil. Ohring and Haldipur (1971) modified the piston and anvil technique by arc-melting a droplet on a water-cooled substrate and quenching to a foil between a hammer and the supporting substrate, thus avoiding crucible problems encountered in handling high melting alloys. The anvil foil so produced is about 15–25 mm in diameter and relatively uniform in thickness of ~ 40 μm, thus making it more suitable than the gun foil for structure, electrical and magnetic property measurements (Yamauchi and Nakagawa 1971).

For technical applications in recent years, effort has been concentrated on the development of continuous (or semi-continuous) fabrication of metallic glasses in wires or tapes. The earliest potentially continuous process applied to metallic glasses was reported by Chen and Miller (1970). In this two-roller or roll quenching process a molten metal is put into a gap between a pair of rapidly rotating rollers. Babic *et al* (1970) built the same apparatus for the preparation of metal ribbon. The product has the shape of a ribbon about 2 mm wide and 50 μm thick. Other commonly used processes are the melt spinning technique of Strange and Pim (1908) and Pond and Maddin (1967) in which the molten stream is cast, in the former, on to the outside and, in the latter, on to the inside of a rotating drum. These processes were developed for fabricating crystalline filaments and later adopted for continuous production of metallic glass ribbons (Masumoto and Maddin 1971, Liebermann and Graham 1976, Bedell 1975).

In comparison with the Strange and Pim process, the Pond and Maddin process yields a higher quenching rate because centrifugal force allows a better thermal contact

between the melt and drum surface, but the quenched filaments could not readily be pulled out from the drum. Chen and Miller (1975) developed a process by impinging a stream of melt on to the inner sloped surface of a rotating drum that ensures good heat transfer between the melt and substrate, while enabling the continuous fabrication of glass filaments. The rates of quenching achieved are $\sim 10^6$ K s^{-1}. Production rates of 2000 m min^{-1} are readily obtainable. These melt spinning methods yield ribbons 20–100 μm thick with reported width up to 5 cm and probably up to 15 cm width in the near future. The roller quenching has the advantage over melt casting by extracting the heat from both sides and in principle yields metallic glasses twice as thick for a given cooling rate and with smooth surfaces of uniform thickness. For some magnetic applications which require high packing density, the uniformity of ribbons becomes a crucial factor.

Wires with circular cross section can be formed by pressure-expulsion of a stream of melt through an orifice into a cooling fluid. Chen (e.g. Gilman 1975a) demonstrated for the first time the formation of a Pd–Cu–Si glassy wire $\sim 0{\cdot}3$ mm diameter by simply injecting a strand of melt into water. This process of forming glass wire has since been pursued further at Allied Chemical Corporation (Kavesh 1978). Alternatively, much finer size (1–100 μm) wire can be produced by the Taylor technique in which metal contained in a glass tube is drawn to very fine wire through a furnace. Glassy wires ~ 10–20 μm diameter of $Ni_{82}P_{18}$ and Fe–P-based alloys have been produced by this technique (Wiesner and Schneider 1974). For easy glass-forming alloys, Pd–Cu–Si, Pd–Ni–P and Pt–Ni–P, a cylindrical rod ~ 1–3 mm diameter of glassy alloy can be produced by quenching a melt-filled quartz capillary in water (Bagley and DiSalvo 1973, Chen 1974a). Other methods of quenching liquid alloys such as plasma spray (Moss *et al* 1964), melt extraction (Maringer and Mobley 1974, Roberge and Herman 1968), melt atomisation (Yamauchi and Narita 1978), and laser glazing (Laridjani *et al* 1972) have not been much explored for the fabrication of metallic glasses.

3.1.2. Atomic condensation. Since structural order in an atomically condensed film is determined largely by the surface mobility of the atoms, a highly disordered amorphous solid would be formed if mobility is low so that the atoms condense at or near the point of impingement, e.g. vapour condensation at liquid helium temperature has yielded high superconducting amorphous films of Bi, Ga, As, Sb and Be. A number of nominally pure metal elements, particularly high melting transition metals, have been produced in amorphous solid films by evaporation or sputtering on to a substrate at very low temperatures. Many amorphous films are very unstable and crystallise at very low temperature ~ 20 K. The stability of the amorphous films is seen to be very sensitive to deposition conditions. Impurity contamination is believed to stabilise the amorphous structure and thus result in the formation of amorphous metal films.

Many alloys of metals or metals and metalloids which have not been prepared in the glassy phase by liquid quenching could form amorphous solids either by vapour deposition or sputtering. Cu–Ag and Co–Au (Mader *et al* 1967), Au–Ni (Herd and Chaudhari 1974), Pb–Au (Scott and Maddin 1976), Fe–Au (Marchal *et al* 1975) and Fe–Si (Mangin *et al* 1977) were produced in amorphous films stable at room temperature by co-evaporation at 80 K substrate temperature. These alloys form the amorphous phase most readily near the equiatomic composition. Mader (1966), based on a jam-up of atom structure, proposed criteria for amorphous phase

formation to be a solid-state immiscibility and a large ($>10\%$) difference in atomic radii of the constituents. This contrasts with liquid quenching in which glass-forming compositions always lie near low melting eutectics. It is not surprising that the criteria for the formation of amorphous phases by atomic condensation and liquid quenching can be different because of the different processes involved during solidification (e.g. Roy 1970). High melting compounds such as superconducting Nb_3Ge (Brown *et al* 1977) and the magnetic bubble materials such as the rare-earth (Gd, Hf) containing $\sim 80\%$ (Co, Fe) form amorphous solids either by sputtering or evaporation (Leamy and Dirks 1977). A limited number of metal–metalloid alloys such as transition metal (Fe, Co, Ni) containing 15–25% P, which can be liquid-quenched into a glassy state, form an amorphous phase by electrodeposition or by vapour condensation. Watanabe and Tanabe (1976) reported the electrodeless plating of amorphous Ni alloys containing $\sim 40\%$ B.

3.1.3. Ion implantation. Ion implantation has been growing steadily as a method to introduce atoms into a surface and modify surface and bulk properties of many materials. Use of implantation technique provides the flexibility of introducing a wide range of atomic species, and obtaining impurity concentrations and distributions of particular interest which in many cases would not be attainable otherwise. The majority of the implantation work is being made in semiconductors and in some cases metals.

Ion implantation provides a unique method for producing very high quenching rates of the order of $\sim 10^{14}$ K s^{-1}, if thermal spikes in the ion implantation process are pictured as localised regions of high lattice temperature. Mechanisms of amorphisation by ion implantation, however, remain unclear (e.g. Grant 1978). Amorphous alloy layers have been produced by implantation of W^+ into Cu (Cullis *et al* 1976), Dy^+ into Ni (Andrews *et al* 1976), Ta^+ into Cu (Poate *et al* 1977), P^+ or B^+ in Fe, Co or Ni (Ali *et al* 1978) and Au^+ into Pt (Singhal *et al* 1978). Amorphous layers form when the concentration of implants reaches compositions of $\sim 15\%$. All amorphous-forming alloy systems exhibit limited solid solubility in the equilibrium states. Ta and W are insoluble even in molten Cu. The Pt–Au alloy system shows a two-phase field in the solid state with a miscibility gap centred at 60 at% Pt and a critical point at 125°C (Hanson 1958).

3.2. Kinetic criteria

Turnbull (1969) adopted simple nucleation theory and, using the criterion for glass formation as being the avoidance of a single homogeneous nucleus, estimated quantitatively the condition for glass formation. The homogeneous nucleation frequency I (cm^{-3} s^{-1}) for normal metals is expressed by

$$I \approx \frac{10^{30}}{\eta} \exp\left(-b\alpha^3\beta/T_r\Delta T_r^2\right) \tag{3.1}$$

where η is viscosity, b is the shape factor (e.g. $16\pi/3$ for a spherical nucleus), the reduced temperature $T_r = T/T_m$ and $\Delta T_r = 1 - T_r$ with T_m the melting temperature. Here α and β are dimensionless parameters related to the liquid–crystal interfacial tension σ and the entropy of fusion ΔS_f and given by $\alpha = (N_0V)^{1/3}\sigma/\Delta H_f$ and $\beta = \Delta S_f/R$, where N_0 is Avogadro's number, V is the molar volume in the crystal, ΔH_f

is the molar heat of fusion and R is the gas constant. For constant $\eta = 10^{-2}$ P, the nucleation frequency I rises steeply with ΔT_r from zero to a broad peaked maximum at $T_r = \frac{1}{3}$. The peak nucleation frequency $I_{max} \approx 10^{32} \exp(-113\alpha^3\beta)$ depends strongly on the thermodynamic parameters and decreases sharply from 10^{31} to 10^{-4} cm^{-3} s^{-1} as $\alpha\beta^{1/3}$ increases from 0·25 to 0·9. Turnbull thus concluded that liquids with $\alpha\beta^{1/3} = 0{\cdot}9$ should readily form glasses, while for those with $\alpha\beta^{1/3} < 0{\cdot}25$ it should be impossible to suppress crystallisation. Glass formation is thus enhanced greatly by a large interfacial tension and entropy of fusion. β is near 1 for metals, SiO_2, GeO_2, organic plastic materials, and many strong acids and bases; while for typical organic and inorganic compounds, β ranges from 4–10. Results of droplet nucleation experiments indicate that $\alpha = 0{\cdot}4$–$0{\cdot}5$ for typical metals and $\alpha = \frac{1}{3}$ for most non-metals. The progressive increase in β certainly goes in parallel with the glass-forming tendency. The ease with which network liquids, such as SiO_2, B_2O_3, P_2O_5, GeO_2, BeF_2, etc, form glasses is due mainly to the extremely high viscosity at T_m. For example, the viscosity (Bockrie *et al* 1955) of fused silica $\approx 10^7$ P at T_m of cristobalite and rises to 10^{12} P at $T_r = \frac{2}{4}$.

A qualitative estimate of the critical quenching rate for glass formation has been carried out by Uhlmann (1971) and Davies (1976) based on the theory of nucleation and growth and using the Johnson–Mehl treatment of transformation kinetics. In this treatment, time–temperature–transformation (TTT) curves corresponding to a small volume fraction of crystalline phase are constructed. From these curves, the minimum quenching rates, q_{cr}, for the formation of various glasses are estimated.

For metals, the reduced glass transition temperature $T_{r0} = T_0/T_m$ is seen to be the most important factor determining the glass-forming abilities, where T_0 is known as an ideal glass transition temperature and is slightly lower than the observed glass transition temperature T_g. The effect of increasing T_{r0} is to drastically lengthen the time at the nose of the TTT curves, to sharpen and shift the nose to smaller undercooling. With a reasonable assumption of the temperature dependence of viscosity of the form, equation (2.2), q_{cr} is evaluated to vary from $\approx 10^9$ K s^{-1} to 10^2 K s^{-1} as T_{r0} increases from 0·3 to 0·6. These values are in reasonable agreement with estimated experimental values, e.g. 10^{10} K s^{-1} for pure metal elements Ni, Pd; 10^6 K s^{-1} for many glass-forming alloys Au–Si, Ni–P, Pd–P; and 10^2 K s^{-1} for easy glass formers Pd–Cu–Si, Pd–Ni–P alloys. For these three glass systems $T_{r0} \approx \frac{1}{4}$, $\frac{1}{2}$ and $\frac{2}{3}$, respectively.

As the glass transition temperature T_g of alloys depends weakly on composition, the increase in T_{r0} and consequent drastic enhancement of glass-forming tendency of these alloy systems arise from the lowering of the liquidus temperature. Those compositions with the lowest liquidus temperature, i.e. near-eutectic compositions, thus form glasses most easily as has been observed for most metallic glasses as well as ionic glasses in which bonding character is not drastically altered. The estimation of q_{cr} by the construction of the TTT curves implicitly assumes that the crystallisation kinetics over the full range of temperature are as rapid as at the temperature of the nose and thus overestimates q_{cr} by about a factor of three estimated from the continuous cooling curves (e.g. Onorato and Uhlmann 1976, Naka *et al* 1978d).

The preceding discussion has focused on the kinetics of homogeneous nucleation. Crystal growth becomes more important than nucleation rate when nuclei or preferred sites are no longer absent. The effect of heterogeneous nucleation on glass formation has been explored recently by Onorato and Uhlmann (1976). They showed that heterogeneities characterised by contact angle $\theta > 100°$ become effective only at sufficiently large undercoolings and that their contribution at the relevant cooling

rates has an insignificant effect on overall crystallisation. Those with $\theta < 100°$, however, have a significant effect on glass-forming ability.

3.3. Glass-forming alloys

Computer simulations demonstrate the formation of a monatomic glass either by atomic deposition (Bennett 1972) or by liquid quenching at rates of 10^{12} K s^{-1} (Rahman *et al* 1976). In practice, however, pure monatomic metal liquids have not been quenched into glasses because of the high quenching rates required to prevent crystallisation. Davies *et al* (1973) reported, for a cooling rate of $\sim 10^{10}$ K s^{-1}, the production of a glassy phase in the thinnest portion of splat-quenched Ni foils only when the quenching was performed in an oxidising atmosphere. Impurity contamination played a role in the stabilisation of the glassy phase as has been observed for atomic depositions of nominal pure metals.

The ability to form glass critically depends on quenching conditions, e.g. thickness of the foil, heat transfer between the melt and the substrate, etc. Many binary alloys, e.g. $Fe_{80}P_{20}$, $Pd_{80}P_{20}$ and $Pt_{75}P_{25}$ produced by the piston and anvil technique (Duwez 1967), reported previously to be partially crystalline nowadays can be readily produced as glassy ribbons by melt spinning, probably due to slight improvements in quenching conditions. In the following, only the metallic glasses which can be quenched readily from the melt at rates of $\sim 10^6$ K s^{-1} are presented. A list of glass-forming alloys has been compiled by Takayama (1976).

Currently known glass-forming binary alloys may be divided into three categories: transition-metal or noble-metal alloys containing about 10–30% semimetal (P, B, Si, C), alloys of early transition metals (Zr, Nb, Ta, Ti) and late transition metals (Fe, Co, Ni, Cu, Pd), and alloys containing Group IIA metals (Mg, Ca, Be). Representative phase diagrams are shown in figure 4 (Hansen 1958).

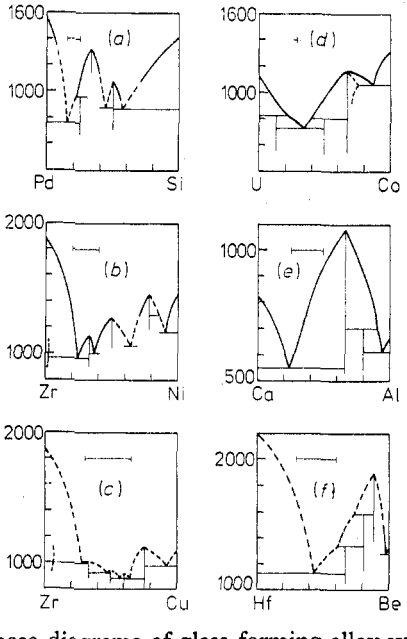

Figure 4. Representative phase diagrams of glass-forming alloy systems. All temperatures are in °C.

The first group is generally known as the metal–metalloid system represented by $Au_{75}Si_{25}$, $Pd_{80}Si_{20}$, $Ni_{80}P_{20}$, $Fe_{80}B_{20}$ and $Pt_{75}P_{25}$ whose glass-forming composition falls into the region of a narrow deep eutectic (figure 4(*a*)). This glassy system has drawn considerable attention because of their technologically interesting properties (Gilman 1975a). The second group is referred to as the inter-transition system. As shown for Zr–Ni alloys in figure 4(*b*), these systems form glasses generally near an early transition-metal-rich eutectic containing 20–40% late transition metal such as Zr_{70}(Ni, Fe, Co, Pd, Rh)$_{30}$, $Ti_{65}Ni_{35}$ and $Nb_{60}Rh_{40}$. However, in alloys of Zr–Cu, Ti–Cu and Nb–Ni (Ray *et al* 1968), glasses can be formed for a broad range of compositions embracing intermetallic phases with relatively low melting temperatures as exemplified by Zr–Cu (figure 4(*c*)). The last glass-forming system consists of Group IIA metals (Be, Mg, Ca) and has been explored only recently. The Mg–Zn system, which consists only of 'simple' metals, forms glass in alloys with 25–35% Zn (Calta *et al* 1977), while Giessen *et al* (1978) have obtained glassy Ca–(20–45%)Mg, and Ca–(25–50%)Al or Zn by melt spinning. It may be noted that Ca and Mg belong to the same Group IIA column. These alloy systems are characterised by relatively high melting intermetallic phases of the AB_2 type, e.g. $MgZn_2$, $CaMg_2$ and $CaAl_2$ participated in relatively low melting eutectic near 40% B element (figure 4(*e*)). In the Be-containing alloys, glasses form in a narrow range of 37–41% Be for Ti–Be alloys, but Zr–Be and Hf–Be alloys (Tanner and Ray 1977) exhibit a wide glass-forming composition of 30–50% Be and 30–60% Be, respectively. This Be alloy system is characterised by a high melting intermetallic phase (Zr, Hf, Ti)$_2Be_{17}$ and eutectic at $\sim$40% Be (figure 4(*f*)).

In addition to these three glass-forming systems, Ray and Musso (1976) reported the production of glassy U alloys containing 20–40% V and Cr. Giessen and Elliott (1978) found the formation of actinide-rich glasses by melt spinning of U–30% Mn, Co, Fe and Ni, and neptunium and plutonium alloys containing $\sim$10–20% transition metal. The glass-forming composition falls near the eutectic which varies from 20–30% transition metal (figure 4(*d*)). Recently, Bauhofer and Simon (1978) reported the formation of glassy alloys of alkali metals (Rb, Cs) containing 13–20% oxygen near eutectic compositions. A number of Al-based alloys near eutectic composition, e.g. Al–17% Cu (Davies and Hull 1974), Al–30% Ge (Ramachandrarao *et al* 1972), Al–7% Cr (Furrer and Warlimont 1977) and Al–7% Ni (Chattopadyay *et al* 1976) also form glasses at higher quenching rates $\gtrsim 10^8$ K s^{-1}. Other glass-forming alloys, e.g. $La_{76}Au_{24}$ (Johnson *et al* 1975), Gd-rich Gd–M with M = Co, Ni, Cu and Pd (Buschow and Beekmans 1978), and $Y_{60}Fe_{40}$ and $Th_{50}Fe_{50}$ (Buschow *et al* 1978) all fall near the eutectic.

All the glass-forming alloys have common features: strong interactions between constituent atoms as indicated by a negative heat of mixing, and a low lying eutectic (figure 4). The heat of mixing $\Delta H_m \approx -2$ kcal (g atom)$^{-1}$ for Au–Ge–Si (Chen and Turnbull 1968), ≈ -8 kcal (g atom)$^{-1}$ for $Ni_{75}B_{25}$ (Omori and Hashimoto 1973), ≈ -10 kcal (g atom)$^{-1}$ for (Fe, Co, Ni)$_{50}Si_{50}$ (Elliot and Gleiser 1960) and ≈ -5 to -10 kcal (g atom)$^{-1}$ for Zr–(Fe, Ni, Ag) and Nb–(Ni, Fe) (Hultgren *et al* 1973, Miedema *et al* 1975). The strong atomic interactions are also seen by the formation of stable intermetallic phases which participate in a relatively low eutectic reaction. The eutectic temperature T_E is about 0·6 of the melting temperature T_m as compared with $T_E/T_m = 0{\cdot}8$ for normal eutectic systems. The additional melting point depression of the glass-forming alloys was shown to arise from the strong atomic interaction and the consequent negative heat of mixing (Chen 1974a).

With a few exceptions such as Pd–Si, Zr–Cu and Zr–Be systems, which manifest thermally the glass transition, binary alloy glasses are not stable and crystallise at temperatures below the effective glass transition temperature. These glasses can be obtained only as thin foils ~ 40 μm thick. A critical quenching rate of 10^5 K s^{-1} or higher is required to retain the glassy phase. The admixture of glass-forming binary alloys or the addition of third elements, which have different atomic radii and different crystalline intermetallic compound symmetry, enhances drastically both the stability and the glass-forming tendency, mainly due to the lowering of the eutectic temperature. The ternary alloy glasses, Pd–Cu–Si, Pd–Ni–P and Pt–Ni–P have been prepared as cylindrical rods of 1–3 mm diameter at quenching rates of 10^2 K s^{-1}. These glasses exhibit a striking thermal stability and remain glassy at the glass transition temperature for several hours. The eutectic point of the ternary alloys are lowered by 50–300 K from that of the constituent binary alloys (Chen and Jackson 1978, Naka *et al* 1978d). The enhancement in the ease of formation and stability of glasses upon alloying is a common phenomenon and has been observed for many metallic glasses, e.g. $Fe_{80}P_{17}C_3$, $(Fe, Co, Ni, Mo, Cr)_{75}P_{16}B_6Al_3$, $Fe_{80}B_{17}Si_3$, and $(Zr, Ti)_{60}Be_{40}$. Interestingly, the glassy phase is seen to form by melt quenching of ternary iron-based alloys $(Fe,M)_{82}C_{18}$ with M = Cr, Mo and W (Inoue *et al* 1978a), while only a partially crystalline phase could be obtained in $Fe_{82}C_{18}$ by splat quenching (Shingu *et al* 1976a, Boswell and Chadwick 1976).

3.4. Factors affecting glass formation

The earliest attempt to correlate the eutectic compositions with liquid structure was made by Hume-Rothery and Anderson (1960). They suggested that the eutectic alloy can take up a special geometrical structure of low free energy. Based on the Frank icosahedral unit, the special geometrical structure occurs at quasi-stoichiometric compositions such as $A_{12}B$, A_5B and A_3B. Bennett *et al* (1971) proposed that the small and softer metalloid atoms fill the large holes inherent in a Bernal dense random packed structure and stabilise the random configuration. Filling all of the large holes, such as in the Archimedian antiprism, trigonal prism and tetragonal dodecahedron with metalloid atoms would yield an alloy of 80% metal content, a composition with which most glassy metal–metalloid alloys have been produced. It was noted, however (Cargill 1975a), that none of the large holes are large enough to accommodate the metalloid atoms. Furthermore, the glass-forming composition of the metal–metalloid system in some cases falls well outside the predicted range, and in many cases the softer metalloid atoms are larger than the metal atoms, e.g. $Pt_{65}Sb_{35}$ (Srivastava *et al* 1972) and $(Au,Ag)_{25}Pb_{75}$ (Predecki *et al* 1965a).

Nagel and Tauc (1975) treated the glass as a nearly free electron solid and argued that the glass phase should be relatively stable at the composition where the Fermi level is at a minimum in the density of states, or where the Fermi vector $2k_F$ equals q_p, the first peak of the structure factor. Thus an alloy with valence electron concentration (VEC) $Z = 1{\cdot}7$ should be most stable against crystallisation. Since $2k_F \sim q_p$ is just the condition for negative temperature coefficient (NTC) of the electrical resistivity in liquid alloys (see §8.1.2), Güntherodt and Künzi (1978) further extended the Nagel and Tauc model such that the glass formation would be favoured for alloy compositions which show NTC (or small temperature dependence of electrical resistivity) in the liquid state. This VEC value and NTC criterion compare favourably with the composition of some metal–metalloid glasses and the wide glass-forming

composition range in the Zr–Cu and Nb–Ni systems, but do not explain the large difference in glass-forming tendency among alloys which satisfy the above criteria. The concentration ranges of NTC for liquid alloys of metal–metalloids, e.g. (Mn, Fe, Co, Ni)–Ge, are centred near the equiatomic composition, contrary to the observed glass-forming range for metal–20% metalloids. Furthermore, no minimum in the density of states is found in many glassy alloys (see §8.1.4). In Cs–O and Rb–O glass-forming compositions (Bauhofer and Simon 1978), $2k_F$ is located near the minimum instead of the maximum in the structure factor.

The models mentioned above are based on the stabilisation of the liquid phase ignoring the composition effect on the stability of the crystalline phases. The rationale of these models has been criticised by Chadwick (1965), who noted that there is very little evidence to substantiate the structural stabilisation in eutectic liquids. As may be seen later (§5), the viscosities of liquids and T_g of alloy glasses are depressed, suggestive of the occurrence of atomic clustering, in the region of eutectic composition. Chen (1974a, 1976b,c) and Chen and Park (1973) then proposed the destabilisation of the crystalline mixture, rather than the stabilisation of the glassy phase, to determine the eutectic composition and the glass-forming range. Chemical affinity due either to electron transfer or to ionisation among constituent atoms, neither of which requires the formation of directional bonding, stabilises crystalline phases of stoichiometric A_3B, A_2B or AB_2 type. The mismatch strain energy associated with the different atomic radii of constituent elements prevents the formation of a continuous crystalline solid solution, thus leading to stoichiometric intermetallic phases and eutectic reactions. This sort of misfit energy is believed to be absent or much reduced in magnitude in the liquid phase. The strong interactions between unlike atoms produce an excessive melting point depression, thus constituting a deep eutectic. Formation of relatively stable intermetallic phases of the A_3B and A_2B type as manifested for the metal–metalloid system leads to the deep eutectic near 20% B, while the eutectic composition falls near 40% Be for Be-containing glass-forming alloys which exhibit high melting intermetallic phases very rich in Be, e.g. Hf_2Be_{17} as shown in figure 6(f). An appreciable size difference, together with the strong interactions of the component atoms, are thus necessary requirements for deep lying eutectic systems and thus of easy glass-forming alloys. For several dozen glass-forming alloys examined (Cargill 1975a), the difference in atomic radii $[(2r_1 - d_{12})/r_1]$ is greater than 0·12, where r_1 is the atomic radius of the major constituent and d_{12} is the interatomic distance between unlike atoms.

In a few cases, the glass-forming composition does not fall at the eutectic but in a composition range more rich in the minor element B. Shingu *et al* (1976b) reported the glass formation at 40–50% Ge in Al–Ge alloys which have a eutectic at 30% Ge. Ca–Mg, –Al and –Zn alloys form glasses over the composition range 25–50% Al, Mg and Zn, where the eutectic compositions are 22% Zn, 27% Mg and 35% Al, respectively. The phenomenon may be due partly to the possible increase in T_g with increasing B content and partly to the higher values of β for Ge ($\beta = 4$) and compounds $CaMg_2$, $CaAl_2$ and $CaZn_2$ due to a low crystalline symmetry (Jackson 1958, 1969).

A qualitative representation of glass-forming elements related to position in the periodic table was given by Masumoto and Maddin (1975). Alloy elements located in different sections in the periodic table facilitate glass formation. Elements of different valence partaking in charge transfer that prefer A–B bonding may be an important factor in promoting glass formation. The valence difference may coincide with the difference in atomic sizes. These two factors would constitute a deep lying

eutectic. An exception to this rule is the Ca–Mg system in which both Ca and Mg belong to the same Group IIA.

Wang and Merz (1976) have correlated the occurrence of amorphous phase with a high degree of bonding anisotropy and extensive polymorphicity and have proposed a microcrystalline structure composed of a finite number of crystalline structure as exhibited by the polymorphs. It may be noted that elements with a high degree of polymorphicity are characterised by a loosely packed open structure with low coordination number, e.g. covalent bonding elements S, Se, As, Bi, P, etc. The open structure of these elements facilitates various atomic configurations with little change in internal energy. The relative ease of amorphisation by atomic deposition in covalent bonding elements, as compared with close-packed metals, can be understood on the basis that, because of the small coordination number, the former require relatively large displacements of the randomly condensed atoms to form the crystalline structure. The Wang and Merz correlation thus coincides with one of the structural criteria for glass formation and the kinetic criterion that elements with low symmetry have relatively low melting temperatures and high entropy of fusion, thus favouring glass formation.

4. Structure

X-ray, neutron and electron diffraction methods have been frequently used to characterise the structure of non-crystalline materials. A radial distribution function (RDF) $4\pi r^2 p(r)$, or reduced radial distribution function $G(r) = 4\pi r[p(r) - p_0]$, is obtained by Fourier inversion of the coherent scattered radiation, where $p(r)$ is the average density of atoms at distance r from a reference atom and p_0 is the overall average density. The RDF yields only a statistical average projection of the structure onto one dimension and thus does not establish a unique description of the atomic configuration in real three-dimensional coordinates. However, the RDF in conjunction with other measurements, e.g. macroscopic density, diffusivity, electronic properties, etc, serves to screen out structural models which are inconsistent with the experimental RDF. Experimental data and model studies of metallic glasses have been exhaustively reviewed by Giessen and Wagner (1972) and Cargill (1975a). Critical reviews of the structural models have been given by Finney (1977), Waseda (1977) and Chaudhari and Turnbull (1978). In this section, various structural models are discussed briefly first, followed by a description of experimental structural data with emphasis laid on more recent work. An attempt is made to unify the structural models of dense random packing of hard spheres (DRPHS) for amorphous pure metals and glassy alloys including metal–metalloid, rare-earth–transition-metal and intertransition-metal systems. The induced structural and compositional anisotropies during preparation, heat treatment and deformation processes are also presented.

4.1. Various structural models

The structural models for amorphous solids can be classified as either the discontinuous type, e.g. microcrystalline and amorphous cluster model, or the continuous random type. Microcrystalline models are heterogeneous in which misoriented microcrystallites containing several hundred atoms are separated by regions of less-ordered non-crystallographic arrangements. Microcrystalline models for amorphous

solids have been proposed for polyatomic systems by Valenkov and Porai-Koshits (1937) and for monatomic systems by Mott and Gurney (1938). The major drawbacks of these models are that the configurations in intercrystalline boundaries and the correlations between crystallite orientations are not described. The calculated distribution functions given by microcrystalline models as compared with experimental data are less satisfactory than those from random dense-packed models.

Amorphous cluster models constitute another type of heterogeneous structural description of amorphous solids similar to the microcrystalline models but with non-crystallographic highly ordered low-energy atomic clusters playing the same role as the microcrystallites. Frank (1952) showed that an icosahedral cluster of 13 atoms with pairwise interactions should have a lower potential energy than either of the close-packed crystalline arrangements (FCC or HCP). Thus such non-crystalline groups would be very common in a simple liquid. Recent calculations by Hoare and Pal (1975) showed that the potential energies of certain non-crystalline clusters up to 50 atoms are lower than those of close-packed crystalline ones. All of the lowest energy clusters essentially formed by distorted tetrahedral units have tetragonal, pentagonal and icosahedral symmetries, and cannot be extended infinitely with lower energy than the corresponding crystalline state. Experimental evidence of amorphous cluster formation was observed by Farges *et al* (1975) in beams of liquid argon ejected from supersonic nozzles in which small argon clusters of about 100 atoms are amorphous. It is reasonable to suppose that in thin films formed by atom condensation, the stable amorphous clusters can be dominant at the initial cluster formation. As in the microcrystalline models, the cluster models lead the unsolved problem regarding the spatial connectivity among clusters.

The continuous random models are homogeneous in contrast to microcrystalline and amorphous cluster models. The well-known models are: (i) the continuous random network (CRN) model proposed by Zachariasen (1932) and Warren (1937) for silica in which tetrahedral units link together to form a continuous irregular three-dimensional network, and (ii) the dense random packings of hard spheres (DRPHS) as a model for monatomic liquids proposed by Bernal (1960) and Scott (1962). The DRPHS model may be thought of as the close-packed analogues of the CRN structure (Chaudhari *et al* 1975, Connell 1975).

There has been considerable discussion of melting phenomena associated with the spontaneous generation of dislocations. The computer simulation of the model by Jensen *et al* (1973) yielded a liquid-like pair distribution when the dislocation density reaches a certain high value $\sim 0{\cdot}15$. Strikingly, the second peak of the pair distribution of the FCC structure (at $\sqrt{2}$ atomic distance) disappears as the dislocation density is increased. This is due to the fact, as noted by Ninomiya (1977), that when a 60° dislocation or screw dislocation is introduced, an octahedron inherent in close-packed crystalline structure is transformed into a tetragonal dodecahedron or trigonal prism, the polyhedra observed in Bernal's random packing structure. The major drawback with the dislocation model is the difficulty in identifying a dislocation in such a high density of dislocations, since they are separated by only about three atomic distances.

4.2. Amorphous metals

4.2.1. Experimental data. Amorphous solids of nominally pure metals have been prepared by vacuum evaporation on to cooled substrates. The structural data were obtained from electron scattering experiments on thin films. Interference functions

and distribution functions for amorphous films among Ni, Fe, Co, Mn and Au are found to be very similar (Cargill 1975a). The interference functions $I(q)$ have, in common, a relatively intense first peak and second peak with a shoulder in the higher q region. The distribution functions RDF(r) and $G(r)$ are characterised by splitting of the second peaks into a strong subpeak and a weak one at larger r, with the ratio of distances of the peaks to that of the first peak being nearly the same, e.g. the ratios r_2/r_1 and r_2'/r_1 equal to $\sim 1{\cdot}67$ and $1{\cdot}93$, respectively, for the second subpeaks. The ratio $r_2/r_1 \approx 1{\cdot}67$ is close to the mean value between the distances $1{\cdot}633\delta$ and $1{\cdot}73\delta$ characteristic of the apex separation in two tetrahedra with common base and with common edge in coplanar, respectively, while the ratio $r_2'/r_1 = 1{\cdot}93$ approaches the separation in three collineated spheres 2δ, where δ is the sphere diameter. Significantly, the $\sqrt{2}\delta$ distance, characteristic of octahedral sites inherent in close-packed crystalline FCC and HCP structures, is absent.

Figure 5 illustrates the interference function $I(q)$ and pair distribution function, $W(r) = p(r)/p_0$, of amorphous Fe film (Ichikawa 1973) and for comparison those of liquid Fe (Waseda and Ohtani 1974). Contrasted to the amorphous film, both $I(q)$ and $W(r)$ of the liquid metal exhibit no splitting in the second peak. The second peak in $W(r)$ of the liquid occurs at $r_2/r_1 \approx 1{\cdot}85$ which falls between the ratios $1{\cdot}67$ and $1{\cdot}93$ observed in the film. The oscillations in both $W(r)$ and $I(q)$ have a larger amplitude and persist to higher q in the amorphous Fe than in the liquid Fe, indicating stronger short-range order in the former.

4.2.2. Dense random packing models. The dense random packing has been established either by packing together as densely as possible a large number of equal steel balls (Finney 1970, Scott and Kilgour 1969), by computer algorithms (Bennett 1972,

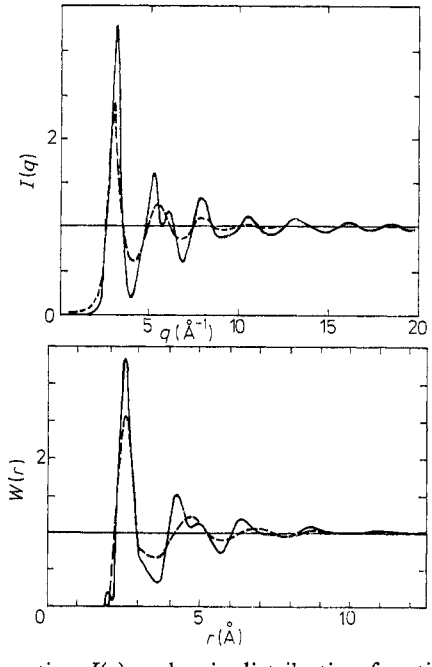

Figure 5. The intensity function $I(q)$ and pair distribution function $W(r)$ of amorphous Fe film (——) and liquid Fe (– – –).

Adams and Matheson 1972), or by integral equation methods (Weeks 1977). The computer-generated dense random packings are similar to those obtained with steel balls, the splitting of the second peaks in $W(r)$ with maxima at 1·73 and 2·0 ball diameters being obtained. The splitting is, however, less pronounced with a significantly weaker maximum at 1·73 ball diameters in the computer-generated structures than in the steel ball models. The packing density of the computer-generated model ($\eta \approx 0{\cdot}63$) is lower and approaches that of the steel ball model ($\eta = 0{\cdot}637$). Weeks showed that both the generalised mean spherical approximation (GMSA) and Percus–Yevick (PY) equation give a $W(r)$ in good agreement with that obtained by Bennett regarding the peak positions and asymmetric shape of the second peak. However, the theory gives a shoulder rather than a split in the second peak.

Qualitatively, the structural models yield a $G(r)$ in good agreement with the experimental data. However, the quantitative agreement is far from perfect. The relative intensities of the two components of the split second peak are reversed and their relative positions r_2/r_1 and r_2'/r_1 are lower. Sadoc *et al* (1973) and Ichikawa (1975) have employed a modified Bennett's algorithm and have succeeded in reproducing the experimental relative peak heights and bringing the r_2/r_1 ratio to 1·65, but have failed to bring r_2'/r_1 closer to the experimental values. All the modifications increase the number of nearly perfect tetrahedra in the structures. These models are not densely packed, having an average density $\sim 20\%$ lower than Bennett's. Better agreement with experimental data has been brought about by relaxing computer-generated or physically constructed models under central forces, pairwise interactions (Heimendal 1975, Connell 1975) and by very rapidly quenching liquid configurations by molecular dynamics (Hiwatari *et al* 1974, Street *et al* 1974, Rahman *et al* 1976, Woodcock *et al* 1976, Yamamoto *et al* 1979). The position of the first component of the split peak is seen to be sensitive to the softness of the potential. The Lennard-Jones 6:12 potential is found to be too hard a repulsive core. The Morse potential employed by Heimendal appears to be more realistic for metal atoms and the model agrees well in many features with the experimental data.

4.3. Glassy alloys

4.3.1. Metal–metalloid alloys. These alloy glasses constitute the most thoroughly studied class of glassy metal systems because of relatively high stability at room temperature and the ease of glass formation either by electrodeposition or liquid quenching. All of the metal–metalloid alloy glasses, e.g. Pd–Si, Ni–P, Fe–P–C, Ni–Pd–P, etc, produce very similar scattering patterns and radial distribution functions. Both $I(q)$ and $G(r)$ of glassy alloys are in many features similar to those for amorphous metal films described in the previous subsection. The ratios $r_2/r_1 \approx 1{\cdot}63$ and $r_2'/r_1 \approx 1{\cdot}90$ for alloys are, however, slightly less than those observed for the metal films. An exception is found for Pt–Ni–P (Sinha and Duwez 1971) in which both $I(q)$ and $G(r)$ show no splitting in the second maximum.

Dixmier and Duwez (1973) reported slight asymmetry in the first peak of $G(r)$ in Pd–Ni–P alloys and attributed it to a contribution from metal–metalloid pairs. Suzuki *et al* (1976) showed that the resolution of RDF(r) is progressively improved as truncation is made at higher q_{max} in the Fourier transform of $I(q)$ as shown in figure 6. $I(q)$ is taken over a wide range of q up to as high as 30 Å^{-1} by means of time-of-flight neutron diffraction using pulsed neutrons produced by an electron linear accelerator. The RDF(r) of the glassy alloy obtained by truncating Fourier transformation at

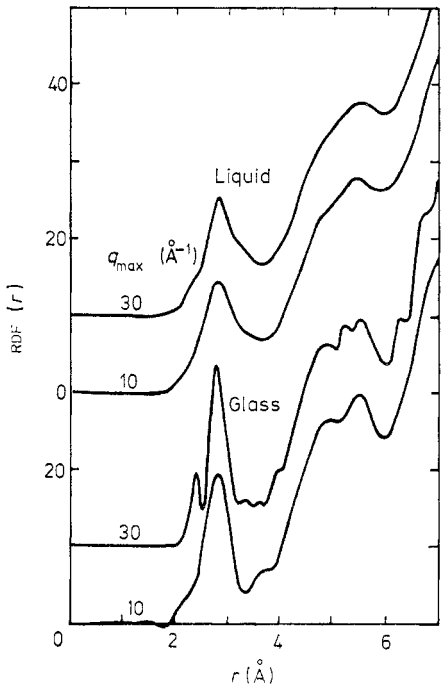

Figure 6. Radial distribution functions, RDF(r), of glassy and liquid $Pd_{80}Si_{20}$ alloy.

$q_{max} = 10$ Å^{-1} shows asymmetry in the first maximum as observed by Dixmier and Duwez. For $q_{max} = 30$ Å^{-1}, the first peak in RDF(r) clearly splits into two subpeaks at $\sim 2{\cdot}42$ Å and 2·81 Å. In the liquid alloy, the RDF(r) shows a shallow hump instead of the distinct subpeak at 2·42 Å because of large thermal fluctuations. Noteworthy is a small tail extending toward lower $r \approx 2{\cdot}20$ Å which is absent in the glassy alloy. Andonov (1976) also observed for the same liquid alloy a similar broad maximum at $\sim 2{\cdot}20$ Å. These features in the RDF for liquid $Pd_{80}Si_{20}$ alloy are seen to be quantitatively reproduced by the Percus–Yevick hard-sphere model for a binary system with a packing density $\eta = 0{\cdot}45$. The peaks (or hump) at 2·81, 2·42 and 2·20 Å correspond to contributions from Pd–Pd, Pd–Si and Si–Si pairs respectively. The Pd–Pd distances in the alloy expand slightly with respect to that in pure metal $\sim 2{\cdot}72$ Å, while the Pd–Si distances are significantly less than the sum of Pd and Si Goldschmidt radii, consistent with the corresponding distances found in the Pd_3Si crystalline structure. The absence of a maximum at 2·20 Å in the RDF(r) of the glassy alloy indicates negligible close contact of Si atoms as found in the intermetallic crystalline structures, Pd_3Si and Pd_2Si.

It may be noted that the essential short-range structure of the glassy alloy already exists in the liquid state but the Si–Si correlation is brought about to avoid a hard contact during cooling from the melt. Considering the particularly strong bonding between metal and metalloid atoms, Chen and Park (1973) speculated that the short-range order in glassy alloys is similar to that in metal-rich intermetallic phase(s). Si atoms are prohibited from hard contact in the glassy phase. However, at high temperatures the large contribution of configurational entropy to the free energy of the system would favour a random mixing and bring about contact among Si–Si atoms in the liquid.

Partial distribution functions provide further information regarding the short-range structure in binary alloys. Recently Sadoc and Dixmier (1976) have obtained three partial distribution functions for amorphous $Co_{80}P_{20}$ alloy by combined x-ray and neutron (polarised and unpolarised) scattering. They observed in the P–P pair distribution function a significant peak which appears only at $r \approx 3{\cdot}34$ Å. This P–P pair distance is much larger than either the covalent (2·12 Å) or metallic (2·56 Å) diameter confirming the P atoms never being in close contact. As with the Pd–Si alloy, the first Co–P pair distance at 2·32 Å is distinctively less than the sum of Goldschmidt radii. Essential features of Co–Co and Co–P partial distribution functions are similar to amorphous monatomic metals. Waseda and his co-workers (Waseda *et al* 1976, 1977a,b) obtained partial distribution functions for amorphous Ni–P and Fe–P glassy alloys by x-ray anomalous scattering techniques. Their results are identical in many features with the findings of Sadoc and Dixmier.

The influence of metalloid concentration on the structure (RDF) has been investigated for phosphorus-containing glasses (Pd, Ni)–P (Dixmier and Duwez 1973), Ni–P (Cargill 1970), Co–P (Chi and Cargill 1976a), Fe–P (Logan 1975a) and Pd–Si and Fe–B (Fukunaga *et al* 1978). Over the composition range from ~15–25% metalloid the peak position of the first peak r_1 increases by ~1% and levels off above 20% metalloid composition, while those of the second subpeaks, r_2 and r_2', remain nearly constant or even decrease, and consequently the ratios $r_2/r_1 \approx 1{\cdot}63$ and $r_2'/r_1 \approx 1{\cdot}90$ decrease. For these P-containing glasses, the first subpeak is more intense than the second at larger r, but the relative intensity in alloys is less than that in pure metals and decreases with increasing metalloid content. The lower ratios r_2/r_1 and r_2'/r_1 in the glassy alloys than in the amorphous metal films, together with the change in relative intensity of the second subpeaks, apparently indicate that the introduction of the metalloid does not simply expand the overall amorphous metal structure.

A quite different effect of metalloid on the structure $G(r)$ of boron-containing glasses has been observed by Waseda and Chen (1978a). In a series of B-containing glasses, Fe–B, Ni–B and Co–B alloys, the second subpeak increases in intensity with decreasing B content, and subsequently becomes more intense than the first subpeak for those containing B less than 20%. In fact, regarding the second peak profile, it resembles rather closely that of the original DRPHS model of Bennett and Finney. On the contrary, Fukunaga *et al* (1978) found $G(r)$ of the Fe–B glasses being in many features similar to that for typical metal–metalloid glasses, e.g. Fe–P, Pd–Si and Ni–P.

4.3.2. Metal–metal glasses. Atomic structure data have been reported for rare-earth–transition metals $Tb_{33}Fe_{67}$ (Rhyne *et al* 1974), $Gd_{36}Fe_{64}$ (Cargill 1974) and $La_{80}Au_{20}$ (Logan 1975b). Both Rhyne *et al* and Cargill observed that the nearest-neighbour maxima could be associated with well-defined RE–RE, RE–TM and TM–TM nearest-neighbour spacings. However, their model calculations of the binary DRPHS structures with these nearest-neighbour spacings were seen to not agree well with experimental data at large distances in $G(r)$. O'Leary (1975) obtained the pair correlation functions from the x-ray data of Cargill and neutron diffraction data of Rhyne *et al* and observed that the correlation numbers for the amorphous RE–TM system are very high and quite similar to those of Laves phase. Logan (1975b) observed similar features in $La_{80}Au_{20}$ in which the first maximum can be associated with a contribution from La–La pairs at 3·75 Å and La–Au pairs at 3·33 Å. These values correspond closely

to that in crystalline La_2Au and the distances expected from the sum of Goldschmidt radii. The contribution from Au–Au was, however, not resolved.

Three partial pair distribution functions have been obtained using x-ray anomalous scattering techniques for Zr–Cu glasses (Waseda *et al* 1976, Mizoguchi *et al* 1978, Sadoc and Lienard 1978) and $Zr_{70}(TM)_{30}$ glasses (Waseda and Chen 1978b), where TM = Fe, Co, Ni and Pd. The basic forms of $G_{ij}(r)$ are similar for all the alloys studied. The pair distribution functions of $Zr_{70}(TM)_{30}$ glasses are exemplified for $Zr_{70}Ni_{30}$ alloy in figure 7. General features of the data are: (i) the interatomic distances of Zr–Zr and Zr–TM pairs are less than the values expected from the Goldschmidt radii, apparently resulting from a nearly empty d shell in Zr atoms through charge transfer. Further evidence of this charge transfer process is provided by the structural studies on Zr–Cu and Nb–Ni alloys (Chen and Waseda 1979) where the interatomic distances of Zr–Zr and Nb–Nb pairs decrease with increasing Cu and Ni contents. (ii) The distribution functions of Zr–TM pairs exhibit a relatively sharp first and second maximum compared with those of like-atom pairs, reflecting preferred interactions of unlike-atom pairs. (iii) Zr–Zr pair distribution functions resemble the $G(r)$ of Fe glasses containing boron. (iv) TM–TM pairs exhibit a hard contact at corresponding Goldschmidt radii, in strong contrast to the metal–metalloid system in which the minor constituent atoms (metalloids) are prohibited from direct contact. The distinct difference in the structure between the metal–metal and the metal–metalloid systems in the glassy state may be partly due to the weaker interatomic interactions in the metal–metal system and partly to the relatively hard-core d-shell characteristic of transition metals, which favour random mixing in the metal–metal system, while the much softer s–p type bonding of metalloid atoms facilitates preferred bonding among metal and metalloids (Chen and Waseda 1979).

4.3.3. Realistic structures of binary alloy glasses. The RDF of typical metal–metalloid glassy alloys are very similar to those observed for amorphous metal films. Polk

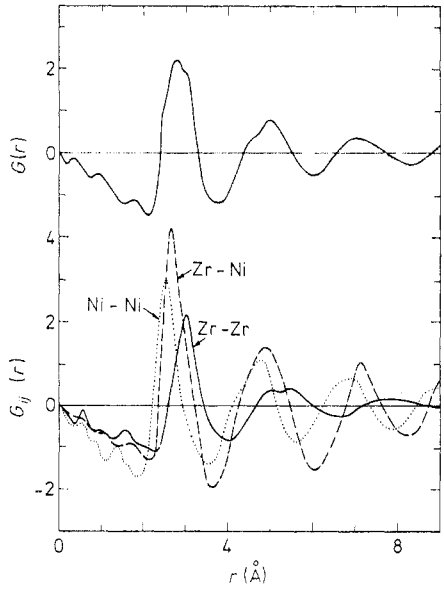

Figure 7. Pair distribution functions of $Zr_{70}Ni_{30}$ glassy alloy.

(1972) thus proposed the simple DRPHS model for these alloys with modification by locating alloying metalloid atoms in the large holes inherent in somewhat expanded dense random packing of hard-sphere structures occupied by larger metal atoms. This ensures that the metalloid atoms are surrounded by metal atoms and are never in close contact. The simplicity of this model is attractive: however, the large holes inherent in the DRPHS structures are too small to accommodate metalloid atoms without drastic structural modification, as evidenced by the observed changes in magnitude and relative positions of radial distribution peaks upon introducing metalloid atoms in the systems. Furthermore, EXAFS measurements of glassy $Pd_{78}Ge_{22}$ (Hayes *et al* 1978) revealed that the RMS half-width of the Ge–Pd pair distribution is less than 0·1 Å, which contrasts with the large variations $\sim 0{\cdot}5$ Å expected in the Polk model.

Using the computer algorithm of Ichikawa (1975), Fukunaga *et al* (1977) simulated partial distribution functions for a binary $Pd_{80}Si_{20}$ with $\delta_{Pd} = 2{\cdot}81$ Å and $\delta_{Si} = 2{\cdot}03$ Å. In one case Si–Si atoms are allowed to be in close contact, and in the other, hard contact is not permitted for Si atoms. In both cases, the partial pair distribution functions $G_{Pd-Pd}(r)$ and $G_{Pd-Si}(r)$ show qualitatively similar features established for the single-size RDPHS model. Prohibiting metalloid–metalloid hard contact seems to sharpen the inner shell of the second peak of the metal–metal pairs. Similar behaviour has been seen in the computer simulation of Fe–P with a similar size ratio by Boudreaux and Gregor (1976), using the $r_{TM}/r_M \approx 1{\cdot}39$ computer algorithm of the Bennett model. The sharpening of the first subpeak can be understood using simple geometrical considerations as advanced by Weeks (1977) and is believed to arise from the increase in the number of collinear metal–metalloid–metal packing sequences whose Fe–Fe distances are about 15% less than the distances in collinear Fe pairs.

Another significant feature of the computer simulation of Boudreaux and Gregor (1976) is the small coordination numbers of P surrounded by P atoms $n_{P-P} \approx 0{\cdot}69$ in the model, where P atoms are allowed to be in hard contact. The value $n_{P-P} \approx 0{\cdot}69$ in the model is less than one-half of the expected coordination number $cn \approx 1{\cdot}70$ in completely random packing structures, where $n \approx 8{\cdot}5$ is the total coordination number, and $c = 0{\cdot}20$ is the concentration of the smaller atoms. This implies that the small atoms (metalloid atoms) tend to avoid close contact in the binary DRPHS models simply due to geometrical constraints in packing atoms together of different sizes. One may therefore conceive that the binary DRPHS structures model approximate the structures of metal–metalloid glasses as well as other metal–metal systems, with the atomic interactions in the real systems playing an additional role in determining the overall packing structures.

Apparently, strong atomic interactions among unlike atoms influence atomic distribution in glassy alloys such that the short-range atomic configuration is often seen to be similar to the corresponding intermetallic phase(s). The absence of splitting in Pt–P glasses may be due to the particular affinities among Pt and P atoms leading to a miscibility gap in the liquid. Emptying the outer electrons through charge transfer is believed to cause the distinct reduction in RE–RE, Zr–Zr pair distances as compared with Goldschmidt radii of the constituents. On the other hand, the geometrical constraint imposed in metal–metalloid alloys, such that metalloid atoms are prohibited from being nearest neighbours, causes the distinct increase in metal–metal pair distances in alloy glasses. The decrease in ratios r_2/r_1 and r_2'/r_1 in $G(r)$ is a natural consequence of binary dense packing of different hard-sphere radii.

4.4. Structural and compositional homogeneity

Chou and Turnbull (1975) observed an increase in the intensity of small-angle scattering (SAS) suggestive of phase separation upon annealing above the glass transition of a liquid-quenched Pd–Au–Si glass. The as-quenched sample is quite homogeneous on several atomic diameters but large-scale compositional inhomogeneities of ~ 200 Å are seen in the annealed ribbons. Glassy ribbons annealed at moderate temperatures below T_g exhibit structural inhomogeneities of smaller scale $\leqslant 100$ Å as evidenced by an increase in positron lifetime (Chen and Chuang 1977). Positron annihilation measurements (Chen and Chuang 1975a, Doyama *et al* 1975), however, reveal negligible vacancy-type defects existed in the glassy metals.

Development of structural and compositional anisotropy is often found in thin films prepared by atomic condensation methods such as electrodeposition, sputtering and evaporation as a consequence of growth kinetics. Staudinger and Nakahara (1977) observed with transmission electron microscopy in thin electrodeposited amorphous Ni–P films a network structure of pipe-like voids of ~ 10–20 Å diameter, while such a void structure is found to be absent in a liquid-quenched Ni–P glass. Chi and Cargill (1976b), based on the SAS data, suggested that the as-deposited films contain macroscopic compositional inhomogeneities with characteristic dimensions ~ 200 Å in the film plane and $\geqslant 2000$ Å normal to the film plane. The magnitude of these inhomogeneities was reduced by annealing. The nature of the inhomogeneities has not been determined.

The presence of a uniaxial magnetic anisotropy is a common feature of the amorphous RE–TM thin films. The origin of this magnetic anisotropy has not yet been established. It has been proposed that an excess of Co–Co nearest-neighbour pairs 'in plane' compared to 'out of plane' is responsible for the perpendicular magnetic anisotropy in Gd–Co alloys (Gambino *et al* 1974). The direct evidence for such compositional anisotropies is provided by x-ray scattering data taken for an amorphous sputtered $Gd_{18}Co_{82}$ with the scattering vector either perpendicular to or parallel to the film surface (Cargill 1975b, Wagner 1976). Leamy and Dirks (1977) discovered that both vapour-deposited and sputtered RE–TM films possess a columnar structure apparently formed during deposition by self-shadowing of the incident atoms by atoms in the growing film. It consists of small (50–250 Å diameter) rod-shaped regions of high density surrounded by a network of less dense material (10–25 Å thickness). This structure in fact occurs most predominantly in amorphous films, such as Ge and Si, whose formation requires limited atomic mobility.

Subtle changes in interference function $I(q)$ of glassy ribbons annealed at moderate temperatures $< T_g$ have been reported for $Pd_{80}Si_{20}$ (Masumoto *et al* 1976a), $Fe_{80}P_{13}C_7$ (Waseda and Masumoto 1975) and $Fe_{40}Ni_{40}P_{14}B_6$ (Egami and Ichikawa 1978). The effect of structural relaxation is seen to increase the amplitude of oscillation in $I(q)$. However, a distinct feature is found in the second maxima in which the peak height increases by $\sim 2\%$ but the height of the shoulder decreases by $\sim 2\%$. At the beginning of crystallisation, in contrast, the second peak becomes lower and the shoulder becomes sharper. The atomic processes of structural relaxation in a glass, being parallel to the structural ordering during cooling of a melt, clearly differ from the crystallisation processes. Aging of glassy Fe–P–C alloys is seen to enhance the phase contrast in TEM (Fujita *et al* 1977) and the intensity of SAS (Osamura *et al* 1979) suggesting the development of structural order of ~ 20 Å in size.

Plastic deformation is shown to produce more disordered (or liquid-like) atomic

structure. Evidence is provided by a decrease in the SAS intensity (Luborsky *et al* 1976) and a broadening in the first and second peaks in $I(q)$ (Masumoto *et al* 1976a, Waseda *et al* 1979) in cold-rolled glass ribbons. Doi *et al* (1977) found a remarkable enhancement in the intensity of x-ray SAS from $Pd_{80}Si_{20}$ glassy ribbons irradiated with fast neutrons (>1 MeV) at a flux of 5×10^{12} neutron cm^{-2} and concluded, from the intensity width of SAS, the macroscopic inhomogeneities to be of ~50 Å size. Whether these inhomogeneities arose from a density deficit of void type or from compositional inhomogeneities, a sort of phase separation, has not been determined. In any case, positron annihilation data have shown that negligible atomic scale defects are induced either by cold rolling of a Pd–Cu–Si glass (Chen and Chuang 1975b) or by 1 MeV electron irradiation of Pd–Ni–Si glass (Chen 1976d).

X-ray diffraction, SAS and positron annihilation measurements yield some information about the changes in structural inhomogeneity. Various spectroscopic techniques, such as NMR (Raj *et al* 1976, Hines *et al* 1978), Mössbauer (e.g. Tsuei *et al* 1968, Kemeny *et al* 1979) and EXAFS studies (e.g. Hayes *et al* 1978, Wong *et al* 1978) have been undertaken to characterise the structure of glassy metals. These studies have confirmed the many structural features obtained through diffraction measurements, and have also shed additional insight on the local environment.

5. Atomic transport and transformation kinetics

The kinetics of crystallisation processes, through nucleation and crystallisation, from a glassy solid and from a liquid would be identical as the glass and liquid belong structurally and thermodynamically to the same phase. The kinetic criteria developed in §3.2 for glass formation would be applicable to the stability, i.e. the resistance to crystallisation of glass, except in the latter process the rates of crystallisation are much slower and the transformation to equilibrium phase(s) occurs through a sequence of progressively more stable phases. Analogous to the kinetic criteria of glass formation in which a critical cooling rate is required to transform a liquid into a glassy solid with the arbitrary viscosity $\eta\sim10^{13}$ P, the relative (or dynamic) stability of a glass may be defined from the critical heating rate required to transform the glassy solid to a liquid without crystallisation through a region at which η equals 10^{12} P, or observed T_g. The relative stability of a glass thus is denoted by the temperature span $\Delta T_x(=T_x-T_g)$ between the onset temperature of crystallisation (T_x) and T_g in a calorimetric scan at certain rates ~20 K min^{-1} (Chen 1976e).

The ease of glass formation and the stability of alloy glasses thus in general, but not always, occur in parallel. Empirically the ternary alloy glasses are more stable than the corresponding binary alloy glasses, and glasses with eutectic composition are observed to be most stable. Many binary alloy glasses crystallise far below the effective glass transition temperature T_g, e.g. T_x is 600 and 710 K for $Ni_{80}P_{20}$ and $Fe_{80}B_{20}$, respectively, while the corresponding T_g is ~620 K and ~780 K, respectively (H S Chen unpublished). Electrodeposited amorphous films Ni–P with P less than 16% (Clements and Cantor 1976) and Ni_3P (Bagley and Turnbull 1970) crystallise at ~450 K which is 150–200 K below the expected T_g. Note that most amorphous metals produced by vapour deposition transform to the crystalline phase at ~20–50 K above the deposition temperature. Estimating T_g of unstable glasses from the crystallisation temperature T_x must thus be employed carefully.

The glass formation tendency and the stability of the resultant glass, as well as the

structural relaxation processes of metallic glass, are critically governed by the atomic transport properties of the liquid (or glass) in the region of the glass transition. Many physical properties, particularly mechanical ductility and magnetic anisotropy, alter drastically upon structural relaxation and crystallisation. Understanding of viscosity and diffusive processes in metallic glasses is thus of technological and scientific importance. In this section, the effects of temperature and composition on viscosities η, glass transition temperatures T_g and diffusivities D are described first, followed by the discussion of stress relief, magnetic aging and crystallisation kinetics. Emphasis is laid on the elucidation of the influence of different structural states, e.g. the relaxed and unrelaxed states, on the temperature dependence and magnitude of diffusion constant, the recovery rate of residual stress, magnetic anisotropy and crystallisation processes.

5.1. Viscosity

Over a broad temperature range in the region of the glass transition, the viscosity η of metallic glasses as well as many non-metallic glasses increases rapidly in the range 10^6–10^{14} P and is described by the Fulcher's expression (equation (2.2)). Most explanations for this general form of the temperature dependence of η have in common the concept that the flow process requires a cooperative motion involving a group of atoms. Adam and Gibbs (1965) derived an equation from a model for polymer glasses by considering cooperative atomic rearrangements, thermally activated over an energy barrier governed by configurational entropy S such that

$$\eta = \eta_0 \exp(\Delta\mu^*/TS) \tag{5.1}$$

where $\Delta\mu^*$ is the activation energy for minimum atomic rearrangement.

Turnbull and Cohen (1958, 1961), based on the idea that diffusive jumps occur only when some critical local concentration of free volume V^* is achieved, derived the temperature dependence of diffusivity

$$D = D_0 \exp(-\gamma V^*/V_f) \tag{5.2}$$

where V_f is the free volume, γ is a constant (of the order of unity). Equations (5.1) and (5.2) reduce to the empirical Vogel–Fulcher's expression (equation (2.2)) with $B = \Delta\mu^*/\Delta C_p = \gamma V^*/\Delta\beta V_0$, as $S \approx \Delta C_p(T - T_0)/T$, $V_f/V_0 \approx \Delta\beta(T - T_0)$ and $D \propto \eta^{-1}$. Here ΔC_p and $\Delta\beta$ are, respectively, the incremental specific heat and the volumetric thermal expansion coefficient at the glass transition, and V_0 is the atomic volume.

Viscosities η near T_g have been obtained from creep measurements for a limited number of metallic glasses, e.g. Au–Ge–Si (Chen and Turnbull 1967), Pd–Si (Chen and Goldstein 1972) and Pd–Ni–P (H S Chen 1979 unpublished). The temperature dependence of η of many stable metallic glasses has also been extracted from the rates of thermal transformations (Chen 1978b,c). The flow behaviour shows a strong compositional dependence as exemplified by (Pd,Ni)–P glasses: the addition of metalloid P raises T_g, T_0 and the apparent activation energy at T_g (Q_g) but lowers S_g, B, and consequently $\Delta\mu^*$ ($= B\Delta C_p$), while alloying between Pd and Ni shows the opposite behaviour (Chen 1978b,c). The increasing T_g and the diminishing S_g with increasing P content may be explained in view of short-range ordering due to strong interactions between metal and metalloid atoms and therefore the reduction in the configurational entropy of the alloy glasses, but the decrease in $\Delta\mu^*$, the mini-

mum energy barrier for diffusive process, is striking and remains unexplained. $Q_g = 4$–8 eV is much higher as compared to that of the lattice diffusion $Q_l = 2$–3 eV. The residual configurational entropy S_g, consisting of structural and compositional contributions, ranges from 0·55 cal mol^{-1} K^{-1} for $(Pd_{0.5}Ni_{0.5})_{73}P_{27}$ to 1·88 cal mol^{-1} K^{-1} for $(Pt_{0.6}Ni_{0.4})_{75}P_{25}$ which is comparable to $S_g \approx 1$ cal mol^{-1} K^{-1} reported for non-metallic glasses (Bestul and Chang 1964), while $V_f/V_0 = 5 \times 10^{-3}$ and $\gamma V^*/V_0 = 0{\cdot}20$ for glassy metals are much less than those observed for other type of glasses, e.g. $V_f/V_0 = 20 \times 10^{-3}$ and $\gamma V^*/V_0 = 0{\cdot}62$ for oxides, but would appear reasonable if the diffusive displacement in liquid metals equals the ionic diameter.

Metallic glasses exhibit viscoelastic behaviour. The glass deforms instantaneously upon applying tensile stress, followed by time-dependent reversible deformation and steady-state viscous flow. The time required for attaining a steady flow is of the order of the structural relaxation time. The recoverable anelastic compliance, J_a, at a stress level of $\sim 10^7$ dyn cm^{-2} in Pd–Si (Chen and Goldstein 1972) and $Pd_{48}Ni_{32}P_{20}$ (H S Chen 1979 unpublished) is small at low temperature (of the order of the elastic compliance) but increases rapidly in a narrow temperature range when viscosities attain 10^{12} P. J_a becomes as high as several hundreds times the elastic compliance. In this temperature range both isothermal J_a and η of the glass remain constant at small stress $\sigma \leqslant 10^7$ dyn cm^{-2} but decrease at higher stress, i.e. the glass becomes non-Newtonian. The total anelastic strain, $\epsilon_a = J_a\sigma$, approaches a constant value $\sim 10^{-2}$. Masumoto and Maddin (1971) reported for a $Pd_{80}Si_{20}$ glass a relatively small $\epsilon_a = 10^{-3}$ at 100°C (far below $T_g = 370$°C) but a large value of $\epsilon_a = 10^{-2}$ at higher temperature ~ 200°C. The high anelastic strain implies the occurrence of a considerable directional structural ordering.

Limited creep measurements below T_g have been reported for $Ni_{76}P_{24}$, $Co_{75}P_{25}$ (Logan and Ashby 1974), $Pd_{80}Si_{20}$ (Maddin and Masumoto 1972), $Cu_{60}Zr_{40}$ and $Fe_{80}P_{13}C_7$ (Murata *et al* 1976a, Kimura *et al* 1977). The significant features of these observations are relatively low activation energy of creep $Q_{cr} \approx 0{\cdot}5$ eV and the increase in η and Q_{cr} upon aging at higher temperature. Taub and Spaepen (1979) reported a higher $Q_{cr} \approx 2$ eV for structurally stabilised glassy $Pd_{82}Si_{18}$. Qualitatively these phenomena may be explained by adopting the entropy model of viscous flow (equation (5.1)) so that the activation energy is expressed as (Chen 1976e)

$$\begin{aligned} Q &= -k \, \mathrm{d} \ln \eta / \mathrm{d}(1/T) \\ &= (k\Delta\mu^*/S)(1 + \mathrm{d} \ln S / \mathrm{d} \ln T) \end{aligned} \tag{5.3}$$

where k is Boltzmann's constant. Equation (5.3) consists of two terms: $Q_{th} \sim k\Delta\mu^*/S$ and $Q_{conf} = (k\Delta\mu^*/S)(\mathrm{d} \ln S/\mathrm{d} \ln T)$. The former arises purely from the temperature dependence of η in an isoconfigurational or unrelaxed structure, and the latter results from the configurational change with temperature. When each atom exercises only a small fraction of an atomic diffusive jump, such as in the case of creep measurement performed on samples at temperatures below the pre-annealed temperature, the structure of glass may be considered unaltered. Q_{cr} thus equals the activation energy for the isoconfigurational viscous flow $Q_{th} = k\Delta\mu^*/S_g$ which is of the order of $\sim 1{\cdot}0$ eV for the as-quenched sample. Pre-annealing lowers S_g and thus raises Q_{cr} and η (equations (5.1) and (5.2)). If creep measurement is performed on the as-quenched sample at successively higher temperatures, structural relaxation occurs during the measurement; thus $\mathrm{d} \ln S/\mathrm{d} \ln T < 0$. The observed activation energy for the viscous creep Q_{cr} would be lower than Q_{th}. Above T_g, the glass attains the equilibrium state,

such that $\mathrm{d}\ln S/\mathrm{d}\ln T = T/(T-T_0) \approx 5$. The apparent activation energy for the relaxed glass $Q_\eta \approx 4$ eV is many times greater than that for creep flow.

5.2. Glass transition temperature

The glass transition temperature T_g of metallic glasses is commonly determined calorimetrically at moderate scanning rates of ~ 20 K min^{-1}. T_g is often taken as the point of inflection in the specific heat C_p against T curve. The composition dependence of T_g shown in figure 8 has been reported for binary alloy glasses $A_{100-y}B_y$, e.g. $Pd_{100-y}Si_y$ (Chen and Turnbull 1969, Lewis and Davies 1976), $(Pd_{0.5}Ni_{0.5})_{100-y}P_y$, $(Pt_{0.8}Ni_{0.2})_{100-y}P_y$ (Chen 1976b), $Zr_{100-y}Cu_y$ (Chen and Krause 1977, Vitek *et al* 1975, Freed and Vander Sande 1978), $(Fe_{0.6}Co_{0.4})_{75}PBAl$ (Chen 1976c) and $Zr_{100-y}Be_y$ (Hasegawa and Tanner 1977). T_g in general increases with increasing y, i.e. towards the stable intermetallic compounds. The increase in T_g of glasses towards the stable intermetallic compound and the viscosity maxima observed in the melt of compound-forming compositions have been attributed to structural and compositional ordering which decreases the configurational states of the systems (Chen 1976b,c).

A slight dip in the T_g against y curves, indicative of suppression in viscosity, in the region of the eutectic may be noted for these alloy glasses. Similar anomalously low viscosities near the region of eutectic composition have been observed in liquid alloys of Pb–Sn, Sb–Cd (Fisher and Phillips 1954), Fe–C (Vostryakov *et al* 1963, Barfield and Kitchener 1955), Fe–P (Dragomir 1973, Romanov and Kochegarov 1964), Pd–Si, Ag–Si and Pd–Cr (Dubinin *et al* 1967) and Au–Si (Polk and Turnbull 1972). In addition to the viscosity minima near the eutectic compositions, Fisher and Phillips found a relative viscosity maximum in the Sb–Cd system for the intermetallic compound SbCd, while Dubinin *et al* reported two maxima in the isotherms of the viscosity of Pd–Si melts at intermetallic compositions of Pd_2Si and PdSi. The causes of the viscosity minimum and the dip in T_g near the eutectic are not clear. It is

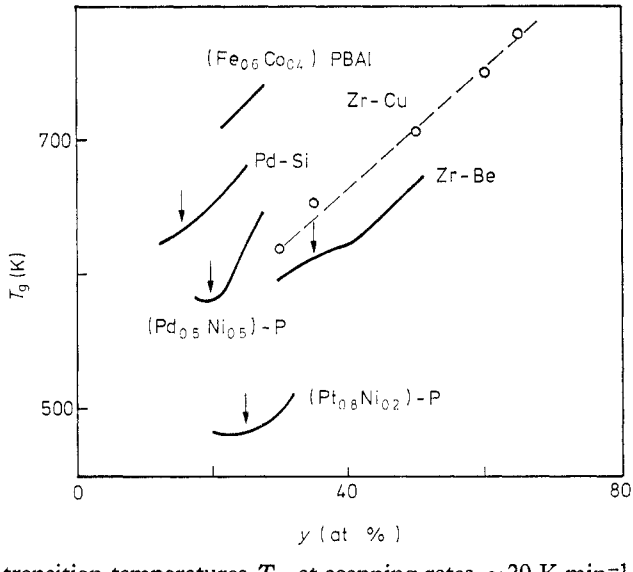

Figure 8. Glass transition temperatures T_g, at scanning rates ~ 20 K min^{-1}, for binary alloys $A_{100-y}B_y$. The arrows indicate the eutectic compositions.

inconceivable to interpret the phenomena from the point of view of structural stabilisation of the eutectic liquid, as any grouping together of atoms in ordered array would result in an increase in viscosity. It is more likely that the structural disordering in liquid melts and probable clustering in glasses in the region of the eutectic composition cause the anomalies observed.

The effect of alloying metallic elements on T_g has been investigated for series of metallic glasses (Chen and Jackson 1978). T_g of $Fe_{75}P_{16}B_6Al_3$ and $Ni_{75}P_{16}B_6Al_3$ alloys initially decreases then increases as Cr or Mo replaces Fe or Ni. Similar behaviour has been observed for Pd–Si glasses when Cu, Fe, Ni or Co replaces Pd. Significantly, T_g against x curves of $(Pd_{1-x}Ni_x)$–P and $(Pt_{1-x}Ni_x)$–P exhibit an absolute minimum. The initial lowering of T_g upon alloying is a very common phenomenon. Similar decrease in the viscosity of dilute liquid alloys has been found in glass-forming systems Fe–C, Fe–P, Au–Si and Fe–(Mn, Cr, V) (Romanov and Kochegarov 1964). It is striking to note that many metal–metalloid liquids, Fe–Si, Co–Si, Ni–Si (Gel'd and Gertman 1961a,b) and Pd–Si (Ukhov *et al* 1968) as well as the pseudo-binary glasses $(Pd,Ni)_{80}P_{20}$ (Chen *et al* 1973/74) exhibit a negative deviation in volume from Vegard's law. The lowering of T_g in alloying glasses and the reduction in η of many metal–metalloid alloying liquids are contrary to the behaviour expected based on the free volume model, which would predict an increase in η and a consequent increase in T_g when the packing density increases. This behaviour otherwise may be explained on the basis of the incremental entropy associated with the addition of alloy elements of different atomic radii to the liquid phase (Chen 1974b). The increase in T_g of glassy alloys upon the addition of $\sim 20\%$ metalloid is apparently due to the development of short-range ordering during cooling from the melt.

T_g of alloy glasses appears to increase with increasing cohesive energy but exhibits considerable scatter (Davies 1976, Chen and Jackson 1978). Au- and Pt-based glasses show relatively low T_g. Thus it appears that the values of T_g also depend upon other factors such as electronic structure and atomic ordering. The reduced glass transition temperature T_{rg} of the glass-forming alloys is $\sim 0{\cdot}5$, in fair agreement with the prediction of kinetic criteria discussed in §3.

5.3. Atomic diffusivities

Diffusion measurement in metallic glasses was first reported by Gupta *et al* (1975). They reported anomalously high values of Ag diffusivities in the as-quenched glass $Pd_{81}Si_{19}$ as compared with the expected values from the viscosity data in an equilibrium state. The activation energy for diffusion was found to be relatively low $\sim 1{\cdot}4$ eV. Birac and Lesueur (1976) observed much faster diffusion of Li $\sim 10^{-15}$ cm^2 s^{-1} as compared with Ag diffusivities $\sim 10^{-17}$ cm^2 s^{-1} in the Pd–Si glass. Recently Chen *et al* (1978) demonstrated that the magnitudes of diffusivities in a $Pd_{77}Cu_6Si_{17}$ glass are critically related to the state of structural relaxation and approach reasonable values in the equilibrium structure. Au diffusivities (D) in the Pd–Cu–Si glass in various states of structure are illustrated in figure 9. Above the glass transition temperature $T_g = 633$ K, the Au diffusivities D of the glass agree fairly well with diffusivities (D_η) evaluated from viscosity data using the Stokes–Einstein relationship. Based on the analysis of the time dependence of the phase-separation process in a similar glassy metal $Pd_{74}Au_8Si_{18}$, Chou and Turnbull (1975) obtained $\sim 3 \times 10^{-17}$ cm^2 s^{-1} for the interdiffusivity in the glass transition range which is in good agreement with D_η as well as the measured $D \approx 10^{-17}$ cm^2 s^{-1} in the Pd–Cu–Si glass.

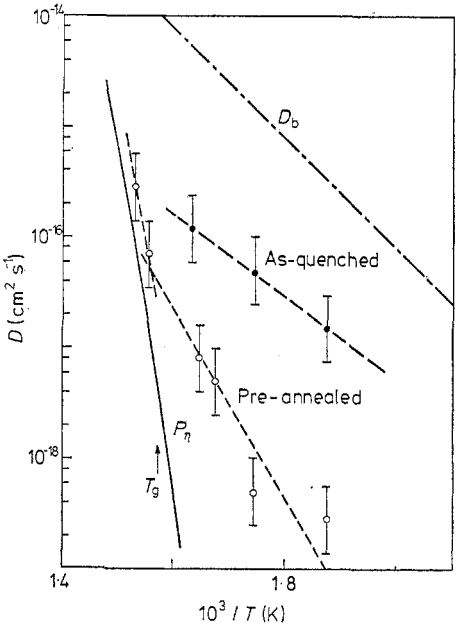

Figure 9. Au diffusivities D in a $Pd_{77.5}Cu_6Si_{16.5}$ glass in various states. D_b is the Au grain boundary diffusivity in polycrystalline Pd films.

Below T_g, however, D up to several orders of magnitude larger than D_η were measured. Slower quenching or subsequent annealing reduces the diffusivity toward D_η. For example, diffusivities of the as-quenched samples are high $\approx 5 \times 10^{-17}$ cm^2 s^{-1} with a relatively low activation energy $Q = 0{\cdot}75$ eV. Pre-annealing at 623 K, 10 K below $T_g = 633$ K, for five minutes leads to lower D by two orders of magnitude and a high $Q = 1{\cdot}67$ eV. The pre-exponential factor $D_0 \approx 10^{-5}$ cm^2 s^{-1} of the metallic glass is much smaller than typical values for crystalline metals (≈ 1 cm^2 s^{-1}) and is more or less characteristic of liquid metal systems. The change in Q and D may be ideally interpreted in terms of an entropy model of viscous flow as discussed in §5.1. For isoconfigurational flow, Q is inversely proportional to the configurational entropy S. The pre-anneal lowers S and therefore increases Q. It is noteworthy that the observed Q are in fair agreement with the evaluated $Q_{th} \sim 1$ eV.

The high diffusivities ($D \gg D_\eta$) below T_g are of significance, because in practice D is observable only after at least one hundred atomic 'jumps', corresponding to composition profile broadening of ~ 20 Å, which is the minimum width broadening required for extracting reasonable diffusivity data. The implication is that the time constant τ_S for the structural relaxation is much larger by at least two order of magnitude than τ_D for the diffusive process. In another word, the free volume (or configurational entropy) which determines the atomic diffusivities in a glass does not disappear until at least one thousand diffusive atomic 'jumps'. A long-range diffusive process analogous to the annihilation of vacancies in crystalline materials at dislocations or at the surfaces of the sample could account for the slow rate of the disappearance of the free volume with respect to the rate of diffusive process in metallic glasses, and thus the time constant ratio $\alpha \equiv \tau_S/\tau_D$ should depend primarily on the details of the long-range atomic structure. Alternatively Spaepen and Turnbull (1978) proposed that the quenched-in structural heterogeneity, on a spatial scale of $\sim 10^2$–10^4 atom

spacings, may be characterised by some distribution of fictive temperatures over the volume of the specimen. If then, the slow rate of structural relaxation, τ_S^{-1}, is determined by those regions of specimens having lower fictive temperatures, then the high diffusivity is due to the areas with high fictive temperature. This proposition, however, is inconsistent with the observed behaviour that the time constant ratio α remains very high in the aged sample in which the quenched-in structural inhomogeneity would diminish through structural relaxation. Significantly, D is seen to scale as η^{-1} according to the Stokes–Einstein relationship in the relaxed state above T_g as well as in the unrelaxed state below T_g.

A viscosity model implies that atoms in a glass do not diffuse by large jumps of lattice distances. Recent molecular dynamics studies of simple liquids by Rahman (1942) and Mössbauer line broadening measurement of ion diffusion in a viscous liquid by Ruby *et al* (1975) tend to suggest that atoms in liquids diffuse by frequent small continuous motions. Whether atoms diffuse by the continuous diffusive process or by infrequent large jumps of lattice distances in a densely packed glass state, however, cannot be unambiguously determined. It is interesting to note that the diffusivity of Au in the Pd–Cu–Si glass is orders of magnitude lower than the grain boundary diffusion D_b, and in fact, D_η, the diffusivity of the stabilised glass, can be many orders of magnitude lower than the Au lattice diffusivity D_l reported by Poate *et al* (1975). This comparison suggests diffusive processes in glass being distinct from the lattice diffusive jumps in grain boundary or crystalline lattice, and provides further support to the conclusion made from the positron annihilation studies (Chen and Chuang 1975a) that the crystallite model may be excluded as a possible structure for metallic glasses.

The high diffusivities $D = 10^{-17}$ cm^2 s^{-1} and the large time constant ratio $\alpha (\equiv \tau_S/\tau_D \geqslant 10^2)$ in unrelaxed glasses are of the utmost importance as will be elaborated in the following subsection. They explain remarkably well many aging phenomena, such as reversible changes in magnetic anisotropy, unattenuated high rates of crystal growth, and the wide spread in activation energies for crystallisation.

5.4. Kinetics of structural relaxation

The structural relaxation near T_g in glass-forming systems has been investigated extensively on ionic glasses and on amorphous polymers. The rate of isothermal isobaric volume (or internal energy) changes can be written as (e.g. Kovacs 1963)

$$\mathrm{d}(V - V_e)/\mathrm{d}t = (V - V_e)/\tau_V \tag{5.4}$$

where t is the experimental time, V and V_e are the actual and equilibrium specific volumes of the glass, respectively, and τ_V is the volume retardation time. The form of equation (5.4) is applicable to the rate of change in various physical properties such as viscosity, magnetic anisotropy and Curie temperature. The temperature dependence of the relaxation time for various physical properties is similar. As the relaxation time is determined not only by the temperature of measurement but also by overall free volume or configurational entropy, the rate of stabilisation depends on the experimental procedure. For example, the rate of approach towards equilibrium by contraction after quenching the specimen from the higher temperature is always greater than that by expansion after reheating the speciment equilibrated at lower

temperature. The rate of structural relaxation is greater for those produced at higher rates of quenching and for glasses with lower T_g (e.g. Chen 1977b, Luborsky and Walter 1978).

Isothermal structural relaxation of metallic glasses near T_g has been investigated from the change in x-ray intensity function (Egami and Ichikawa 1978), from enthalpy recovery, and Curie temperature aging (Chen 1978e). The rate of equilibration obeys approximately a lg t law. It distinguishes itself from the exponential t dependence commonly observed in magnetic aging (Luborsky 1976, Berry and Pritchet 1976a) and anelastic relaxation kinetics (Maddin and Masumoto 1972, Chi *et al* 1978) in which the relaxation kinetics are described by the first-order rate reaction with a single relaxation time. Most analysis of the logarithmic t recovery is based on a variable activation energy, e.g. the linearly decreasing activation energy either with increasing number of lattice defects or with increasing disorder (Dienes 1953, Chen 1978e).

In cases of stress relief and magnetic aging experiments performed below T_g, the kinetics of annealing is best given by equation (5.4) with a single thermally activated process having a relatively low $Q \sim 1$ eV. The stress relief of as-quenched glasses exhibits two distinguishable processes, the initial short-time relaxation and the final long-time relaxation (Chi *et al* 1978, Williams and Egami 1976, Luborsky and Walter 1978). The former process is believed to be associated with an irreversible structural relaxation, but it is not determined whether the latter process is purely anelastic or viscoelastic. The rates of stress relief are reduced drastically but the apparent activation energies Q_{re} are little affected in the samples produced at slower rates of quenching. Q_{re} is $\sim 0{\cdot}5$ eV for the short relaxation process and is ~ 1 eV for the long relaxation one.

Luborsky (1976) performed the first studies of the detailed kinetics of field-induced magnetic ordering in metallic glass ferromagnets. The kinetics of the reorientation of magnetically induced anisotropy measured by the remanence to saturation ratio for well-stabilised glassy samples of $Fe_{40}Ni_{40}P_{14}B_6$ obey the simple first-order rate reaction kinetics. Berry and Pritchet (1976a,b) carried out a kinetic study of directional magnetic ordering in $Fe_{40}Ni_{40}P_{14}B_6$ and $Fe_{75}P_{15}C_{10}$ glass from the change in the ΔE effect produced by transverse magnetic annealing of an initially longitudinally annealed sample. The relaxation time was taken as the annealing time at which the ΔE effect attains a maximum value. Their data for $Fe_{40}Ni_{40}Pi_{14}B_6$ are in excellent agreement with Luborsky's data. Q is approximately 1·4 eV for the FeNi glass and ~ 1 eV for the Fe glass.

Another important feature of the magnetic anneal is that the induced magnetic anisotropy is reversible, suggesting directional ordering processes involving thermally activated local atom movements. Because of the lower activation energies involved, Berry and Pritchet suggested that magnetic ordering involves movement of the metalloid atoms P, B or C. We may recall, however, that the diffusion of Au (or Ag) in the unrelaxed (below T_g) Pd–Cu–Si glass involves a relatively low activation energy ~ 1 eV and the time constant for structural relaxation is much longer than that for diffusive processes. The high diffusivities would persist until several hundred atomic 'jumps'. Thus the reversible atomic ordering involving the low activation energy could also occur through ordinary diffusive process without invoking the interstitial type diffusion of the metalloids. The observed relaxation times at temperatures 200–300 K below T_g for the magnetic and stress relief range from 10^3–10^6 s, corresponding to diffusivities 10^{-19}–10^{-22} cm^2 s^{-1} which are of the same order of magnitude at the

corresponding temperatures extrapolated from the high-temperature diffusivities of Au in the unrelaxed states of Pd–Cu–Si glass.

5.5. Crystallisation processes

The rates of crystallisation have been investigated for a number of glasses. The kinetics of the transformation were analysed through the use of the generalised theory of phase transformation (Christian 1965, Turnbull 1956), $x=1-\exp(-k_n t^n)$ where x is the volume fraction transformed in time t, k_n is a kinetic constant, and the exponent n is determined by transformation mode. n ranges from 2·5 to 4 for Pd–Si glasses (Bagley and Vogel 1975, Chou and Turnbull 1975, Burton and Ray 1971), whereas values from 3 to 5 have been obtained in Fe-based glasses (Yeh and Maddin 1976, Scott and Ramachandrarao 1977, Shingu *et al* 1978). Funakoshi *et al* (1977) reported $n=1$ in a Pd–Ag–Si alloy. Transformations for which $3<n<4$ may imply a diffusion-controlled process with decreasing nucleation frequency with time, while for $n=1$ one-dimensional growth of crystal (plate form) from a fixed number of nuclei may be conceived. The description of the transformation mode simply based on the kinetic data, however, can be erroneous, and thus direct electron microscopy in conjunction with the kinetic measurement should be employed (Duhaj *et al* 1976, Yeh 1976, Shingu *et al* 1978). Under hydrostatic pressure, the glass–crystalline transformation in a $Pd_{75}Ag_5Si_{20}$ is shifted to higher temperature by 1·4 K kbar^{-1} (Emmes *et al* 1975). In addition to the retardation of crystallisation process, a modification of crystalline phases to simpler structure under a pressure of ≈ 100 kbar^{-1} have been reported for $Pd_{80}Si_{20}$ by Iwasaki and Masumoto (1978). One expects $dT_x/dP<0$ if $P\Delta V$ terms in the free energy are dominant and $dT_x/dP>0$ if diffusivities are the controlling factor. The results indicate that the latter applies.

The activation energy, Q_x, for crystallisation varies widely with composition and temperature of transformation. In stable glasses, such as $Pd_{77}Cu_6Si_{17}$ (Bagley and Vogel 1975), $Fe_{40}Ni_{40}P_{14}B_6$ (Luborsky 1977), $Zr_{40}Cu_{60}$ (Pratten and Scott 1978), $Ti_{50}Be_{40}Zr_{10}$ (Tanner and Ray 1977), $(Fe,Ni)_{75}P_{16}B_6Al_3$ (Coleman 1976) and $(Pd_{0·5}Ni_{0·5})_{82}P_{18}$ (Boswell 1977) in which crystallisation occurs above T_g, Q_x is high, >4 eV, and comparable to the Q_η for the viscous flow in an equilibrium glass. Q_x of stable glasses, $Pd_{77}Cu_6Si_{17}$ and $Pd_{48}Ni_{32}P_{20}$ (Chen 1978a), indeed equals Q_η and decreases with increasing temperature of transformation as $Q_\eta=kBT^2/(T-T_0)^2$. It suggests the viscosity as the rate controlling factor during crystallisation of the stable glasses.

For most metallic glasses which crystallise near or below T_g, Q_x ranges from 4 eV to 2 eV (Coleman 1976, Luborsky 1977, Masumoto *et al* 1976b, 1977, Masumoto and Maddin 1971). Q_x was seen to be lower for glass with less stability, i.e. lower value of $\Delta T_x=(T_x-T_g)$. Amorphous metals such as Bi, Fe, Co and Ni produced by atomic condensation which are thermally least stable exhibit a very low $Q_x\leqslant 1$ eV, the same magnitude observed for the activation energy for diffusion in an isoconfigurational glassy state.

A significant but often overlooked feature during the crystallisation of glasses at low temperature ($\ll T_g$) is that crystals once nucleated grow at high constant growth rates to several hundred ångströms in size (Masumoto and Maddin 1971, Masumoto and Kimura 1975a, Masumoto *et al* 1976a), and occasionally to large crystals of several microns in size (Bagley and Turnbull 1970, Duwez 1967, Mader 1966). Although the diffusionless transformation in the amorphous state was suggested

(Turnbull and Bagley 1975) to be responsible for the low Q_x and the high rate of crystallisation, the processes of crystallisation as well as structural relaxation, in metallic glasses (or amorphous metals) however may as well simply reflect the diffusive processes in the various glassy states. The diffusion constants estimated from the crystal growth rates (Shingu *et al* 1976a, Herold and Köster 1978) are $\sim 10^{-15}$ cm^2 s^{-1} which are higher than that for Au diffusivities $\sim 10^{-17}$ cm^2 s^{-1} in the Pd–Cu–Si glass. Considering the similar high growth rates observed in eutectic crystallisation, which involves interdiffusion of both metal and metalloid atoms, the high D found in crystal growth simply reflect the highly disordered frozen-in structure in these alloy glasses, Fe–C and Fe–B, rather than due to fast diffusion of metalloid atoms.

The correlation between the magnitude of Q_x and the stability ΔT_x can be interpreted in the light of the structural relaxation model (Chen 1976e). The occurrence of crystallisation in many metallic glasses far below T_g is simply the reflection of high nucleation frequency and diffusivity in the quenched state. The persistently high rates of crystal growth imply that the time constant is many orders of magnitude longer in structural relaxation than in diffusive processes as observed. Thus the growth of crystals ceases only after hundreds or thousands of atomic diffusive 'jumps' when the glassy matrix relaxes to the equilibrium state at which atomic diffusivities are negligibly small.

6. Mechanical properties

Mechanical properties constitute the most unique characteristics of glassy metals. Fracture in glassy metals proceeds by highly localised shear deformations which contrasts with the brittle fracture commonly observed in non-metallic glasses. Because of the lack of translational periodicity, the fracture strength σ_f of glassy metals approaches the theoretical strength ($\sigma_f \approx E/50$) as compared with $\sigma_f \approx E/10^5$ to $E/10^2$ observed for crystalline metals in which dislocations are created and propagate through the crystalline lattice. Here E is the Young's modulus. There has been considerable interest in understanding and characterising this behaviour. Extensive treatments on this subject can be found in articles by Masumoto and Maddin (1975), Gilman (1975b), Masumoto (1977), Berry (1978) and Davis (1978). In this section, density, thermal expansion, elastic constants and anelastic properties will be presented first with emphasis on the effect of modification on these properties associated with changes in structure and the state of magnetisation. It will be followed by a description of modes of deformation, strength, toughness and ductility. Various flow models, structural changes at deformation bands and causes of embrittlement will be discussed.

6.1. Density and thermal expansion

The density of metal–metalloid glasses varies linearly with alloy composition in Ni–P (Cargill 1970) and Pd–Cu–Si (Chen and Park 1973). Negative deviation from a linearity is found at the equiatomic composition in (Pd, Ni)–P (Chen *et al* 1973/74), and in Fe–B near the eutectic $\sim 20\%$ B (Ray *et al* 1977) and $\sim 16\%$ B (Fukamichi *et al* 1978). The density in the glassy alloys is only about 1–2% less than in the corresponding crystalline alloys. Cargill (1975a) noted that the packing fraction for many glassy metal–metalloid alloys is indeed high, being about $0{\cdot}67 \pm 0{\cdot}02$ if 12 coordinated

Goldschmidt radii for metals and tetragonal covalent radii for metalloids are employed in the evaluation of the occupied volume. The observed molar volume of inter-transition alloy glasses Zr–Cu as well as crystalline Zr_2Cu equals approximately within 2% the average of the atomic volume of the pure crystalline constituents Zr and Cu (Turnbull 1977).

Quenched glasses contract in volume by $\sim 0{\cdot}5\%$ with structural relaxation (Chen *et al* 1973/74, Chen 1978b, Liebermann *et al* 1977). The volumetric thermal expansivity, $\beta = (1/V)(dV/dT)$, of the glassy alloys Pd–Cu–Si, Pd–Ni–P and Pt–Ni–P in the unrelaxed state is $\sim 40 \times 10^{-6}$ K^{-1} which is approximately equal to the corresponding crystalline counterpart. β of the glasses as shown in figure 2 increases by a factor of ~ 2 at the glass transition. This is normally observed in other glasses as well. However, the opposite occurs in a few materials which exhibit open network structures, e.g. SiO_2 (Douglas and Isard 1951) and aqueous lithium acetate solutions (Williams and Angell 1973). The thermal contraction of alloys from T_m to T_g eventually reduces the volume difference, ΔV, between the glass and corresponding crystalline phase to a small fraction ($\frac{1}{3}$ to $\frac{1}{2}$) of the volume change $\Delta V_m/V_m \sim 40\%$ at T_m. The small volume change ~ 1–2% associated with glass (or liquid)–crystalline transformation in metals is in strong contrast to the large change of $\sim 10\%$ in non-metallic materials and in the structural models of DRPHS. The near equality in molar volume in the glassy and crystalline phases which the DRPHS model fails to predict necessitates the introduction of soft potentials into the DRPHS model. This characteristic of the metallic system may be attributed to the metallic bonding which is such that the electronic contribution to the total energy is dominant and structure-insensitive (Barrett and Massalski 1966).

An appreciable volume contraction near the Curie temperature associated with spontaneous volume magnetostriction has been reported in a number of metallic glass ferromagnets. The thermal expansion anomaly is large in Fe-based alloys and increases with decreasing metalloid content, while Co-based alloys exhibit no distinct anomaly. Some Fe–B alloy glasses show Invar type behaviour (Fukamichi *et al* 1977a,b). The thermal expansion coefficient is negative in $Fe_{91}B_9$ and becomes positive for the higher boron-containing alloy $Fe_{79}B_{21}$. The $Fe_{83}B_{17}$ alloy exhibits an excellent Invar characteristic in a very wide temperature range. Almost invariably for all glasses, the volume contracts by $\sim 1\%$ upon crystallisation. The magnitude of the spontaneous volume magnetostriction for the $Fe_{83}B_{17}$ glass estimated from the difference in thermal expansion curves below and above T_c is $\sim 10^{-2}$ at room temperature, which is of the same order of magnitude observed for crystalline Invar alloy (Sumiyama *et al* 1976). The non-linear composition dependence of density in Fe–B glassy alloys (Ray *et al* 1977) thus may result partly from the large spontaneous volume magnetostriction of the Fe-rich alloys.

6.2. Elastic constants

The Young's modulus E and shear stiffness μ are generally lower by 20–40% but the bulk modulus K by only $\sim 7\%$ in the quenched glassy alloys than in the crystalline state (Golding *et al* 1972). The relatively large decrease in shear stiffness in the glassy state has been attributed to the interatomic shear displacements inherent in a disordered structure (Orowan 1952, Weaire *et al* 1971, Simpson and Hodkinson 1972). Chen *et al* (1975b) noted the charge transfer among constituent atoms being partially responsible for the softening of the shear stiffness in alloy glasses. The shear stiffness

softening $\Delta\mu_S$, however, is reduced considerably upon structural relaxation, and the difference in μ between the completely relaxed glassy alloys and the crystalline counterparts is small, $< 10\%$. The large $\Delta\mu_S$ observed in quenched glass samples thus arises mainly from the frozen-in excess volume (Chen 1978b). The increase in E associated with the decrease in volume V, $-\mathrm{d}\ln E/\mathrm{d}\ln V$, during the structural relaxation is large, ~ 15, which is comparable to that accompanied by crystallisation, ~ 17, and thermal expansion, ~ 10. The temperature eoefficient of E, $-\mathrm{d}\ln E/\mathrm{d}T$, is about 4×10^{-4} K^{-1} for the glassy alloys, and increases by about a factor of two through the glass–liquid transition.

The uniaxial-stress dependence of the Young's modulus E is found to have an unusually large value $\mathrm{d}E/\mathrm{d}\sigma \approx -12$ in $Pd_{77\cdot5}Cu_6Si_{16\cdot5}$ alloys (Testardi *et al* 1973). Smaller values $\mathrm{d}E/\mathrm{d}\sigma \approx -5$ are observed in series of alloy glasses $(Fe, Ni)_{75}P_{16}B_6Al_3$ (Krause and Chen 1976). The anharmonicity is calculated to contribute to the high-temperature specific heat (linear in temperature) and the ultrasonic attenuation observed in the Pd–Cu–Si glass. Since the large anharmonicity is associated with shear modes, it makes no contribution to the thermal expansion as evidenced by the negligible difference in thermal expansion between glassy alloys and the crystalline phase.

The Young's modulus of metal–metalloid glasses, $(Pd_{1-x}Ni_x)_{80}P_{20}$ (Chen *et al* 1975b), $[Fe_{1-x}(Ni,Co)_x]_{75}P_{16}B_6Al_3$ (Chen 1976g) and $[Fe_{1-x}(Ni,Co)_x]_{80}B_{20}$ (Chou 1976) is found to exhibit a positive deviation with x from a linearity. The enhanced E in the alloyed glasses is correlated to the magnetic ordering by Chou. The influence of magnetic ordering, however, is found to be insignificant in a ferromagnetic metallic glass $Fe_{75}P_{15}C_{10}$ (Berry and Pritchet 1976b) and FeNi-based alloys (Hausch and Török 1978) as evidenced by the absence of a noticeable change of slope in the saturation Young's modulus E_S against T curve on passing through the Curie temperature. Fukamichi *et al* (1977a,b) showed that spontaneous volumetric magnetisation is negligible in Co-based glasses.

The Young's modulus E of metal–metalloid glasses (Chen and Krause 1977) is found to increase with increasing boron content but remains nearly constant with phosphorus content. E decreases in the order (Fe,Co), (Pd,Ni) and Pt glasses while the bulk modulus of the corresponding crystalline metals show just the opposite behaviour, decreasing in the order, Pt, (Pd,Ni), Co and Fe. Chen (1978d) indeed noted that the Poisson's ratio ν is highest for Pt–P ($\sim 0{\cdot}42$) and lowest for Fe–B ($\sim 0{\cdot}34$). Considering the composition dependence of E and the magnetic moment, magnetic ordering apparently is not a dominant factor in determining elastic constants in these metallic glasses. The short-range ordering which arises from the strong interactions among metal and metalloid atoms is suggested to be responsible for the increasing trend of E.

6.3. Anelasticity

Metallic glasses are not perfectly elastic. An appreciable creep strain $\sim 1\%$ which is recoverable with time on removal of load can be induced under uniaxial stress as mentioned in §5.1. This subsection deals with the anelastic behaviour of metallic glasses at low stress–strain levels to obtain insight into their structure and atomic movements. Many results obtained, however, will be shown to be of interest also to the material applications.

6.3.1. Thermally-activated relaxation. Metallic glasses are characterised by low acoustic loss ($Q^{-1}=10^{-5}$–10^{-4}) at room temperature. Exceptionally low attenuation of longitudinal sound waves has been observed in Pd–Ag–Si alloys (Dutoit and Chen 1973). The attenuation at 100 MHz is 0·06 dB μs^{-1}, which equals the lowest value reported for fused silica. Q^{-1} of many metallic glasses increases exponentially with temperature with apparent activation energy $A=0{\cdot}5$–1 eV (Chen *et al* 1971, Berry and Pritchet 1973, Soshiroda *et al* 1976). The onset of the exponential damping behaviour shifts to higher temperature and A increases upon progressive annealing or crystallisation. As pointed out by Berry (1978), although the parameter A has the dimension of an energy, it does not have a direct physical significance because of a broad distribution in relaxation time for atomic motion in the glassy state. It may be shown that if the distribution is defined by a single activation energy Q and a spectrum of pre-exponential factors, such that $G(\tau)\propto\tau_0^{\gamma}\exp(Q/RT)$, then $A=\gamma Q$, where γ is a distribution parameter. The Q value obtained from the frequency-shift method is $\sim$1·2 eV for the Pd–Si glasses and is higher, $\sim$2·5 eV, for the Fe-based alloys. The value of $\gamma=A/Q$ is found to range from $\frac{1}{4}$ to $\frac{1}{2}$ for the glassy state (Berry 1978).

6.3.2. Thermoelastic behaviour. Elastic relaxation may originate from the change in temperature induced during flexural vibration. Berry and Pritchet (1973) obtained from thermoelastic relaxation measurements in glassy alloys the thermal diffusivities $D_{th}\approx 0{\cdot}05$ cm^2 s^{-1} for $Pd_{82}Si_{18}$ and 0·012 for $Fe_{75}P_{15}C_{10}$ which are only one-half to one-third of those for the crystalline phase(s). This is consistent with the higher electrical and thus thermal resistivity in the glassy state. The results of Barmatz and Chen (1974) are very similar to Berry and Pritchet's data. The expansion coefficients of the glassy and crystalline samples are similar and equal to about 10^{-5} K^{-1} from the relaxation measurements. These values are in good agreement with the dilatometric data.

6.3.3. Magnetoelastic behaviour. Magnetoelastic phenomena, such as the ΔE effect, have long been known and studied in crystalline ferromagnetic materials. The ΔE effect arises from the additional magnetostrictive strain generated by stress-induced domain motion. In the last few years certain ferromagnetic metallic glasses have been discovered to exhibit striking ΔE behaviour (Berry and Pritchet 1975, 1976a, Arai *et al* 1976a, Arai and Tsuya 1978). The effects can be large and are readily manifested at room temperature with moderate magnetic field $\sim$5 Oe. The large ΔE effect can not only reduce the elastic stiffness of materials, but also can significantly alter or even reverse the sign of the temperature coefficient $(1/E)\,\mathrm{d}E/\mathrm{d}T$ (e.g. Berry 1978).

The magneto-mechanical coupling factor k_c and the resonant frequency f_R of glassy ribbons depend on the bias field. Arai *et al* (1976a) observed that in a glassy $Fe_{80}P_{13}C_7$ annealed for 100 min at 300°C in a magnetic field of 1200 Oe applied perpendicular to the length of the ribbon, the coupling factor k_c increases with increasing applied field H_b and attains a maximum value of 0·43 at $H_b\sim 5$ Oe and then decreases with further increase in H_b. The resonant frequency f_R shows just the opposite behaviour. A modulus minimum has also been observed around an applied field of 5–10 Oe in a $Fe_{75}P_{15}C_{10}$ and $Fe_{40}Ni_{40}P_{14}B_6$ glass (Berry and Pritchet 1975, 1976a). This maximum in k_c factor or minimum in modulus, which corresponds to a maximum value of ΔE effect, occurs near a magnetisation of 0·5 M_s.

The magnitude and field dependence of the ΔE effect can be varied considerably by prior magnetic annealing that reduces internal stress and induces a uniaxial

magnetic anisotropy in the sample. The maximum ΔE effect, $(E_s - E_m)/E_m$ of metallic glasses is exceptionally large, $\sim 0{\cdot}4$, for the $Fe_{40}Ni_{40}P_{14}B_6$ and even larger, $\sim 0{\cdot}8$, for $Fe_{75}P_{15}C_{10}$. The same value $\Delta E/E_m \sim 0{\cdot}8$ was also reported for the $Fe_{80}P_{13}C_7$ ribbon annealed at 350°C for 20 min by Arai *et al* (1976b). A much higher value of 1·9 was seen in $Fe_{78}Si_{10}B_{12}$ (Arai and Tsuya 1978). In the as-prepared ribbon, the ΔE effect is smaller (about 0·1) but is still the same as that in Ni and 10 times larger than the ΔE effect in pure crystalline iron (Bozorth 1951). The magnitude of the ΔE effect of the Fe glasses is unaltered up to a frequency of 9 kHz and shows a clear decline for the range 0·1–1·0 MHz. The ΔE effect disappears completely near 1 MHz. The decline in the ΔE effect is probably due to the macroeddy current relaxation and 0·1 MHz marks the relaxation frequency (Berry 1978).

The maximum coupling factor k_c obtained is 0·53 in the $Fe_{80}P_{13}C_7$ ribbon and attains 0·75 in $Fe_{78}Si_{10}B_{12}$ which is as large as that reported by Savage *et al* (1975) in high magnetostriction rare-earth–Fe_2 compounds. In these compounds the maximum k_c occurs at large applied field of a few hundred Oe, while in the Fe ribbons the required field is only about 5 Oe. The large magnetoelastic phenomena of metallic glass ferromagnets arise from the absence of strong restraints to the motion of domains, or low magnetic anisotropies, and not from an unusually large magnetostriction.

In parallel with the bias applied magnetic field, uniaxial stress modifies domain structure and thus influences the ΔE effect, e.g. the as-quenched glassy alloys $(Fe_{1-x}Ni_x)_{75}P_{16}B_6Al_3$ (Krause and Chen 1976). For those compositions rich in Fe, there is shown a ΔE effect superimposed on the anharmonic behaviour. For composition $x = 0$, the ΔE effect peaks at ~ 4 kg mm^{-2} and completely diminishes at ~ 45 kg mm^{-2}. From additional studies using an applied H field these stress levels were found to correspond, respectively, to the bias magnetic field of ~ 5 Oe for the maximum ΔE effect and to the saturation magnetic field of ~ 50 Oe. The ΔE effect is small ($< 0{\cdot}1$) as reported for Fe glasses in the as-quenched state. As Ni replaces Fe, the ΔE effect decreases in magnitude and the stress level required for saturation also decreases, apparently, as a result of decreasing magnetostriction and magnetic moment. No ΔE effect is observed for $x \geqslant 0{\cdot}6$ as well as for those composition rich in Co.

6.4. Deformation and fracture

6.4.1. Fracture morphology. Plastic flow in metallic glasses at temperatures well below the glass transition temperature T_g was seen for the first time by Chen and Wang (1970), Leamy *et al* (1972) and Masumoto and Maddin (1971) to occur in the form of highly localised shear deformation bands. Leamy *et al* (1972) revealed that metallic glasses, deformed in tension, initially undergo localised shear along the direction of maximum shear stress. The samples then fracture by decohesion within the locally deformed material. The fracture surfaces exhibit two morphologically distinct zones as shown in figure 10 (plate). One zone is smooth and relatively featureless and the other consists of a vein pattern of local necking protrusions which resembles that on fractured liquid adhesive. The large local plastic shear produces the smooth zone, while the local necking protrusions are formed during rupture. The opposing fracture surfaces are essentially mirror images of one another. The smooth layer extends to larger areas while the vein pattern becomes more distinct when the strain rates and test temperature of the sample are increased (Masumoto and Kimura 1975b). Davis and Kavesh (1975) observed an enhancement in the shear displacement prior to failure under hydrostatic pressure resulting from the suppression of crack nucleation.

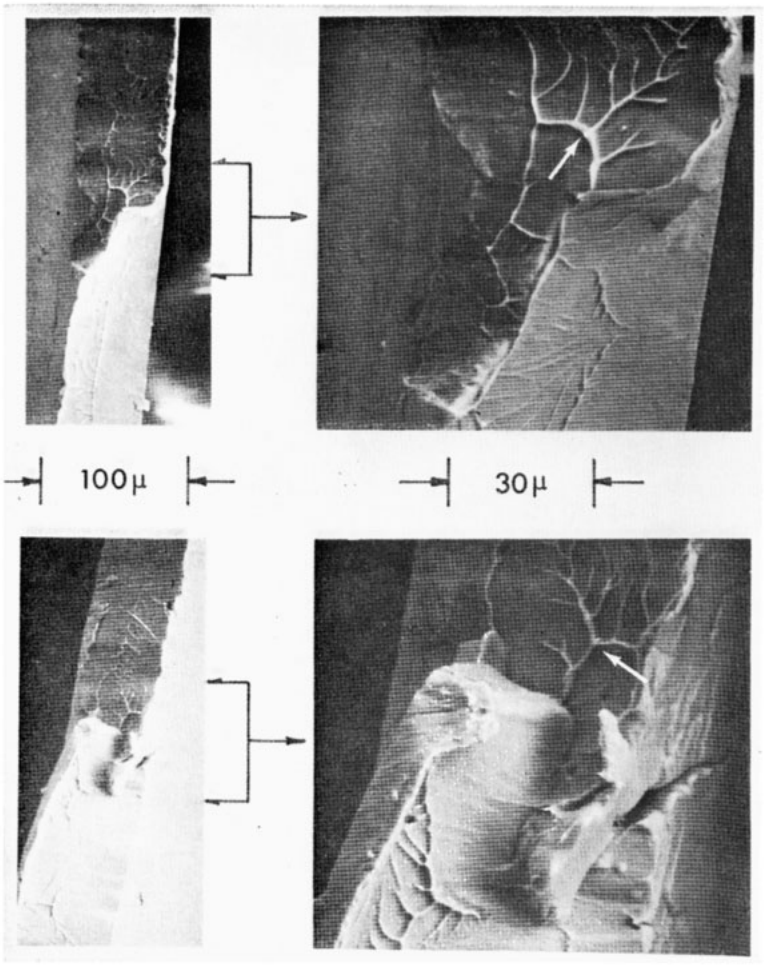

Figure 10. SEM micrograph of tensile fractured surfaces of a Pd–Cu–Si glassy ribbon.

Aging of the glassy samples is found to show the opposite behaviour. Under mechanical constraint such as in uniaxial compression, bending, rolling, drawing, and indentation, the catastrophic instability is avoided and multiple shear bands are observed. Some slip lines terminate inside the material.

As temperature increases toward the glass temperature, the mode of deformation changes from the inhomogeneous localised shear to homogeneous flow (or viscous creep) around a critical temperature depending on the strain rate. In the homogeneous region the tensile strength increases as the strain rate increases or temperature decreases, while in the inhomogeneous region its dependence is small or opposite (Maddin and Masumoto 1972). The hardness indentation produces deformation markings of a coronet below the critical temperature but no such markings are observed above it (Masumoto 1977). The highly localised deformation and temperature-insensitive fracture strength at lower temperature imply that the inhomogeneous flow is athermal with little or no work hardening.

The absence of work hardening in metallic glasses is evidenced by the compression experiments of Pampillo and Chen (1974). A specimen of $Pd_{77.5}Cu_6Si_{16.5}$ was first compressed to initiate deformation and then repolished to remove the associated surface steps. Reloading resulted in reinitiation of existing bands. This behaviour was further demonstrated by bending and then rebending of glassy ribbons which exhibited slip bands regenerated on the initial bending (Pampillo 1975, Krishnanand and Cahn 1975).

6.4.2. Structure of deformation bands. If a specimen is deformed, polished, and then etched, preferential attack occurs at the sites of the shear deformation bands (Pampillo and Chen 1974, Chen *et al* 1973). This demonstrates clearly a change in the local chemical potential of the deformed zones. The susceptibility to preferential etching is expected to disappear by annealing the deformed glass near the glass transition temperature at which structure relaxation occurs. The energetic state of the deformed material is demonstrated further by the stored energy measurement of cold-rolled Pd–Cu–Si ribbons (Chen 1976f). On heating, energy is released over a broad temperature range. The relaxation spectrum with a slight shift to low temperature resembles that observed for the quenched glass. About 4% of the expended energy is stored in the slip bands. The relaxation spectra shift to lower temperature in the cold-rolled glass which implies the introduction of more disorder structure of high atomic mobility in the glass material. This point of view is also borne out by the enhanced magnetic aging in plastically deformed glass ribbons (Luborsky *et al* 1976, Williams and Egami 1976).

To determine whether vacancy-type defects exist in the deformed bands, the structure of a cold-rolled Pd–Cu–Si glass has been investigated using positron annihilation methods (Chen and Chuang 1975b). Both the positron lifetime and angular correlation of the glass exhibit a negligible change on cold rolling, whereas large changes have been observed for crystalline Pd. In fact, upon cold rolling, the angular distribution in crystalline Pd becomes sharper, and the intensity of the narrow component increases drastically. In addition, the positron lifetime is higher in the cold-rolled Pd than in the glassy material. These results lead to the proposition that plastic deformation of metallic glasses induces no vacancy-type defects. Similarly, no vacancy-type defects are produced in a 1 MeV electron-irradiated Pd–Ni–Si (Chen 1976d). It is plausible, however, that the 'vacancy–interstitial' pairs created during irradiation recombine either by diffusive processes or through local atomic regrouping. The

structure of the shear deformation bands of metallic glasses was suggested to resemble that of the quenched 'frozen-in' disorder.

6.4.3. Deformation mechanism. The similarity in the inhomogeneous slip in glassy metals to that in crystalline metals leads to postulates of the existence of dislocations in glassy materials (Gilman 1973, 1975b). Li (1976) proposed a dislocation lattice model for glass structure. The shear modulus, the critical shear stress and localised inhomogeneous deformation were explained in terms of the cooperative motion of dislocations. However, the formal geometric definition of such a dislocation and strain field around it have been questioned by Ashby and Logan (1973). They proposed instead, in a random network structure, the existence of disjunctions or broken bonds at which structure relaxes and the long-range strain field would diminish around them. Furthermore, the existence of dislocations in glassy metals appears to be inconsistent with the results of positron annihilation data which suggest no vacancy-type defects existing in the glasses. Leamy *et al* (1972) proposed that plastic flow occurs via the motion of localised strain concentration without using the term dislocation.

Alternatively, localised slip is supposed to arise from strain softening within the slip either due to chemical and/or structural disordering (Polk and Turnbull 1972), adiabatic heating (Leamy *et al* 1972, Chen 1973), or due to applied stress (Spaepen and Turnbull 1974). The shear band is viewed as a fluid layer based on a 'vein pattern' observed on tensile surfaces of glassy ribbons (Argon and Salama 1976, Spaepen 1975). When a tensile crack is nucleated in this 'fluid layer', it can propagate by pushing away the fluid. The problem is then the well-known Taylor instability (Taylor 1950) of a moving interface between two immiscible fluids. The model of formation of viscous layers at deformation bands was criticised by Davis (1978) because the vein pattern morphology of fracture surfaces of glasses is also exhibited by some crystalline materials, e.g. by the shear rupture failure of 304 stainless steel (Lee and Devine 1976). In addition, the concept based on the formation of viscous layer due to dilatation field is not applicable to a screw-type front in which triaxial tension is absent. Li (1978) pointed out that slip can be automatically localised with or without strain softening if slip is heterogeneously nucleated and the slip area spreads into a band.

All of these models appear to depend too much on forced analogies between either fluid or crystalline material and glassy solid. All of them are not well founded on experimental evidence. A different point of view was expressed recently by Li (1978) who proposed that there exist density variations (or excess volume) of the proper kind and the slip process merely transfers this variation to a different location. Since the slip is variable both in direction and magnitude, the excess volume may not be transferred completely. Some excess volume may be left behind and act as a source for further slip. The slip process occurs through a series of repeated nucleation events at density variations, both at and behind the slip front. This distinguishes itself from the concept of propagation of slip in crystalline metals in which the slip front moves with a steady configuration, and there is no further slip behind it. Slip localisation can occur by the concentration of excess volume into the slip area by the stress field of the 'Somigliana' dislocation.

Another approach is the computer simulation of deformation in two-dimensional amorphous structure (Maeda and Takeuchi 1978) and in three-dimensional random structure (Yamamoto *et al* 1979) using the Johnson potential. Maeda and Takeuchi

demonstrate a number of interesting features: (i) the elemental process of plastic deformation consists of chain-reacting collapses of holes separated by 5–8 atomic distances in the direction of the maximum shear; (ii) since the simulation was performed under isovolumic condition, collapse of holes simultaneously creates new holes at their vicinity as if they move an atomic distance; and (iii) thus-created holes occasionally revive to participate in further slips at which the environment favours the collapse. These features are more or less similar to those described by the excess volume model of Li.

Distinctly, holes do not move independently but with a correlation with each other. In this way the deformation proceeds by repeated collapse and reproduction of holes. Although this model has a drawback for containing too few atoms and being structurally unstable, this concept of deformation process is believed to be applicable also to the plastic deformation in actual three-dimensional glassy metals. The holes visualised in the two-dimensional model being relatively large would be much smaller in three-dimensional amorphous structure. Further exploration in this line would be very fruitful for the understanding of deformation mechanisms in metallic glasses.

6.5. Strength, toughness and embrittlement

Metallic glasses exhibit an interesting combination of mechanical properties, a very high fracture strength and a high fracture toughness. Fe-based glasses are seen to have fracture strength $\sigma_f \approx 350$ kg mm^{-2} which is comparable with the best hard-drawn piano wires. Remarkably, despite the high σ_f, metallic glasses exhibit a high toughness contrary to the brittle behaviour inherent in non-metallic glasses and high strength crystalline metals. The tearing energy of metallic glasses $\Gamma \approx 10^8$ erg cm^{-2} is many orders of magnitude larger than that in crystalline metals ($\sim 10^5$ erg cm^{-2}) and than the surface tension ($\sim 10^3$ erg cm^{-2}).

The ductility and toughness of Fe-based glasses are very susceptible to thermal annealing and hydrogen environment. A complete loss in ductility of Fe glasses may occur after annealing without crystallisation. This subsection deals with the influence of composition, atomic ordering and electronic configuration on the strength, hardness and fracture strain of metallic glasses. Alloying effects and possible mechanisms for the thermal embrittlement in metal–metalloid glasses are also presented.

6.5.1. Strength and hardness. The fracture strength σ_f, hardness H_v, Young's modulus E, Poisson's ratio ν and fracture tensile strain $\epsilon_y \approx H_v/3E$ of some typical glassy metals are listed in table 1. The ratio $E/\sigma_f \sim 50$ may be compared with that for Fe whiskers, $E/\sigma_f \sim 15{\cdot}5$ (Brenner 1956). H_v/σ_f equals $\sim 3{\cdot}0$ as expected for metallic glasses in which the indentation is accompanied with a large compressive plastic flow with little strain hardening. The Vickers hardness H_v and the tensile yield strain $\epsilon_y (\approx H_v/3E)$ of a series of metal–metalloid glasses have been reported by Chen (1978d). The influence of composition on H_v and ϵ_y is very similar to that on E. With increasing metalloid content y, both H_v and ϵ_y increase for the Fe and Co glasses, while remaining nearly constant for Pd–Ni–P and Pt–Ni–P glasses. Masumoto (1977) noted similar increases in H_v with increasing content of C, P, B or Si in Fe- and Co-based glasses. Both H_v and ϵ_y decrease in the order Fe, Co, Ni, Pd and Pt glasses as does E. A correlation between the average number of d and s electrons of metallic atoms and H_v of metal–metalloid glasses has been noted (Naka *et al* 1976b). For fixed metalloid composition, H_v of Fe-based glass increases when elements to the

Table 1. Fracture strength of glassy metals. Vicker's hardness H (kg mm^{-2}), fracture strength σ_f (kg mm^{-2}), Young's modulus (10^3 kg mm^{-2}), Poisson's ratio ν, and tensile yield strain ϵ_y (10^{-2}).

	H	σ_f	H/σ_f	E	ν	$\epsilon_y = H/3E$
$Pd_{77}Cu_6Si_{17}$	455	157	2·91	9·3	0·41	1·52
$Pd_{64}Ni_{16}P_{20}$	452	160	2·83	9·4	0·41	1·50
$Pd_{16}Ni_{64}P_{20}$	541	180	3·01	10·6	0·40	1·74
$Pt_{75}P_{25}$	344	—	—	9·3	0·43	1·23
$Co_{75}B_{25}$	1155	—	—	18·0	0·34	2·15
$Fe_{75}B_{25}$	1314	—	—	17·9	0·32	2·45
$Nb_{50}Ni_{50}$	893	—	—	13·2	0·37	2·26
$Zr_{50}Cu_{50}$	580	—	—	8·5	0·36	2·27
$Ti_{50}Cu_{50}$	610	—	—	10·0	0·36	2·06

left of Fe in the periodic table (Cr, V, Ti) are substituted for Fe, while it decreases on replacing Fe with elements of higher atomic number (Co, Ni, Cu).

Contrary to the proposition of Davis *et al* (1976) that H_ν scales as E, $\epsilon_y (= H_\nu/3E)$ depends strongly on the transition element and increases with the addition of metalloids. ϵ_y is lowest for Pt–P glasses ($\epsilon_y \sim 1{\cdot}3 \times 10^{-2}$) and highest for Fe–B alloys ($\epsilon_y \sim 2{\cdot}5 \times 10^{-2}$). To demonstrate the correlation between elastic stiffness and the flow strength, the yield strain ϵ_y is plotted against Poisson's ratio ν for a number of metallic glasses including metal–metal glasses, Nb–Ni, Cu–Zr and Ti–Be in figure 11. ϵ_y increases in the order Pt–P, Pd–Ni–P, Co–B and Fe–B glasses from $1{\cdot}23 \times 10^{-2}$ to $2{\cdot}45 \times 10^{-2}$

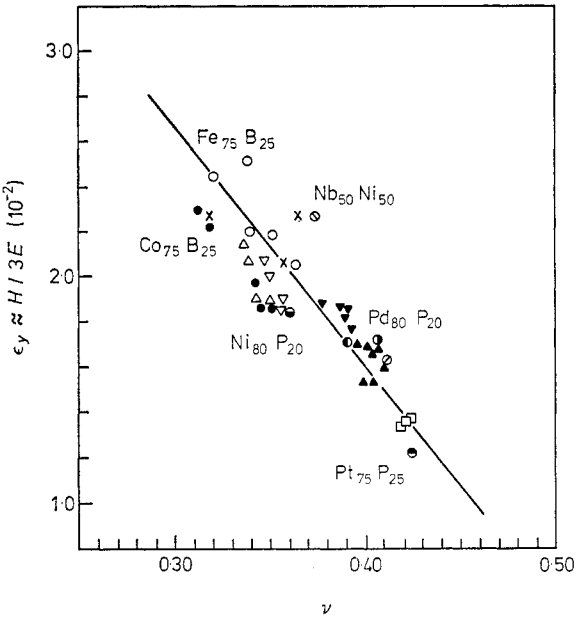

Figure 11. The correlation between the critical yield strain ϵ_y and Poisson's ratio ν for glassy alloys. Fe–B (○), Fe–Si_3B (●), Co–B (△), Fe–Al_3P (▼), (Pd,Fe)–P (▲), (Pd,Ni)–P (▽), (Pt,Ni)–P (□) and metal–metal (×).

as ν decreases from 0·42 to 0·32. It should be noted that the data for metal–metal glasses fall on the ϵ_y against ν relationship established for metal–metalloid glasses.

These results, together with the composition dependence of Young's modulus (§ 6.2), demonstrate that atomic ordering and electronic structure which influence elastic constants, flow strength and glass transition temperature also affect the yield strain. The increasing directionality of interatomic forces (or central forces) due to either atomic ordering or d-bonding characteristics in transition metals was suggested to be responsible for the lowering of ν and the increase in ϵ_y as well as E and T_g. In some 'ductile' glassy alloys with constant numbers of s and d electrons, e.g. $(Pd_{1-x}Ni_x)_{80}P_{20}$ and $(Pd_{1-x}Ni_x)_{83}Si_{17}$, (Chen *et al* 1975b,c) the yield strain ϵ_y correlates well with the glass transition temperature T_g such that the ϵ_y against x curve of the Pd–Ni–P glasses shows a negative deviation as does the T_g against x curve, while the ϵ_y against x curve of the Pd–Ni–Si is S-shaped and resembles the composition dependence of T_g. In these alloys, atomic ordering is the dominant factor and the incremental configurational entropy associated with disorder upon alloying lowers T_g and ϵ_y.

6.5.2. Fatigue and toughness. The fatigue lifetime data have been reported for $Pd_{80}Si_{20}$ glass (Ogura *et al* 1975) and for glassy $Pd_{77\cdot5}Cu_6Si_{16\cdot5}$ and $Fe_{29}Ni_{48}P_{14}B_6Al_3$ (Davis 1976). Qualitatively similar stress (S) against stress cycle (N) behaviour was observed. In all cases the lifetimes are time-independent and depend only on stress cycles. The S–N curve has a distinct fatigue limit σ^* with $\sigma^*/\sigma_f \approx 0{\cdot}3$ at a critical number of cycles $\sim 10^5$. The rate of fatigue crack propagation (dl/dN) in glassy metal ribbons is described by a power law of the stress intensity factor with exponent $m=2$ for $Ni_{39}Fe_{38}P_{14}B_6Al_3$ (Davis 1975) to $m=4$ for $Ni_{40}Fe_{40}P_{14}B_6$ (Ast and Krenitsky 1976) and $Pd_{80}Si_{20}$ (Ogura *et al* 1976) as has been observed for a variety of steels.

A well-defined plastic zone consisting of slip bands around a fatigue crack increases in size with increase in crack length. The fatigue crack propagates along slip bands formed ahead of the crack. Such a cracking behaviour in a glass is very similar to that in crystalline metals. However, the fatigue slip bands, which have a single slip step of $\sim 0{\cdot}5$ μm as a consequence of the absence of work hardening in the glass, are distinct from the so-called extrusions or intrusions as generally observed in crystalline metals. The width of plastic zone was related to the stress intensity factor for mode I(K_I) in the range $K_I \geqslant 50$ kg mm^{-2} as $Z_p \propto aK_I^m$ with $m=2$. This type of power relationship is expected according to the elastic–plastic theory of cracks.

The mode III fracture toughness K_{III} for $Fe_{80}P_{13}C_7$, $Pd_{80}Si_{20}$ and $Zr_{43}Cu_{57}$ glass has been determined using tear tests by Kimura and Masumoto (1975). The tearing energy Γ was seen to be proportional to the yield stress σ_y: $\Gamma/\sigma_y \approx 0{\cdot}03$ mm. Γ of the glasses is $\sim 10^8$ erg cm^{-2} and many orders of magnitude higher than that of inorganic glasses $\sim 10^3$ and polymers $\sim 10^5$. Γ increases with increasing the rate of tearing, u, below a critical value of $u_{cr} \approx 10$ mm min^{-1} and then decreases at higher u as the mode of deformation alters from a steady tearing to serrative one, or from thermally activated mode analogous to viscous flow to athermal plastic deformation. In the steady-state mode of tearing, Γ thus increases as the temperature is reduced, contrary to crystalline metals in which fracture energy decreases approaching the intrinsic surface energy value. K_{III} values obtained are 320, 140 and 190 kg mm$^{-3/2}$, respectively, for the Fe, Pd–Si and Cu–Zr glasses.

Davis (1975) measured the shear toughness K_c for Fe–Ni-based glasses from single-

edge-notch and centre-cracked-panel tension tests. K_c for the $Ni_{39}Fe_{38}P_{14}B_6Al_3$ glass increases with decreasing thickness of ribbon as the state of mechanical constraint changes from plane strain toward plane stress. K_c peaks in a thickness range 4–8 μm, equivalent to twice the shear slip thickness. The peak value ~ 210 kg mm$^{3/2}$ is less than the $Fe_{80}P_{13}C_7$ values ~ 320 kg mm$^{-3/2}$ of Kimura and Masumoto by a factor of 1·5 which is roughly the ratio of the fracture strengths. The minimum toughness observed ~ 30 kg mm^{-2} being the plane strain (mode I) fracture toughness, K_c falls reasonably on the K_c against σ_f relationship established for high strength steel.

6.5.3. Embrittlement. Chen and Polk (1974) first observed that Fe-based glasses were very susceptible to quenching conditions and tend to be brittle, whereas glass-forming Ni, Pd and Pt alloys exhibit a high ductility even in a partially crystalline state. Subsequent observation by Chen *et al* (1973) of bent glassy ribbons indeed revealed that the large strains induced at shear band intersections during bending deformation are relieved by plastic flow in Pd- and Ni-based alloys, but not in Fe-based glasses. Many Fe-based glasses which are ductile in the as-quenched state become brittle upon annealing apparently as the result of structural relaxation (Chen 1976g, 1977a,b, Luborsky *et al* 1976, Davis *et al* 1976, Ast and Krenitsky 1976).

In simple alloy systems such as binary Fe–B, Fe–P, Zr–Cu, the alloy glasses embrittle as a result of crystallisation. However, kinetics of embrittlement in many metallic glasses often correlate neither to the rate of stress relief nor to the crystallisation process (Chen 1976g, 1977b, Inoue *et al* 1978a,b). In fact $Fe_{40}Ni_{40}B_{20}$ glass ribbons produced at slower quenching rate are seen to undergo stress relief at slower rates but to embrittle at much lower temperatures with low apparent activation energy ~ 1 eV (Chi *et al* 1978). Embrittlement temperature, T_B, defined as the annealing temperature (for ~ 2 h) after which the glass becomes brittle, can differ by ~ 100 K from sample to sample apparently resulting from different frozen-in structure at various rates of quenching (Chen 1977b).

It has been proposed (Walter *et al* 1976, Davis *et al* 1976) for phosphorus-containing glasses that either segregation or clustering of phosphorus causes the embrittlement of glasses, based on observations (Luborsky *et al* 1976, Masumoto 1977) that $Fe_{80}P_{13}C_7$ and $Fe_{40}Ni_{40}P_{14}B_6$ lose ductility at lower temperatures of annealing than do $Fe_{78}B_{12}Si_{10}$, $Fe_{80}B_{20}$ and $Fe_{40}Ni_{40}B_{20}$ which contain no phosphorus. Walter *et al* (1976) concluded, from the relative decrease in the P peak in Auger spectra of an embrittled glass $Fe_{40}Ni_{40}P_{14}B_6$ before and after ion milling to a depth of about 60 Å, the presence of high P content clusters of ~ 60 Å in diameter. Their interpretation, however, is not conclusive, as the depletion of lighter elements in binary alloy on the surface layer ~ 20 Å after ion milling has been commonly observed (Ho *et al* 1976, 1977). The enrichment in heavy atoms after ion bombardment has been seen also in Pt–Si, Au–Al and Ta_2O_5 (Liou *et al* 1977). The change in peak height ratio observed may simply reflect a preferred sputtering of P resulting in the enrichment of Fe on surface layer ~ 60 Å depth during milling process. Further observation (Chen 1977b) on the influence of alloying among metalloids, in fact, demonstrates that the enhanced loss of ductility of glasses occurs only in the alloys containing two or more metalloid elements. Some phosphorus-containing glasses with a small fraction $\sim 3\%$ of other metalloids, $Fe_{80}P_{17}(B,Si,C)_3$ are found to exhibit a mechanical stability comparable to or surpassing those of B-containing glasses, $Fe_{80}B_{20}$ and $Fe_{40}Ni_{40}B_{20}$.

The atomic nature of embrittlement process in metallic glasses is not known. Phenomenologically it has been proposed (Chen 1976g, 1977b) that local structural

and compositional fluctuations somewhat analogous to phase separation in the regions of ~ 20 Å accompanied by structural relaxation may be responsible for the enhanced embrittlement in alloy glasses. The embrittlement arises from the resulting stress concentration around the clusters. This proposition seems to be in harmony with the observations that ternary alloys, Fe–P–B, Fe–P–Si and Fe–Co–P, exhibit a higher tendency to phase separate and consequently are more susceptible to embrittlement than do the corresponding binary alloys, Fe–P, Fe–B and Co–P. Experimental evidence of the clustering in the embrittled glasses is provided by an increase in electrical resistivity (Yeh 1976), in positron lifetime (Chen and Chuang 1977) and in the intensity of x-ray small-angle scattering (Luborsky *et al* 1975, Osamura *et al* 1979).

Fe-based alloy glasses were observed to be susceptible to hydrogen embrittlement. Kawashima *et al* (1976) observed in highly corrosion-resistant alloys $Fe_{59}Cr_8Ni_{23}P_{13}C_7$ that hydrogen embrittlement occurs under cathodic polarisation where the reduction of hydrogen ions take place, while in the passive potential region the glass is susceptible to embrittlement only under the influence of stress in strong acid solutions. The amount of absorbed hydrogen is higher than in crystalline metals probably due to the strong affinity of hydrogen to metalloids in the glass alloys (Nagumo and Takahashi 1976). Degassing of hydrogen occurs gradually in air even at room temperature and fracture stress is completely recoverable. It indicates that the absorbed hydrogen does not induce internal crackings or shear. The diffusion constant is smaller by 10^{-4} than that in iron or steel. Interestingly, it is consistent with the observation by Kawashima *et al* (1976) that the hydrogenised specimen embrittles under tensile testing at room temperature only below a critical strain rate $\sim 10^{-4}$ s^{-1}. The glass exhibits a ductile fracture above the critical strain rate apparently resulting from the absence of hydrogen diffusion into inhomogeneous shear slip bands. The critical strain rate is much lower at liquid nitrogen temperature so that the glass remains ductile at a slower strain rate $\sim 10^{-5}$ s^{-1}.

7. Magnetic properties

At first glance the coexistence of long-range ferromagnetic ordering with a structurally disordered material appears striking. However, ferromagnetism is supposed to arise from nearest-neighbour interactions (Gubanov 1960), and as described in §5 the very short-range order structure in the glassy state does not differ significantly from that in the corresponding crystalline material. Metallic amorphous ferromagnets have been obtained by vapour deposition of Co–Au (Mader and Nowick 1965), Fe–(Si,Ge) (Felsch 1969), by quenching from a melt of FePC (Duwez and Lin 1967) and Pd–Si alloys containing Co and Fe (Tsuei and Duwez 1966), and by electrodeposition of Co–P (Bagley and Turnbull 1965, Simpson and Brambley 1971). These amorphous alloys were reported to have a coercive force $H_c = 1$–10 Oe. These values are significantly lower than the corresponding crystalline values but are still much higher than conventional soft magnetic materials. Recent investigations (e.g. Dietz and Klett 1978, Kobliska *et al* 1978, Egami and Dahlgren 1978, Heiman *et al* 1978) revealed, however, that magnetisation behaviour of amorphous alloys critically depends on the deposition process and a soft magnetisation characteristic comparable with the melt-quenched glasses can be obtained for amorphous films by the proper choice of deposition conditions.

For practical applications as soft magnetic materials the ribbon form appears to be

most useful. Recent studies of magnetic behaviour of glassy metal have therefore been centred on glassy ribbons obtained by continuous melt spinning (Sherwood *et al* 1974, Egami *et al* 1974, Fujimori *et al* 1974). The glassy metal ribbons having the general composition, transition metal $\sim 20\%$ metalloid, exhibit low $H_c \sim 0{\cdot}1$–$0{\cdot}001$ Oe and high permeabilities comparable to soft magnetic alloys. The static coercive forces and dynamic properties of typical glassy ferromagnets are compared with those of conventional supermalloy in table 2.

Table 2. Magnetic properties of glassy metals. Saturation moment $4\pi M_s$, remanence B_r, coercive force H_c, and AC permeability μ.

	$\lambda = 0$ alloys	$Fe_{40}Ni_{40}P_{14}B_6$	$Fe_{72}Co_8Si_5B_{15}$	Supermalloy
$4\pi M_s$ (kG)	6·3	8·3	16	8·0
B_r (kG)	4·5	7·0	15	6·5
H_c (mOe)	13	8	7	30
μ (10^3)†	90‡	12	—	45

† The applied magnetic field $B(G) = 1000$, $f = 1000$ Hz.
‡ Water-quenched from 700 K.

Glassy metals are not structurally and magnetically isotropic as evidenced by the presence of macroscopic magnetic anisotropy. Residual strain, field heat treatment, or directional ordering during solidification induces anisotropies which determine the domain structure of the glasses and thus their magnetic behaviour. The domain structures in glassy metals are essentially similar to those observed in crystalline counterparts. Most models developed for crystalline magnetic materials to describe the static and dynamic properties are shown to be also applicable to glassy metals (Gyorgy *et al* 1975, Gyorgy 1978, Fujimori and Masumoto 1978, Graham and Egami 1978).

This section reviews experimental results on ferromagnetism in glassy metals, with particular emphasis on the influence of chemical and structural disorder on magnetic properties such as the magnetic moment, Curie temperature, magnetoelastic effects and induced magnetic anisotropies. Spin wave excitations, critical behaviour and low-temperature magnetisation will also be discussed.

7.1. Magnetic moments and Curie temperature

Whereas comparisons between glasses and crystals have been made, the experimental data show that the low-temperature magnetic moment is not strongly affected by structural disorder (Felsch 1969, 1970a,b, Kazama and Kameda 1976, Durand 1976). Felsch found that above a critical concentration of Si at 1% and Ge at 7% in Fe–Si and Fe–Ge alloys, the magnetic moment per Fe atom (μ_B) is identical in amorphous and crystalline BCC phase, but below the critical concentration μ_B of the amorphous films, is lower than that of crystalline phase. Similar anomalous behaviour was also observed in Fe–Au alloys. The causes of the anomalous behaviour in the Fe-rich amorphous alloys are not clear. The short-range order of dense close-packed structure in the amorphous Fe which is distinctively different from the local environment in the less-dense-packed BCC structure may account for the anomaly.

The addition of metalloid atoms is expected to alter μ_B and the Curie temperature T_c of glassy alloys resulting from the modification on local atomic environments. Figure 12 illustrates the influence of B, Si and P on μ_B and T_c of melt-quenched $Fe_{100-y}M_y$, where M are the metalloid atoms. Maxima in μ_B and T_c against y curves are clearly seen (Chen *et al* 1977, Fukamichi *et al* 1977a,b, Hiroyoshi *et al* 1978, Narita *et al* 1978). μ_B attains a maximum value of 2·2 and 2·04 Bohr magnetons at $y=15$ and 20%, respectively, for the FeB and FeSiB alloys. No clear maximum is found in the FePBAl alloys; however, the composition dependence of μ_B in the FePBAl is identical to the FeSiB alloys. T_c of both the FeSiB and FePBAl alloys peaks at $y=25\%$ but T_c is lower by ~ 100 K in the latter. The maximum in T_c seems to occur in FeB at higher B content $y>25\%$. The influence of metalloids on μ_B is different from that on T_c. T_c is seen to be very sensitive to the detailed atomic configuration as evidenced by the large change in T_c, e.g. an increase as much

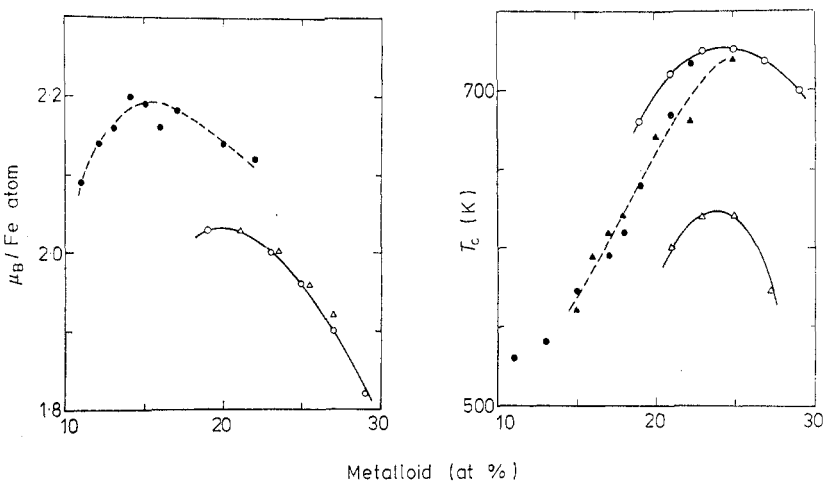

Figure 12. The Bohr magnetons per Fe atom μ_B and Curie temperature T_c as a function of metalloid content of Fe-based alloys: Fe–B (●), Fe–BSi_3 (▲), Fe–SiB_{10} (○) and Fe–PB_6Al_3 (△).

as 40 K in FeNiPBAl (Chen *et al* 1976, Chen 1978e, Lieberman *et al* 1977), upon annealing of the quenched glassy ribbons. Subsequently T_c of crystalline alloys, e.g. 878 K for Fe_3B, 716 K for Fe_3P and 830 K in Fe_3Si is, in general, much higher than that in the glassy state.

In the glass-forming alloys examined, either the addition of metalloid atoms to Co or Ni or replacing Fe with Co or Ni in general reduces the moment. Qualitatively the moment of metal–metalloid glasses was explained by taking the number of Bohr magnetons per atom 2·6, 1·6 and 0·6 for Fe, Co and Ni, then assuming each B, Si and P contributing 1, 2 and 3 electrons, respectively, filling the d shell in the rigid band model (Mizoguchi *et al* 1973, Yamauchi and Mizoguchi 1975, O'Handley *et al* 1976). The Fe and Co glasses may be approximated to have $\mu_B=2{\cdot}0$ and 1·0, respectively, while the Ni alloys are seen to be weakly temperature-dependent paramagnets. This simple picture is not really expected to be valid, and is inconsistent with the decreasing μ_B with y of the Fe-rich glassy metals. Furthermore, replacing B with either C, Si, and Ge has been found to increase μ_B of Fe–B glasses (Kazama *et al* 1978, Hatta *et al* 1978).

The influence of composition on T_c has been investigated by Chen *et al* (1977) for a number of alloy systems. The addition of a metalloid which expands Fe–Fe interatomic distances raises T_c while the increase in Co–Co and Ni–Ni pair distances lowers T_c. $Fe_{1-x}Co_x$ and $Fe_{1-x}Ni_x$-based glassy alloys show a broad maximum in T_c at $x=0{\cdot}50$ and $x=0{\cdot}25$, respectively. T_c of Co–Ni-based glasses drops rapidly as Ni replaces Co. This behaviour may be qualitatively understood in the framework of the Bethe–Slater curve. The influence of alloy constituents on T_c is, however, complicated and is far from understood. The magnitude of T_c shows no apparent correlations either to the valence electrons or to the size of the glass formers.

7.2. Mictomagnet and spin glass

Replacing either Fe or Co with Mn, Cr and Mo drastically reduces both μ_B and T_c (Mizoguchi *et al* 1973). The Mn-rich alloys (Sinha 1971) exhibit complex magnetic properties, with maxima in the temperature–magnetisation curves indicating ferromagnetic behaviour. Sherwood *et al* (1976) observed that in $(Fe_{0{\cdot}5}Mn_{0{\cdot}5})_{75}P_{16}B_6Al_3$ the magnetisation against temperature curve exhibits a maximum near 20 K when cooled in zero applied field. Cooling from higher temperatures in the presence of a 15·3 kOe applied field essentially eliminates the broad maximum. The field-quenched alloy exhibits an asymmetrical displaced hysteresis loop at 1·5 K. Magnetic cycling changes the magnetic state of the specimen resulting in a nearly symmetrical loop. These magnetic properties are interpreted as evidence for ferromagnetic–antiferromagnetic 'exchange anisotropy' or mictomagnet behaviour in this glassy alloy.

A transition to a spin glass state at low temperature ~ 10 K has been reported in glassy alloys containing magnetic impurity atoms of less than $\sim 10\%$, e.g. $Pd_{80-x}Fe_xSi_{20}$, $Pd_{80-x}Fe_xSi_{20}$ (Zentko *et al* 1975) and $Ni_{80-x}Fe_xP_{14}B_6$ (Onn *et al* 1978). The susceptibility χ exhibits a sharp cusp in a low field $H_a < 10$ Oe. Above the transition T_f, χ follows a Curie–Weiss law. Application of a small magnetic field greatly reduces and rounds the cusp. In addition to the cusp in χ against T curves, Mizoguchi *et al* (1977) observed in an amorphous sputtered $Gd_{37}Al_{63}$ film thermal hysteresis and relaxation in magnetic properties below the transition temperature $T_f = 16$ K.

7.3. Magnetisation processes

Glassy ferromagnets are not magnetically isotropic. Local anisotropies may be produced by non-uniform strains (Egami *et al* 1974, Fujimori *et al* 1976a,b, Schroeder *et al* 1978), field annealing (Sherwood *et al* 1974, Chen *et al* 1975a) or structural and compositional anisotropies which occur during quenching processes (Leamy *et al* 1975a). The value of the induced anisotropy (K_u) ranges from 500 erg cm^{-3} for magnetically annealed near zero-magnetostrictive CoFe alloy (Chen *et al* 1975c) to 5×10^4 erg cm^{-3} for as-quenched $Fe_{80}P_{13}C_7$ (Fujimori *et al* 1974).

The magnetic domain structure can be observed by Bitter's method (Fujimori *et al* 1976c), magneto-optical Kerr effect (Schroeder *et al* 1978) or by scanning electron microscopy (Leamy *et al* 1975a, 1976). Figure 13 (plate) shows the domain structure for an as-quenched zero-magnetostrictive alloy $(Co_{0{\cdot}96}Fe_{0{\cdot}04})_{75}P_{16}B_6Al_3$. The glassy ribbon was prepared by centrifugal spinning and the resultant domain structure appears to reflect the flow pattern such that the direction of magnetisation is parallel to the direction of spin, $\bar{R}$, in the centre of the ribbon and perpendicular to $\bar{R}$ at the

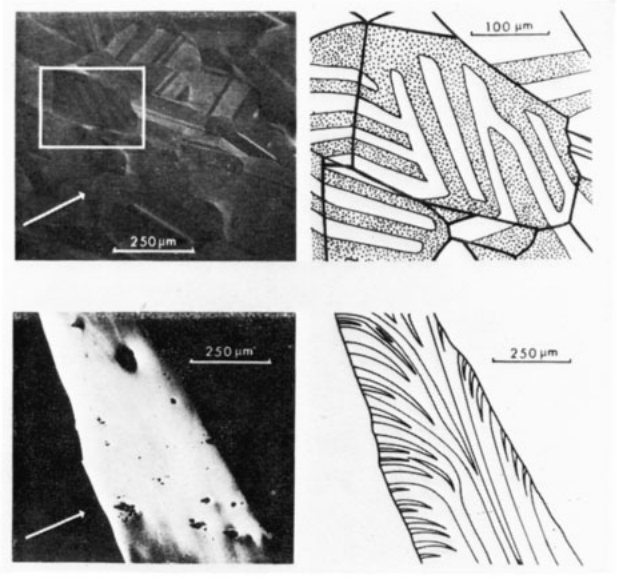

Figure 13. The domain structure of permalloy (top) and of the as-melt spin-quenched $\lambda = 0$ glassy ribbon.

ribbon edges. The magnetisation curve or the B–H loop is quite square, with a coercive force of 0·02 Oe, but exhibits a relatively low remanence ratio, $B_r/B_s = 0{\cdot}45$, as expected from the domain structure. The square part of the loop arises from the motion of the 180° domain walls present in the sample, and the low remanence results from the presence of domains whose directions of magnetisation are not parallel to the spinning direction. Large jumps (Barkhausen jumps) in magnetisation are often observed, suggesting the nucleation and irregular motion of a large-scale domain structure. The saturation applied field is approximately 60 Oe corresponding to a value of $1{\cdot}5 \times 10^3$ erg cm^{-3} for K_u. The domain structure after a magnetic anneal is modified such that the domain patterns exhibit the easy direction of magnetisation parallel to the magnetic field during annealing. Annealing the sample with an applied field along the ribbon direction substantially increases the remanence ratio, and decreases the coercive force and K_u, while with the magnetic field perpendicular to spin direction the remanence ratio decreases practically to zero.

Under the condition that an AC field, $H = H_0 \sin 2\pi ft$, is large enough to reverse the magnetisation through the B–H loop, it is assumed in well-annealed glasses that the domain walls are essentially free and the dynamic coercive force H_{AC} arises from the eddy current damping. A straightforward calculation adopting the models developed for crystalline soft magnetic materials (Gyorgy 1978, Gyorgy *et al* 1975) gives

$$H_{AC} = (\pi f L H_0 \beta / M_s)^{1/2} \tag{7.1}$$

where β is the damping constant, L is the average domain spacing and M_s is the saturation magnetisation. The experimental results for the as-quenched $\lambda = 0$ alloy are shown in figure 14. H_{AC} is proportional to the cubic root rather than the square root of frequency f, suggesting, in terms of the model, that the domain spacing must be a function of frequency, $L \propto f^{-1/3}$. This frequency dependence of L can be under-

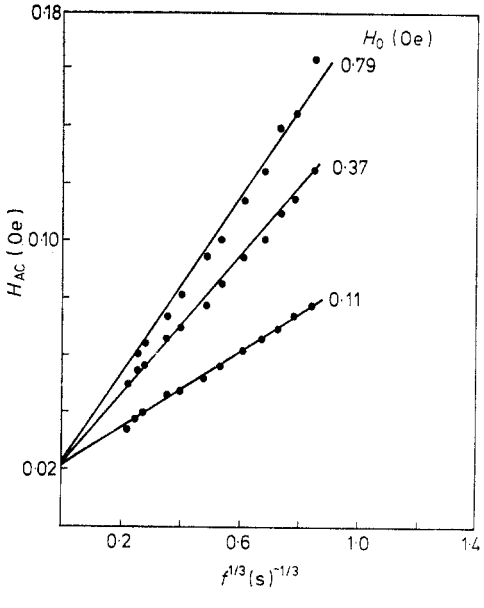

Figure 14. The AC coercive force as a function of $f^{1/3}$, where f is the drive field frequency. H_0 is the field amplitude.

stood phenomenologically that potential wall nucleation sites, which are operative at high frequencies, are swept away by a wall nucleated at an energetically more favourable site at lower frequencies. The slopes of the three curves vary as $H_0^{1/2}$. The domain spacing L at 100 Hz is deduced to be 0·1 cm for the annealed sample which is high compared with the static domain spacing $\sim 0{\cdot}1$ mm (Chen *et al* 1975c) but is not unreasonable considering that the domain walls must be nucleated at each cycle.

7.4. Magnetostriction and induced magnetic anisotropy

The magnetostrictive constant (λ_s) has been investigated in the FeCoNi system (Sherwood *et al* 1974, Arai *et al* 1976b, Jagielinski *et al* 1977). The Fe-rich glasses show large positive magnetostrictions $\lambda_s = (20\text{–}40) \times 10^{-6}$, while λ_s is negative in the Co glasses. In the Fe–Co systems $\lambda_s = 0$ occurs at approximately the same Fe/Co ratio ($\sim 0{\cdot}05$) relatively independent of the glass formers (Brooks 1976, Brooks and Chen 1977, O'Handley *et al* 1976). The addition of Ni to an Fe alloy decreases λ_s.

For glasses in an as-quenched state, the origin of K_u is most likely due to the internal residual stress. This is substantiated by the reduction in K_u with stress relief (Luborsky *et al* 1975) and the existence of the same temperature dependence of anisotropy $K_u(T)$ and the magnetostriction $\lambda_s(T)$ (Egami and Flanders 1975). The kinetics of the stress relief process depends strongly on the structural state of the glass as discussed in §5. Pre-annealing or slower quenching decreases the rate of stress relief and cold rolling enhances it (Williams and Egami 1976, Luborsky *et al* 1976, Chi *et al* 1978). In the FeCo system (Fujimori *et al* 1976a) and $(Fe,Ni)_{80}B_{20}$ (O'Handley 1975) a linear dependence of K_u with λ_s is found. A minimum K_u and H_c is seen for the $\lambda_s = 0$ composition. The residual stress of the as-quenched ribbons is evaluated to be $\sim 10^9$ dyn cm^{-2} (Fujimori *et al* 1976a, Schroeder *et al* 1978) which is comparable to the tensile stress $\sim 2 \times 10^9$ dyn cm^{-2} required for the disappearance of the maze domain structure (Krause and Chen 1976).

For the $\lambda_s = 0$ alloy, residual stresses do not account for the induced anisotropy. Pair ordering of some sort is postulated (Chen *et al* 1975c) to occur during the cooling process. The direction of the pair ordering seems to be determined by the flow directions during cooling in as-quenched ribbons (figure 13) and by the direction of the applied magnetic field in the annealed samples. It appears that even in non-zero magnetostrictive alloys, after stress relief, the induced K_u may arise from the directional pair ordering. Luborsky and Walter (1977a) investigated the uniaxial-field-induced K_u for stress-relieved glassy alloys of $(Fe_yNi_{1-y})_{80}B_{20}$. The temperature and composition dependence of the glasses are seen to be consistent with the directional order theory (Chikazumi and Graham 1969) such that

$$K_u = AN(y)\,(M_m/M_0)^2\,(M_a/M_0)^2/T_a \tag{7.2}$$

where A is a constant depending on the atomic arrangement and the range of interaction, $N(y)$ is a function of the concentrations of the ordering species and can be approximated to be proportional to $y^2(1-y)^2$ in the binary alloys, and M_m, M_a and M_0 are the magnetisations at the measuring temperature, the annealing temperature T_a and 0 K, respectively. The normalised anisotropy $K_u' = K_u T_a\,(M_m^2 M_a^2/M_0^4)^{-1}$ corrected for its temperature dependence attains a maximum at $y = 0{\cdot}5$. However K_u' does not diminish at $y = 1$ as predicted if only Fe–Ni ordering occurs and is about 25% of the maximum value. In contrast to the FeNiB system,

$(Fe_yNi_{1-y})_{80}P_{14}B_6$ alloys (Luborsky and Walter 1977b) have neither the composition nor the temperature dependence of equation (7.2). These results have been attributed to the presence of a large contribution to K_u from the metalloid atoms and fast diffusive process during cooling which disturbs the pair ordering established at higher temperatures. In the alloy series $(Fe_yCo_{1-y})_{78}Si_{10}B_{12}$, Fujimori *et al* (1977) found the composition dependence of K_u' well described by equation (7.2) only for the Fe-rich alloys in the range $y > 0{\cdot}7$, while Miyazaki and Takahashi (1978) showed that the induced uniaxial magnetic anisotropy of the Fe–Co glasses can be explained by the directional pair model over the whole composition range provided that the measured magnetic field is high, ~ 3 kOe.

The field-induced anisotropy cannot be eliminated by cooling from above T_c in zero magnetic field as an anisotropy is induced below T_c by the local direction of magnetisation, if the kinetics of equilibration below T_c are high compared with the rate of cooling. K_u, however, can be greatly reduced, and consequently the initial permeability μ_e should increase substantially by heat treatment above T_c followed by a cooling fast enough to prevent atomic rearrangement. An increase in μ_e by a factor of five has been achieved for the $\lambda_s = 0$ FeCoPBAl glass (Gyorgy *et al* 1975) and $(Fe_{0{\cdot}1}\ Co_{0{\cdot}4}\ Ni_{0{\cdot}5})_{78}Si_8B_{14}$ (Ohnuma and Masumoto 1978) by water quenching from 700 K. Takahashi *et al* (1977) observed in series of (Fe,Co,Ni)SiB that a drastic improvement in μ_e can be obtained by air cooling ($\sim 150\,^\circ$C h^{-1}) from 450 °C for $\lambda_s = 0$ glassy alloys with $T_c < 200\,^\circ$C,while for $\lambda_s = 0$ glasses with higher T_c $\gtrsim 300\,^\circ$C, a similar achievement can be obtained only by water quenching. Apparently the quenching rates required to prevent magnetic reordering below T_c are lower for those with low T_c as the diffusivities decrease drastically with lowering temperature.

7.5. Invar and Elinvar behaviour

Iron-based glassy alloys are found to have relatively large forced volume magnetostrictions $\partial\omega/\partial H \approx 2 \times 10^{-9}$ Oe^{-1} (Tsuya *et al* 1975a,b, Fujimori *et al* 1976a, Jagielinski *et al* 1977). The large positive $\partial\omega/\partial H$ implies a large negative thermal expansion $\alpha_M(T)$ associated with magnetisation and consequently the thermal expansion of the Fe alloys exhibit anomalous contraction upon heating through T_c (Fukamichi *et al* 1977b). The anomalous thermal expansion $\alpha_M(T)$ is more pronounced in the Fe-rich alloys. No distinct anomaly is detected in Co-based glasses apparently as a result of the small $\partial\omega/\partial H \approx 3 \times 10^{-10}$ observed. Yamauchi and Mizoguchi (1975) reported a relatively large pressure effect on T_c and μ_B in series of $(Fe,M)_{80}P_{10}B_{10}$ glasses with M = Ni or Co, $dT_c/dP \approx -0{\cdot}7$ K kbar^{-1} and $d \ln \mu_B/dP = -2 \times 10^{-2}$ kbar^{-1}, resulting from the large $\partial\omega/\partial H$. A much larger effect of pressure on T_c, e.g. $dT_c/dP = -6$ K kbar^{-1} is found in Fe–B Invar system (Fukamichi *et al* 1978).

An excellent Invar characteristic was found in the Fe–B system (Fukamichi *et al* 1977a). The alloy with 17% B exhibits nearly zero thermal expansion for a wide temperature range of ~ 300 K near room temperature. As in the crystalline ferromagnetic Invar alloys, the reduced magnetisation curves of the FeB alloys decrease much more rapidly than the Brillouin function for the spin $S = \frac{1}{2}$. In the Invar composition region the low-temperature (4·2 K) magnetic moment μ_B/Fe atom decreases and the high-field susceptibility χ_{HF} increases drastically as the B content decreases (Hiroyoshi *et al* 1978). The room-temperature $\chi_{HF} \sim 5 \times 10^{-5}$ emu g^{-1} is similar in both the glassy alloys and crystalline Invar alloys (e.g. $Fe_{66}Ni_{34}$) but is ten times higher than the crystalline pure Fe or Ni. The origin of Invar anomalies is still

controversial. The large χ_{HF} and the flattening of the magnetisation curve may reflect exchange fluctuation which is governed mainly by the number of Fe atoms surrounding the Fe atom and Fe–Fe pair distribution.

In §6.3.3, it is shown that Fe-based glassy alloy ferromagnets show a large ΔE effect resulting from the large magnetostriction $\lambda_s \approx 20 \times 10^{-6}$ and large coupling constant $k_c \approx 1$. The temperature coefficient of Young's modulus E depends on domain structure and thus changes sensitively to the preparation processes and heat treatments of samples (Berry and Pritchet 1976b, Kikuchi *et al* 1977). Excellent Elinvar characteristics are thus in principle obtainable for most ferromagnetic glassy alloys which exhibit a large ΔE effect.

7.6. Spin wave excitations and critical behaviour

In the past few years a number of studies have been reported on the spin wave excitation in glassy metals inferred from inelastic neutron scattering measurements (Pickart *et al* 1974, Axe *et al* 1974, 1977, Mook *et al* 1974, Lynn *et al* 1976, Tarvin *et al* 1978) and from low-temperature magnetisation measurements (Cochrane and Cargill 1974, Tsuei and Lilienthal 1976, Chien and Hasegawa 1977). The inelastic neutron scattering measurements are consistent with a normal ferromagnetic dispersion relation $\hbar w(q) = \Delta + Dq^2 + Eq^4 + \ldots$, where the gap Δ arises due to dipole–dipole interactions. The low-temperature magnetisation is consistent with the Heisenberg model prediction $M = M_0\,(1 - BT^{3/2} - CT^{5/2})$. B and D are related by the equation (Ketter 1966)

$$B = 2{\cdot}612\,\frac{g\mu_B}{M(0)}\left(\frac{k_B}{4\pi D}\right)^{3/2}. \tag{7.3}$$

A persistent discrepancy, however, has been found between the coefficient B obtained from the magnetisation measurements and the B calculated from the spin wave stiffness constant D. The latter is consistently 30–40% smaller than the former. For example, $B_{obs} = 4{\cdot}5 \times 10^{-5}\ K^{-3/2}$ and $2{\cdot}2 \times 10^{-5}\ K^{-3/2}$, respectively, for $(Fe_{0{\cdot}93}\ Mo_{0{\cdot}07})_{80}P_{10}B_{10}$ and $Fe_{75}P_{15}C_{10}$, while the corresponding $D = 85$ meV Å^2 and 165 meV Å^2 which yield $B_{cal} = 3{\cdot}12 \times 10^{-5}\ K^{3/2}$ and $1{\cdot}3 \times 10^{-5}\ K^{-3/2}$, respectively.

Birgeneau *et al* (1978) have recently studied systematically the spin wave excitation and low-temperature magnetisation in a series of glassy alloys $(Fe_xNi_{1-x})_{75}P_{16}B_6Al_3$. Their results are summarised in table 3. For $x = 1$, 0·65 and 0·5 alloys in which the measured magnetisation is field-independent, excellent agreement is found between D and B related by equation (7.3) of ordinary spin wave theory. Thus there exists no evidence of localised non-propagating modes. The cause of the discrepancy

Table 3. Spin wave stiffness of $(Fe_xNi_{1-x})_{75}P_{16}B_6Al_3$ glasses.

Alloys	T_c (K)	B (10^{-6} K$^{-3/2}$)		$D(0)_{calc}$ (meV Å^2)	$D(0)_{meas}$ (meV Å^2)
		Mössbauer	Magnetisation		
$x = 1{\cdot}0$	630	19 ± 2	$18{\cdot}6 \pm 2$	117 ± 10	134 ± 5
$x = 0{\cdot}65$	576	28 ± 2	$28{\cdot}4 \pm 2$	114 ± 10	115 ± 3
$x = 0{\cdot}5$	482	43 ± 3	$46{\cdot}3 \pm 3$	94 ± 10	91 ± 3
$x = 0{\cdot}3$	258	117 ± 10	124 ± 10	61 ± 10	36 ± 3
Crystalline Fe	1042		3·4	285	281

observed previously remains unexplained. In an $x=0{\cdot}30$ sample, a significant discrepancy is seen but of the opposite sign to that observed previously. Here the measured stiffness $D=36$ meV Å^2 is smaller than the calculated $D_{cal}=61$ meV Å^2 from the measured $B\approx 12\times 10^{-5}$ K$^{-3/2}$. It is believed that in this alloy where Fe constitutes only $\sim 22\%$ of the atoms, dilute alloy effects dominate. A spin wave description is probably not valid as is evidenced by the marked field dependence of magnetisation (Leamy *et al* 1975b) and lack of sharp excitations of spin waves in these glassy alloy samples.

In a more complete study on the high-temperature spin dynamics of $(Fe_{0{\cdot}65}Ni_{0{\cdot}35})_{75}P_{16}B_6Al_3$ (Tarvin *et al* 1978), the spin wave stiffness D is well described by $D(T)=115[1-0{\cdot}45(T/T_c)^{5/2}]$. The 5/2 law, as predicted by simple spin wave theory for the Heisenberg ferromagnet, appears to hold up to 450 K for the FeNi sample ($T_c=572$ K). Furthermore the spin wave damping at 450 K is consistent with the Heisenberg model prediction $\Gamma(q)\sim q^4\ln^2[k_BT/\hbar w(q)]$. Similar results are seen by Axe *et al* (1977) in FeMoPB alloy. In the critical region, the spin wave stiffness is found to follow the power law $D\sim(1-T/T_c)^{0{\cdot}5\pm 0{\cdot}1}$ for $0{\cdot}02\leqslant 1-T/T_c\leqslant 0{\cdot}2$, while at T_c the energy width is described by $\gamma_c(q)\sim q^{2{\cdot}7\pm 0{\cdot}2}$ for $0{\cdot}05\leqslant q\leqslant 0{\cdot}18$ Å^{-1}. These results agree satisfactorily with dynamical scaling theory for the Heisenberg ferromagnet.

A detailed experimental magnetisation study of a glassy $Co_{70}B_{20}P_{10}$ (Mizoguchi and Yamauchi 1974) near the critical point shows a definite second-order phase transition with equations of state $M_s\propto(T_c-T)^{0{\cdot}04}$ for $T<T_c$, $\chi_0^{-1}\propto(T-T_c)^{1{\cdot}34}$ for $T>T_c$ and $M\propto H^{1/4{\cdot}4}$ at $T=T_c$. The specific heat associated with the magnetic transition has been reported previously (Chen 1973), for Fe-based glasses which exhibit a sharp peak at T_c. Chen *et al* (1977) have demonstrated further from specific heat measurements the evidence of a well-defined second-order magnetic order–disorder transition in an 'undercooled liquid state' in some (Fe,Co) alloys. In the critical region the correlation length becomes so large that the critical behaviour is governed mainly by macroscopic structure. In this sense glassy metals may be considered as ideal isotropic ferromagnets and exhibit better-defined critical behaviour predicted for Heisenberg ferromagnet than do crystalline alloys.

8. Electrical properties, low-temperature behaviour and corrosion resistance

8.1. Electrical resistivity

A Kondo-type resistivity minimum below which the resistivity ρ obeys $\ln T$ law is seen in most glassy alloys containing magnetic impurity atoms, and is the subject of much controversy in recent years. A model based on Kondo-type s–d exchange scattering (Hasegawa and Tsuei 1970) and a two-level configurational tunnelling (Cochrane *et al* 1975) have been proposed to explain this resistance-minimum phenomenon. These two models are practically identical in theoretical formalism but based on quite different origins contributing to the $\ln T$ dependence of ρ.

A clearer picture in comparison has emerged for the origin of high-temperature ρ behaviour. The high values of ρ, small temperature coefficient $\alpha=(1/\rho)\,d\rho/dT$, and quadratic temperature dependence of ρ below ~ 50 K can be explained satisfactorily in the framework of generalised Ziman theory (e.g. Cote and Meisel 1977, Güntherodt and Künzi 1978). Experimental results will be discussed in terms of these viewpoints.

8.1.1. Resistivity minimum. The existence of a resistance-minimum phenomenon has been found in most glassy alloys ranging from weakly paramagnetic to strongly ferromagnetic, e.g. Pd–Si containing magnetic elements Co, Fe, Cr and Mn (Tsuei and Hasegawa 1969, Hasegawa and Tsuei 1970, 1971). Ni–P (Cote *et al* 1977b), Pd–Ni–P (Maitrepierre 1970), Fe–P–C (Lin 1969), Co–P (Cochrane *et al* 1975), Fe–Ni–PBAl and Fe–Mn–PBAl (Räpp *et al* 1978a, Gudmundsson *et al* 1978). The resistivity minimum anomaly is strikingly similar in the non-ferromagnetic and ferromagnetic glassy alloys. The temperature of resistivity minimum, $T_{\min}$, can be as high as 500 K in alloys containing Cr. Below $T_{\min}$, the resistivity can be described by the sum of a ln T term ($\Delta\rho$) which levels off at low temperature, a residual resistivity ρ_0, and a power law temperature dependence term T^n with $n=2$ for $T<50$ K and $n=1$ at higher temperature.

A Kondo-type effect has been suggested to account for the ln T contribution to the resistivity (Tsuei and Hasegawa 1969, Tsuei 1977). Kondo-logarithmic resistivity arises from exchange scattering between conduction electrons and localised moments (Kondo 1975, Heeger 1975). The levelling off of $\Delta\rho$ as T approaches 0 K suggests the formation of the spin-compensated state. The coexistence of the resistivity minimum and ferromagnetism in glassy metals is striking. This is quite in contrast to the case of crystalline systems in which the Kondo-type resistivity minimum is observed only for very dilute magnetic impurity alloys of less than 0·1%, and is completely suppressed due to spin–spin correlation for alloys with higher magnetic impurity content. It is not clear how the Kondo effect could be dominant in amorphous ferromagnets well below the Curie temperature.

Cochrane *et al* (1975), based on the observation that the ln T dependence is unaltered by an applied field of 45 kOe, concluded that the resistivity minimum anomaly was non-magnetic in origin. They adopted a two-level tunnelling model originally proposed by Anderson *et al* (1972) for the interpretation of the low-temperature anomalies in glassy materials and arrived at an expression for the low-temperature resistivity depending only on the glassy structure,

$$\Delta\rho \sim V_c^3 \ln (k^2T^2+\Delta^2) \tag{8.1}$$

where Δ is a characteristic energy gap and V_c is the Coulomb attraction between the ion and electron. Experimental data of the Fe-based alloy glasses (Räpp *et al* 1978a, Gudmundsson *et al* 1978) qualitatively fit expression (8.1) but with some deviations. The Δ/k values obtained, however, depend strongly on the magnetic species such as Cr and Mn, and are typically orders of magnitude larger (>10 K) than predicted from the model ~ 1 K. The data of Gudmundsson *et al* in fact fit well with a simple exponential power dependence. Hasegawa and Tsuei (1970), on the other hand, found no resistivity minimum in Pd–Si alloys of very high purity. In addition, a number of amorphous vapour-deposited films of polyvalence alloys such as $Ga_{95}Ag_5$, $Sn_{84}Cu_{16}$ and $Pb_{80}Ag_{20}$ (Korn *et al* 1973, 1974) do not exhibit the resistivity-minimum phenomenon. This may suggest localised moment formation is unlikely in high-valence metals (Anderson 1961). At present, very little is known about the interaction of electrons with configurational systems in glasses; however, considering the absence of a resistance minimum in Pd–Cu–Si of high purity which exhibits a considerable two-level density of state (§8.2), this interaction, if present, is at least an order of magnitude smaller than generally observed (Golding *et al* 1977, 1978). Furthermore, since atomic structure among glassy alloys is identical, a structural model can hardly be consistent with the strong composition effect on the resistivity anomaly.

8.1.2. Temperature coefficient of resistivity. Beside the resistivity minimum phenomenon, the resistivity of glassy alloys exhibits two other common features: (i) the resistivity ρ is relatively high ~ 200 $\mu\Omega$ cm and varies with temperature quadratically at low temperature $T < 50$ K and linearly near room temperature, and (ii) the temperature coefficients of resistivity, $\alpha_R = (1/\rho)d\rho/dT$, are small and change sign with changing composition. The suggested explanations for these common characteristics include localised spin fluctuations (Hasegawa 1972), Mott s–d scattering (Mott 1972, Tangonan 1975) and a generalised Ziman theory (Ziman 1961, Sinha 1970, Evans *et al* 1971, Cote and Meisel 1977). All these models yield T^2 dependence of ρ at low temperature and T behaviour at high temperature. Quantitative comparison with the localised spin fluctuation theory and the s–d scattering, however, is not accessible because of the lack of knowledge of the density of states and of the phonon-scattering contribution to $\rho(T)$. Since the liquid and glassy states belong thermodynamically and structurally to the same phase, the Ziman theory which has successfully explained the resistivity of liquid transition metals and their alloys, e.g. Busch and Güntherodt (1974), has proved to be very satisfactory in the understanding of the resistivity in glassy alloys. Following the approach of Dreirach *et al* (1972) for the resistivity of liquid transition metals, theoretical calculations of resistivity $\rho(T)$ based on experimental structure factors $a_{ij}(q,T)$ performed for a Zr–Cu glass (Waseda and Chen 1978c) have been seen to agree fairly well with the experimental data.

Although three partial structure factors are required to discuss properly the resistivity of binary alloys, for quantitative discussion of metal–metalloid glassy alloys in which the resistivity behaviour is predominantly determined by the transition metals, the three partials may be replaced by a single structure factor of the transition metal. In transition metals, the d-phase shift is dominant at the Fermi energy, the resistivity can be given by

$$\rho \propto a(2k_F) \frac{\Gamma^2}{\Gamma^2 + 4(E_{res} - E_F)^2} \tag{8.2}$$

where Γ is the width and E_{res} is the energy of the scattering resonance, lying approximately at the centre of the 3d band. There are two main contributions to the electrical resistivity of liquid (or glass) transition metals, resulting from resonance scattering and from the pair correlation function $a(2k_F)$. The latter is identical for Fe, Ni and Cu. Since Mn has a half-filled d band, the difference $(E_{res} - E_F)$ is small in this metal, the resistivity of transition metals decreases with increasing number of 3d electrons going from Mn to Fe, Co, Ni and Cu. This is indeed observed in glassy alloys (Fe, Mn)PBAl such that a relatively high $\rho \sim 370$ $\mu\Omega$ cm is found in the Mn alloy and a lower value ~ 160 $\mu\Omega$ cm in the Fe one. Relatively low resistivity ~ 100 $\mu\Omega$ cm is seen in Au–Ge–Si (Chen and Turnbull 1968, Hauser and Tauc 1978).

The influence of composition and temperature on ρ of alloy glasses may be explained by the relative position of $2k_F$ with respect to K_p and temperature dependence of $a(K)$ as shown in figure 15. The valence of liquid transition metals Z is ~ 1. The $2k_F$ values of pure transition metals then are of the same magnitude as for monovalent noble metals and lie far below K_p. On alloying with polyvalent metals, Z increases and so does $2k_F$ giving rise to a large increase in ρ via structure factor term. In the composition range, e.g. Ni_3P where $2k_F = K_p$ and in which $a(2k_F)$ decreases with increasing temperature, the temperature coefficient of resistivity becomes negative.

Many glass-forming alloys fall near this composition range. Consequently, with increasing concentration of polyvalent metals such as metalloids and early transition

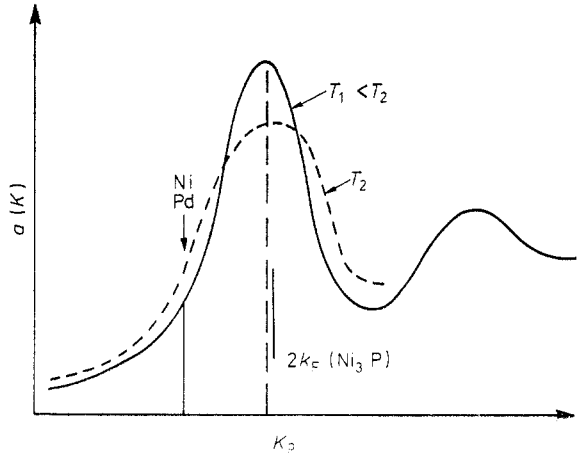

Figure 15. The structure factor $a(K)$ plotted against K for two temperatures T_1 and T_2. The arrow indicates the $2k_F$ of transition metals.

metals, ρ increases and negative temperature coefficients, α_R, occur. This has been borne out experimentally in a number of glassy alloys. In liquid-quenched $(Pd_{0.5}Ni_{0.5})$–P (Boucher 1972) and electrodeposited Ni–P (Cote *et al* 1977b), ρ increases with P content and α_R changes sign from positive to negative at 25% P content. Hauser and Tauc (1978) found that in sputtered amorphous Au–Si alloys, α_R changes sign at lower concentration of metalloid Si at 15%. All the intertransition alloy glasses studied, e.g. Nb–Ni (Nagel *et al* 1978), Zr–Cu (Murata *et al* 1976b, Szofran *et al* 1976), Zr–Ni,Co (Räpp *et al* 1978b), $Zr_{70}Pd_{30}$ (Graebner *et al* 1977) and Ti–Be–Zr (Hasegawa and Tanner 1977), are found to have a negative temperature coefficient $\approx -10^{-4}$ K^{-1} as may be expected if $Z \approx 2$ is taken for Zr, Nb and Ti so that in these alloys $2k_F$ lies near K_p.

In glassy alloys $(Pd_{1-x}Cu_x)_{80}P_{20}$ (Tangonan 1975), the resistivity varies from $\rho = 150$ $\mu\Omega$ cm and $\alpha_R = 7 \times 10^{-5}$ K^{-1} for $x = 0{\cdot}1$ to $\rho = 260$ $\mu\Omega$ cm and $\alpha_R = -8 \times 10^{-5}$ K^{-1} for $x = 0{\cdot}5$ which contrasts with the weak dependence of both ρ and α_R on x in $(Ni_{1-x}Pd_x)_{80}P_{20}$ alloys. Similar behaviour in α_R upon replacing Ni with Pt is seen previously by Sinha (1970) for $(Ni_{1-x}Pt_x)_{75}P_{25}$. This decrease in α_R as more Cu is added is interpreted (Oberle *et al* 1976, Güntherodt and Künzi 1978) under the proposition that Cu has one electron per atom and Pd or Ni has valence Z less than one, thus bringing about $2k_F \approx K_p$ for Cu-rich alloys containing 20% P. But for the corresponding Pd-rich or Ni-rich alloys the value of $2k_F$ falls below K_p. This viewpoint is in accord with the finding that the negative temperature coefficient of resistivity occurs at a lower concentration of metalloid in Au–Si and Cu–P than in Pd–Si and Ni–P alloys.

It can be shown (Cote and Meisel 1977) that at high temperature ρ varies as a constant $\pm T/\theta^2$ and ρ goes as a constant $\pm T^2/\theta^3$ at low temperature. Here θ is the Debye temperature and the sign is determined by the relative position of $2k_F$ to K_p. A quadratic temperature dependence of ρ at low temperature is indeed observed in all glassy alloys. In the unrelaxed or isoconfigurational glassy state, $2k_F$ can be assumed to expand or contract to exactly compensate for any peak shifts in the structure factor (Cote *et al* 1977a). The temperature coefficient of resistivity may be approximated from the temperature dependence of the structure factor. For glassy alloys

with $2k_F \approx K_p$, $\alpha_R \approx 1/a(K_p)\, da\,(K_p)/dT \approx (1/W)\, dW/dT$ where $W(T)$ is the Debye–Waller factor. The reduction in the structure factor peaks is measured to be of the order of -10^{-4} K^{-1} in $Ni_{75}P_{25}$ (Cote *et al* 1977a), Zr–Cu (Waseda *et al* 1977a) and $Nb_{40}Ni_{60}$ (Basak *et al* 1979). This is also the value estimated from the temperature dependence of $W(T)$ and is in fair agreement with the maximum negative temperature coefficient observed.

The change in resistivity associated with structural relaxation has been reported for Au–Ge–Si (Chen and Turnbull 1968), Zr–Cu (H S Chen unpublished) and Pd–Si (Chen and Turnbull 1968). As shown in figure 16, the $Zr_{65}Cu_{35}$ glass which exhibits a negative temperature coefficient of resistivity shows an irreversible increase in resistivity ρ associated with structural stabilisation above 400 K and a rapidly decreas-

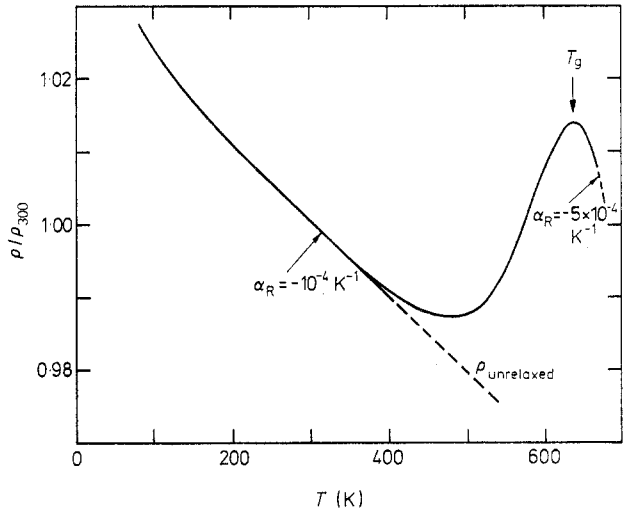

Figure 16. The variation in resistivity ρ upon heating (~ 10 K min^{-1}) a glassy $Zr_{65}Cu_{35}$. T_g is the glass transition temperature.

ing ρ through the glass transition temperature, T_g, with the temperature coefficient $\alpha_R \approx -5 \times 10^{-4}$ K^{-1}, many times larger than that ($\alpha_R \approx -10^{-4}$ K^{-1}) of the unrelaxed structure at room temperature. The change in ρ through the glass transition is reversible. The total incremental resistivity due to structural relaxation of the quenched Zr–Cu is $\sim 5\%$. In Pd–Si glassy alloys which show a small positive $\alpha_R \approx 0{\cdot}5 \times 10^{-4}$ K^{-1}, the change in ρ associated with structural changes exhibits just the opposite behaviour and is less pronounced. Available structure data indeed indicate an increase of $\sim 3\%$ in $a(K_p)$ of quenched glasses upon annealing, e.g. Pd–Si (Masumoto *et al* 1976a) and FeNiPB (Egami and Ichikawa 1978). $a(K_p)$ of the glass would decrease through the glass transition as it does in liquid metals with increasing temperature. Quantitative comparison between experiment and theory is, however, complicated by observed non-uniform shifts in peak positions in $a(K)$ resulting from the structural rearrangement involved (§4.4).

8.1.3. Superconducting properties. For over two decades, it has been demonstrated that a wide variety of amorphous metal films, obtained by vapour deposition on to a

substrate at liquid helium temperature, are superconducting with a T_c usually higher than the equilibrium crystalline value (Buckel and Hilsch 1954, Bergman 1976). These amorphous films are stabilised by impurities and anneal into crystalline phase at relatively low temperatures. Quantitative property studies of these films are quite limited because of gaseous contamination and large internal surface area which may play a significant role in the superconductivity. These films are often characterised as strong coupled superconductors with the ratio of energy gap $\Delta_0 \approx 2{\cdot}25 k_B T_c$. A systematic study of T_c has been reported recently in series of 4d and 5d transition-metal alloy films (Collver and Hammond 1973, 1977). They found that T_c is a triangular function of the average number of electrons per atom (e/a) peaking at $e/a = 6{\cdot}4$ with $T_c \approx 10$ K, in contrast to the well-known double-peaked structure of the Matthias rule for crystalline superconductors (Matthias 1955). The peak location at $e/a = 6{\cdot}4$, which corresponds to where the d shell of the atom is half-filled with five electrons with parallel spins, suggests the dominance of atom-like parameters in determining the superconducting properties of these amorphous materials.

A number of glassy superconductors have been obtained in the form of disc or ribbon by melt quenching with T_c ranging from 1 to 5 K, e.g. $Au_{24}La_{76}$, $T_c = 3{\cdot}3$ K (Johnson *et al* 1975), $Nb_{58}Rh_{42}$, $T_c = 4{\cdot}7$ K; $Zr_{70}Pd_{30}$, $T_c = 2{\cdot}4$ K (Johnson and Poon 1975), $Zr_{76}Rh_{24}$, $T_c = 4{\cdot}2$ K (Togano and Tachikawa 1975), $Zr_{70}Be_{30}$, $T_c = 2{\cdot}8$ K (Hasegawa and Tanner 1977), $(Mo,Ru)_{80}P_{20}$, $T_c = 3{\cdot}5$–9 K (Johnson *et al* 1978) and $Zr_{70}M_{30}$ with M = Co, Ni or Cu, $T_c = 2$–$3{\cdot}5$ K (Räpp *et al* 1978b). The transition is well defined with the width of transition less than 0·1 K. The transition temperature of the glassy alloys is generally lower than that of amorphous transition metals at corresponding e/a values. Since an increasing distance in the periodic table between alloying elements was found to decrease T_c of disordered alloys (Collver and Hammond 1977), the difference in T_c observed may be related to the fact that the T_c against e/a curve for the amorphous metals is based on alloys of neighbouring elements in the periodic table, while the results of the liquid-quenched glasses are for binary alloys with elements far apart. The very short electronic mean free path in these glasses suggests that the electronic interaction leading to pairing is of a local nature. The early transition metals contribute about two free electrons/atom, while the late transition metals give about one free electron/atom, so that the density of states at the Fermi surface $N(k_F)$ varies smoothly upon alloying. T_c of glassy alloys thus is essentially determined by the strength of an atomic-based electron–phonon coupling and is expected to show no abrupt change with composition.

An increase in T_c by a factor of two or more is generally seen following the crystallisation to intermetallic states. An enhancement of T_c from 3 to 7 K is achieved (Hasegawa and Tanner 1978) in partially crystalline $Be_{20}Nb_{15}Zr_{65}$ ribbons apparently resulting from a glassy Be–Zr base matrix containing high T_c crystalline precipitated superconducting particles. Interestingly, the partially crystalline sample retains high strength and toughness characteristics of glassy metals.

The transition from the superconducting to the normal state in a magnetic field is reversible which may be expected as the coherence length $\epsilon \sim 10^{-6}$ cm is much larger than atomic scale disorder $\sim 10^{-7}$ cm so that favourable centres for flux pinning are absent. The critical current $J_c(H)$ varies as H^{-1} or $J_c(T)H_{c2}(T) = \alpha_c(T)$. $\alpha_c(0)$ is observed to be of the order 2×10^8 A G cm^{-2}. The maximum values of J_c(at $T = 2$ K, $H = 0$) are relatively low, e.g. $\sim 10^4$ A cm^{-2} for $La_{76}Au_{24}$ and 3×10^4 A cm^{-2} for $Nb_{58}Rh_{42}$ as compared with reported $J_c = 2 \times 10^6$ A cm^{-2} for liquid-quenched microcrystalline Nb_3Al (Lo *et al* 1977).

The superconducting behaviour of these glassy alloys agrees with the BCS theory in the weak-coupled limit and they may be considered as ideal type-II superconductors. This contrasts to the previous results on amorphous non-transition metals which are characterised by a strong electron–phonon coupling (Bergman 1973). The energy gap Δ_0 for the former is found from specific heat measurements to be small $\sim 1{\cdot}47\, k_B T_c$ for $Zr_{70}Pd_{30}$ (Graebner *et al* 1977). Shull and Naugle (1977) estimated from the incremental specific heat at T_c a relatively small electron–phonon coupling constant $\lambda \sim 0{\cdot}8$ in LaAu compared to the amorphous non-transition metals ($\lambda = 2{\cdot}0$). Tunnelling experiments reveal that the energy gap in many amorphous transition-metal-based superconductors behaves in accordance with the BCS weak-coupling limit (e.g. Tsuei *et al* 1977). Apparently the structural disorder alone does not significantly enhance electron–phonon interactions.

8.1.4. Electronic properties. Electronic properties of glassy metals have been investigated with various measurements, e.g. specific heat in Pd–Si alloys (Chen and Haemmerle 1972, Golding *et al* 1972, Mizutani *et al* 1978, Lasjaunias *et al* 1978) and in $Zr_{70}Pd_{30}$ (Graebner *et al* 1977), the angular correlation of positron annihilation radiation in Pd–Cu–Si and Ni–P (Chuang *et al* 1975, Doyama *et al* 1975), photoemission measurements in Pd–Cu–Si and Nb–Ni (Nagel *et al* 1976, 1977), K_β emission spectra from Al and Si dissolved in Fe, Ni or Cu (Tanaka *et al* 1975), energy loss spectra of Pd–Ni–P (Shen *et al* 1978), optical properties of Au–Si (Hauser *et al* 1978), Auger electron microscopy of vapour-quenched films of (Au, Ag or Cu)–Si alloys (Hiraki *et al* 1975), and nuclear magnetic resonance measurements of Pd–Ni–P and Pt–Ni–P (Heiman *et al* 1978). These studies reveal three common phenomena: (i) the metalloid impurity Si is metallic in metal-rich alloys, (ii) there is no significant difference in electronic structure such as the density of states at the Fermi surface, core levels and valence bands, between the glassy and crystalline alloys, and (iii) a slight shift of core levels to higher binding energy by 0·3 eV and reduction in the density of state $N(k_F)$ in the alloys are seen as compared with that of constituent metal elements.

The temperature coefficient (γ_e) of the electronic contribution to the specific heat of non-magnetic alloys both in glassy and crystalline phases ranges from $\sim 1{\cdot}2 \times 10^{-3}$ J mol^{-1} K^{-2} in Pd–Cu–Si to $\sim 3 \times 10^{-3}$ J mol^{-1} K^{-2} in Zr–Pd which, for comparison, is 2–4 times larger than the values typically observed in noble metals but is much lower than that found in Pd($\gamma_e \sim 10 \times 10^{-3}$ J mol^{-1} K^{-2}). The reduction in γ_e is due to the filling of the Pd valence band by free electrons in Si or Zr. However, undoubtedly a part of γ_e in alloys may be attributed to the possible presence of a tail of the d electrons.

Whether a minimum in the density of states $N(k_F)$ would occur in the glass-forming composition (Nagel and Tauc 1975) has raised a considerable debate, although the reduction in $N(k_F)$ observed via the measurements of photoemission spectra in the Pd–Cu–Si and Nb–Ni alloys has been interpreted to indicate the existence of a minimum in $N(k_F)$. Careful specific heat measurements in series of Pd–Si alloys (Mizutani *et al* 1978) show to the contrary a maximum at electrons per atom $\sim 1{\cdot}60$. Furthermore, the density of states $N(k_F)$ evaluated from the electronic specific heat is found to be higher in the ferromagnetic Fe-based glassy alloys than in similar crystalline metals, Fe or Ni (Onn *et al* 1977, Stewart and Phillips 1978). NMR studies of Pd–Ni–P alloys (Hines *et al* 1978) indicate a smooth variation of the Knight shift with P content suggesting the absence of any minimum in the density of states.

8.2. Thermal properties at low temperatures

For the past decade there has been an intensive effort to understand the properties of glassy materials (Pohl and Salinger 1976, Halperin 1976). Experimental measurements reveal great regularity in the behaviour of thermal property for all non-metallic glasses, but this behaviour distinctively differs from that for crystalline materials. For example, below 1 K the dominant contribution to specific heat varies linearly with temperature and the thermal conductivity approaches a temperature dependence T^2 in non-crystalline materials. This contrasts remarkably with the behaviour of non-metallic crystals in which the specific heat varies as T^3 and the addition of minute impurities can drastically lower the thermal conductivity. Anomalous behaviour has been also seen in acoustic attenuation and velocity dispersion measurements. Among a number of models proposed to explain these phenomena a two-level tunnelling model (Anderson *et al* 1972, Phillips 1972, Jäckle 1972) has been most satisfactory. However, the connection between these two levels and the nature of the glassy state is still not known.

Glassy alloys being atomically densely packed constitute a structurally distinct non-crystalline system. Availability of glassy metals either in ribbon or cylindrical form have kindled in recent years a number of investigations at low temperatures of acoustic behaviour, thermal conductivity and specific heat measurements. The problem of separating the phonon contribution from the electronic contribution to the thermal property in metals can be eliminated in the superconducting state (Graebner *et al* 1977). Despite the distinct difference in structural packing between the dense-packed glassy metals and loose-packed non-metallic glasses, experimental data reveal striking similarity between these two classes of glasses in behaviour and magnitude of many low-temperature thermal properties.

8.2.1. Acoustic behaviour above 2 K. A broad absorption peak and velocity dispersion at temperatures 2–20 K have been seen in a number of glassy metals at frequencies ranging from kHz (Barmatz and Chen 1974) to 500 MHz (Dutoit 1974). The absorption is characterised by a broad distribution of relaxation times which is similar to that observed in fused silica glasses (Scott and MacCrone 1970). The data exhibit a large asymmetry in the low-temperature regime. Associated with it, the Young's modulus shows dispersion effects. Crystallisation removes the asymmetry. The attenuation maximum obeys the Arrhenius expression with low activation energy of 5·7 meV in Pd–Si and ~ 30 meV for $Fe_{75}P_{16}C_4Si_2Al_3$. A similar broad asymmetric distribution of the internal-friction peak in sputtered films of Nb_3Ge has been observed lately by Berry *et al* (1978), but the peak occurs at a higher temperature, ~ 260 K, with a higher activation energy, $\sim 0{\cdot}52$ eV, and is attributed to the diffusion of H atoms. As with the internal friction measurements, the magnitude of dispersion in the cold-rolled sample is greater by three-fold than in the as-quenched sample (Barmatz *et al* 1976). Annealing reduces both the velocity dispersion and internal friction. Recent measurements show that the temperature dependence of velocity is linear between 4–20 K in amorphous Ni–P, Co–P and glassy Pd–Si (Bellessa *et al* 1977, Bellessa 1977, 1978) as well as in amorphous selenium and fused silica. It is in strong contrast to the usual T^4 law of the decrease in sound velocity in crystals. The observed low-temperature asymmetry in relaxation processes is explained by the coupling of localised atomic arrangements to the bulk through a Grüneisen parameter, which leads to temperature-dependent relaxation strength (Scott and MacCrone 1970).

Bellessa (1978) argued that the linear temperature dependence of the sound velocity cannot be explained with relaxation processes. Golding *et al* (1978) demonstrated, however, that a linear T dependence in the region 4–20 K can be interpreted with a tunnelling model with a broad spectrum of decay rate.

8.2.2. Thermal property anomaly below 1 K. It has been seen in electrodeposited amorphous Ni–P and Co–P (Bellessa *et al* 1977, Bellessa 1977) and in a liquid-quenched glassy Pd–Cu–Si (Bellessa and Bethoux 1977, Golding *et al* 1977) that the sound velocity (v) increases with increasing temperature below ~ 2 K then decreases at higher temperatures, as exemplified for the Pd–Cu–Si in figure 17. Below 1 K the experimental data are well fitted with a logarithmic temperature law. Above 5 K, v decreases linearly with T. The temperature dependence is larger for the transverse

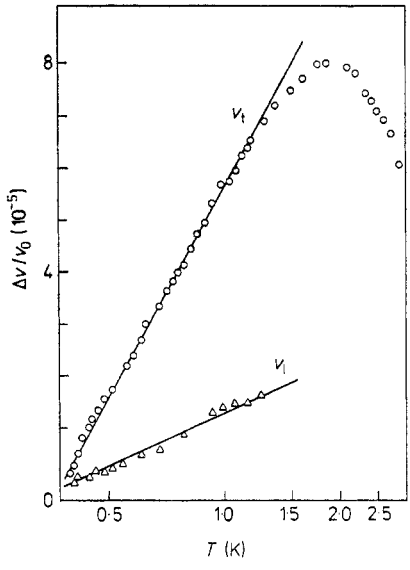

Figure 17. Relative variation of the sound velocity as a function of temperature in glassy $Pd_{77\cdot5}Cu_6Si_{16\cdot5}$. The longitudinal v_l and transverse wave velocity v_t are, respectively, 4·6 km s^{-1} and 1·8 km s^{-1} (Bellessa and Bethoux 1977).

waves than for the longitudinal waves. The peculiar temperature dependence of the velocity has been supposed to arise from the interaction of the sound wave with the two-level systems. At low temperatures, a resonant acoustic attenuation leads to an increase in sound velocity and the velocity variation is given by Pichê *et al* (1974):

$$[v(T)-v(T_0)]/v(T_0)=(n_0\gamma^2/\rho v)\ln(T/T_0) \tag{8.3}$$

where n_0 is the two-level system density of states, γ is the coupling constant between the two-level systems and the ultrasonic wave, v is the sound velocity and T_0 is an arbitrary reference temperature. The coupling constants $n_0\gamma^2$ deduced from equation (8.3) are of the order of 2×10^7 erg cm^{-3} for Pd–Cu–Si and Ni–P, and are smaller, $\sim 5\times10^6$ erg cm^{-3}, for Co–P. These values are one order of magnitude smaller than in vitreous silica in which $n_0\gamma^2\approx10^8$ erg cm^{-3}.

An increase in the absorption as the temperature is lowered below 100 mK is seen in the Pd–Cu–Si (Golding *et al* 1977, 1978). The sound velocity varies nearly logarithmically above 0·10 K and passes through to a minimum near 20 mK. This behaviour

is similar to that in fused silica and is consistent with the two-level tunnelling model. In contrast to studies of fused silica, however, no saturation in the resonant absorption at 20 mK is observed over a wide range of acoustic intensities. This difference arises from the fact that the process of the decay of configurational states in a glassy metal is very rapid compared to insulating glasses. The interactions between conduction electrons and a two-level system in which the states can give up their energy to the electrons, rather than to phonons, are suggested to drastically shorten the lifetime of the states.

Matey and Anderson (1977) find in glassy Pd–Cu–Si samples the same anomalous behaviour as found for insulating glasses that the thermal conductivity κ decreases with decreasing temperature, becomes nearly independent of T near 10 K, and varies as T^2 at lower temperature. However, in this study, it is necessary to subtract from the measured conductivity the electronic contribution which is important at low temperatures. This problem is overcome by making measurements on superconductors far below the transition temperatures so that the electronic contributions to thermal conductivity and specific heat become negligible.

The specific heat and thermal conductivity of a superconducting glassy $Zr_{70}Pd_{30}$ (Graebner *et al* 1977) are shown in figure 18. The onset of superconductivity is found at $T_c = 2{\cdot}53$ K with a resistive transition width of 10 mK and a C_p width of 30 mK. Below 1 K, the specific heat may be fitted by the expression

$$C_p = DT + BT^3 + E \exp(-F/T) \tag{8.4}$$

and the thermal conductivity by a single power law

$$\kappa = 8{\cdot}6 \times 10^{-4}\, T^{1{\cdot}9} \qquad \text{W cm}^{-1}\,\text{K}^{-1}. \tag{8.5}$$

The T^3 coefficient corresponds to a Debye temperature $\theta \approx 180$ K and the exponent F can be identified with Δ_0/k_B, where Δ_0 is the energy gap at $T=0$ and is found to be

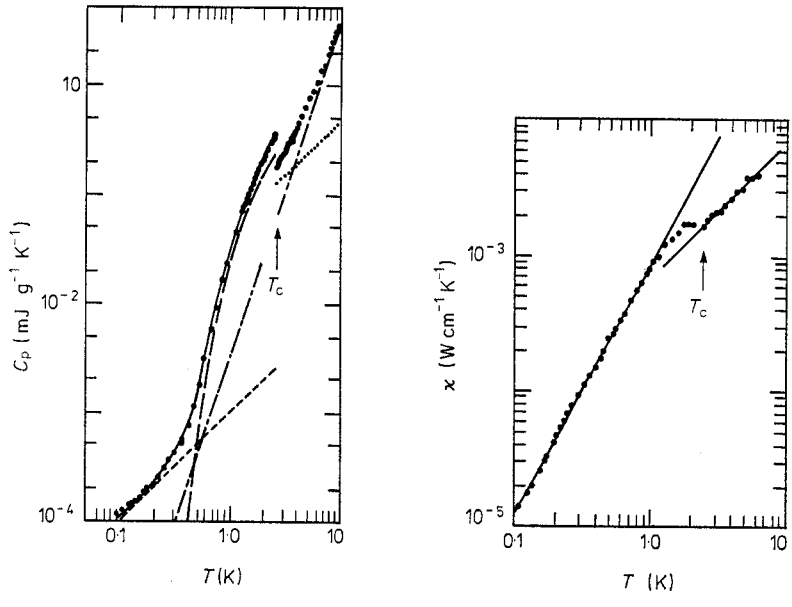

Figure 18. Heat capacity C_p and thermal conductivity κ of the superconducting glassy alloy $Zr_{70}Pd_{30}$ (Graebner *et al* 1977).

$1{\cdot}47\ k_B T_c$. The linear term (equation (8.4)) in the specific heat at the lowest temperatures and the $T^{1{\cdot}9}$ dependence of κ are both supposed to arise from a two-level configurational system. The former yields a density of states $n_0 = 6D\rho/\pi^2 k_B{}^2 = 2{\cdot}7 \times 10^{33}$ erg^{-1} cm^{-3}. Here the density of the glass equals 7·86 g cm^{-3}. Under reasonable assumptions, the coupling strength can be estimated from thermal conductivity data. It gives $\bar{n}\gamma_T{}^2 = 5 \times 10^7$ erg cm^{-3} for the $Zr_{70}Pd_{30}$ glass which is strikingly close to the value of 9×10^7 erg cm^{-3} found in fused silica. Here γ_T is the deformation potential for the two-level systems coupled to transverse waves, and $\bar{n}$ is the density of two-level systems which participate in resonant absorbing phonons and is approximately 4% of n_0.

The linear specific heat and approximately quadratic thermal conductivity of this material below T_c are strikingly similar to those properties in typical insulating glasses (e.g. Stephens 1976) for which the coefficient of the linear term in C_p lies in the range $(0{\cdot}4\text{–}6) \times 10^{-3}$ mJ g^{-1} K^{-2} and the coefficient of the $T^{1{\cdot}9}$ thermal conductivity is in the range 10^{-4}–10^{-3} W cm^{-1} K^{-3}. The present values are thus near the low end of the C_p range and the high end of the κ range. It may be concluded that the anomalous specific heat, thermal conductivity, velocity dispersion, and the sound absorption in glassy metals below 1 K are due to the intrinsic defects characteristic of the disordered state. The microscopic nature of these two-level states is still unknown.

8.3. Corrosion behaviour

Glassy alloys containing certain amounts of chromium and phosphorus are seen to exhibit extremely high corrosion resistance in acid and neutral solutions such as 1 M H_2SO_4, 6% $FeCl_3$ and 1 N HCl (Naka *et al* 1974, 1976a). Glassy $Fe_{80}P_{13}C_7$ alloy is seen to be fairly unstable in corrosive environments. However, the addition of Cr remarkably improves the corrosion resistance. Glassy Fe–$CrP_{13}C_7$ alloys containing more than 8% Cr show extremely high corrosion resistance far surpassing commercial 18Cr–8Ni stainless steel, particularly in $FeCl_3$ solution in which the latter suffers pitting and crevice corrosion. This superior corrosion resistance of the FeCrPC glasses has been attributed to the rapid formation of thick uniform highly corrosion-resistant passive films.

ESCA studies (Asami *et al* 1976) reveal that the passive film formed on the glassy FeCrPC alloys consists mainly of $CrO_x(OH)_y$, bound water and oxidised phosphorus. The main composition is not essentially different from the passive films on ordinary stainless steels, except for oxidised phosphorus. Thus the extremely high corrosion resistance of the glassy metals must arise from causes other than the composition of passive film and may lie in the kinetics of passivation and the defect densities in substrates. Further investigations with potentiodynamic polarisation and potentiostatic anodic polarisation measurements (Hashimoto *et al* 1976a) find that the corrosion potential of the glassy alloys is generally high and shows higher reactivity as compared with the 18Cr–8Ni stainless steel, apparently resulting from the presence of a large amount of semimetallic elements. Paradoxically it is the high reactivity of the glassy alloys which prompts the rapid formation of thick highly corrosion-resistant passive films enriched in chromium via rapid dissolution of other elements in the alloys. The high reactivity of glassy alloys also constitutes a rapid recovery of rupture sites of the passive film. The chromium enrichment process in forming passive films thus enables the glassy alloy to exhibit a superior corrosion behaviour at lower Cr content as compared with stainless steel.

The addition of nickel to chromium-bearing glassy Fe alloys is seen (Hashimoto *et al* 1976b) to raise the corrosion potential through the acceleration of oxygen reduction and retardation of anodic dissolution, and thus prompts the formation of a protective passive film which consists mainly of $(CrO)_x(OH)_y$. Consequently the nickel addition is particularly effective in improving corrosion resistance for the glassy alloys containing a small amount, $\sim 3\%$, of Cr.

The rate of formation of the chromium-enriched passive film in the active state depends on the rate of active dissolution. Consequently the effectiveness of additive metalloids on the corrosion resistance of Fe–Cr-based glasses simply reflects whether the individual element accelerates the active dissolution. The alloys containing phosphorus and carbon have the highest corrosion potential and thus are the best corrosion-resistive while the alloys with Si or B are less reactive and exhibit a poor corrosion resistance (Naka *et al* 1978a).

The high corrosion resistance of Cr-bearing Fe-based glassy alloys is further enhanced by the structurally and chemically homogeneous single-phase nature of the glassy state which ensures the formation of 'uniform' passive films. The high reactivity of the crystalline alloys can arise from high densities of crystal defects such as grain boundaries, impurity segregates, etc, which act as nucleation sites for corrosion. The dominant role played by the chemical homogeneity of the glassy phase is demonstrated further in $Zr_{50}Cu_{50}$ and $Ti_{50}Cu_{50}$ alloys (Naka *et al* 1978b) in which the corrosion resistance of the glassy alloys is higher than that of crystalline alloys of the same composition. The addition of P to the TiCu glass increases greatly the corrosion resistance as a result of spontaneous passivation due to the rapid enrichment of Ti in the alloy–solution interface.

Strikingly a small amount of molybdenum additive ($< 3\%$) to FePC alloys is more effective than a chromium additive in reducing the corrosion rates (Naka *et al* 1978c, Hashimoto *et al* 1978). The glassy alloys containing 4% or more Mo are passivated without pitting even in 1 N HCl, contrary to the crystalline Fe–Mo alloys in which passivation of iron is hindered by the addition of Mo in 1 N H_2SO_4. X-ray photoelectron spectroscopy (XPS) reveals that the passive films of the glassy alloys consist mainly of ferric oxyhydroxide which is the same as the main constituent of passive films formed on crystalline iron in 1 N H_2SO_4. The increasing tendency for anodic passivation with the addition of Mo is attributed to the lowering of the active dissolution of the alloy owing to the formation of a hexavalent molybdenum species on the alloy surface. Tungsten addition is found to be a less effective corrosion inhibitor than Cr or Mo.

9. Conclusion

A glass, upon subsequent annealing, exhibits three characteristic features: (*a*) structural relaxation to more stable states, (*b*) devitrification into crystalline phase(s), and (*c*) transformation from a glass to a liquid at the glass transition. Structural relaxation can occur far below the glass transition. The rate and magnitude of structural relaxation are higher for glasses obtained at higher quenching rate and for those subjected to plastic deformation or irradiation. The modes of structural relaxation may be identified as (i) a low-temperature one with a relatively low activation energy ~ 1 eV, and (ii) a high-temperature one near the glass transition. The latter has been extensively investigated for non-metallic glasses, while the former, in comparison, has not been much explored and reported only in glassy metals. The low-

temperature structural relaxation often causes a drastic reduction in mechanical ductility and a considerable modification in magnetic anisotropies, and thus deserves further exploration. The devitrification process generally proceeds through nucleation and growth. The most commonly observed dendritic and facet growth morphologies are the expected modes of crystallisation of a glass. Many glassy metals crystallise without any indication of glass transition. Apparently, in these glassy alloys the nucleation barrier for crystallisation is so low that devitrification occurs concurrently with the structural relaxation processes. In practice, the glass transition observed is a kinetic phenomenon and not a thermodynamic phase transition. The glass transition temperature which marks the transition from a non-equilibrium glassy structure to an internal equilibrium liquid state or vice versa increases with the rates of heating or cooling. The glass transition temperature can be higher by ~ 100 K when the rate of cooling varies from 1 K s^{-1} to 10^6 K s^{-1}.

Limited diffusion data of Pd–Si glasses reveal three significant features. Firstly diffusivities (D) appear to scale as the reciprocal of viscosities following a Stoke–Einstein relationship. Secondly D are critically dependent on the state of glassy structure. D of the unrelaxed glass can be many orders of magnitude higher than the relaxed one, with a relatively low activation energy ~ 1 eV. Thirdly, below T_g the diffusivities in the unrelaxed glass remain even after a hundred atomic 'jumps'. This implies that the time constant τ_s for structural relaxation is at least two orders of magnitude longer than that (τ_D) for diffusive process. The high diffusivities $D \approx 10^{-17}$ cm^2 s^{-1} and the large time constant ratio $\tau_s/\tau_D \geqslant 10^2$ in the unrelaxed glasses explain remarkably well many aging phenomena, such as the reversible aging of magnetic anisotropy, unattenuated high rates of crystal growth and a wide spread in the activation energy for crystallisation.

The kinetic criteria predict fairly well the ease of glass forming of alloys. The interactions among constituent atoms, which lead to the low-lying eutectic and raise T_g of the alloy, facilitate the glass formation and enhance the thermal stability of the resultant glass. A number of models have been proposed to account for the eutectic formation and the stability of glassy alloys. The structure and electronic models based on the stabilisation of the liquid phase are seen to be inconsistent with many experimental results. Alternatively the strong composition dependence of liquidus temperatures may simply reflect the destabilisation of the crystalline mixtures and the stability of the intermetallic phases which constitute the eutectic system. Further thermodynamic and electronic property measurements of glass-forming alloys near the eutectic composition would be of great interest.

Homogeneous dense random packing structures are nowadays the most widely accepted models for the structures of most glassy metals. Microcrystalline models yield distribution functions and structure factors which are less satisfactory with experimental data as compared with the random packing models. Furthermore many physical properties of glassy metals, e.g. the low diffusivities in the glassy state as compared with the grain-boundary diffusivities, and only slight change in the lifetime and angular correlation of positron annihilation radiation upon vitrification, suggest the absence of grain boundaries in glassy metals. Strong atomic interactions may lead to a short-range order which often resembles that in intermetallic crystalline phases. In metal-metalloid systems the metalloid atoms are prohibited from direct contact in the glassy state, while the structures of amorphous RE–TM and glassy TM–TM alloys are described by more or less random distribution of constituent atoms. Causes of these distinctively different structures between the metal–metalloid and

metal–metal system are not clear. The weaker atomic interactions and the steeper core potential of the d shell in transition metals are suggested to favour the random mixing in the metal–metal glasses.

Glassy metals are not perfectly isotropic. Structural anisotropies can be induced during solidification, plastic deformation and magnetic aging of glasses. They are manifested by recoverable time-dependent deformations and magnetic anisotropies. Development of structural and compositional anisotropies is often detectable by x-ray diffraction and electron microscopy in thin films obtained by atomic condensation, but is less pronounced in liquid-quenched glassy metals. Structural and compositional inhomogeneities on a larger scale, ~ 100 Å, however, have been observed for glassy metals subjected to prolonged heat treatments and neutron irradiation.

Glassy metals exhibit many unique properties arising from the absence of crystalline symmetry and grain-boundary-type inhomogeneities. Because of the lack of translational periodicity, the fracture strength of glassy metals, $\sigma_f = E/50$, approaches the theoretical strength $\sigma_{th} \approx E/20$. Fracture proceeds by highly localised shear deformations, apparently resulting from the absence of work hardening. Magnetic anisotropy may arise from either magnetostrictive or structural origins. Magnetic aging that reduces residual strains would lead ideally to soft magnetic behaviour. The absence of structural and compositional inhomogeneities leads to the low acoustic losses in many glasses, and to the high corrosion resistance of Cr-containing glassy alloys by forming 'uniform' protective passive films enriched in chromium.

Atomic processes which cause plastic deformation may differ, although macroscopic fracture and fatigue behaviour are very similar in many features between glassy metals and high-strength crystalline metals. The rate of fatigue crack propagation and the width of the plastic zone in glassy metals obey a power law of the stress intensity very similar to those observed for a variety of steels, according to the expected behaviour from the elastic–plastic theory of cracks. The loss of ductility in aged Fe-based glasses is believed to arise from the induced structural and compositional inhomogeneities resulting in stress concentrations around the clusters. Phenomenologically it is similar to the temper embrittlement behaviour of steels. The atomic nature of the embrittlement processes is, however, still not clear. Both atomic ordering and electronic structure of constituent atoms are found to influence the flow strength and critical yield strain of glassy alloys.

Changes in the structure and the state of magnetisation modify the density, thermal expansion and Young's modulus of glasses. Certain ferromagnetic glassy metals exhibit a strikingly large magnetoelastic behaviour. Magnetic annealing that induces a uniaxial magnetic anisotropy can alter considerably the magnitude, field and temperature dependence of the ΔE effect. Elinvar characteristics thus can be obtained for most ferromagnetic glassy alloys by proper heat treatments. Excellent Invar characteristics are found in the Fe–B and Fe–P systems containing $\sim 17\%$ metalloid element.

Since the coherence length or correlation distance for magnetic ordering becomes much larger than the atomic scale disorder $\sim 10^{-7}$ cm, the critical behaviour is governed mainly by macroscopic structure. In this sense, glassy metals may be considered as ideal isotropic ferromagnets and would exhibit better-defined critical behaviour than do crystalline alloys. This has been borne out by magnetisation and neutron scattering measurements of Fe-based glassy alloys, in which the low-temperature spin wave excitations and critical behaviour are in excellent agreement with theory for a crystalline Heisenberg ferromagnet. Remarkably, models developed for

crystalline magnetic materials describing the static and dynamic properties are also found to be applicable to glassy metals.

Electrical resistivity of glassy metals shows two main characteristics: (i) a resistivity minimum below which ρ obeys a ln T law, and (ii) a relatively high resistivity $\sim 10^{-4}$ Ω cm varying quadratically with temperature at $T \leqslant 50$ K and linearly near room temperature. The temperature coefficient of resistivity is small and changes sign with composition. The origins of the resistivity minimum is still controversial. In comparison the quadratic and linear temperature dependence of resistivity can be explained satisfactorily in the framework of extended Ziman theory for liquid alloys. The resistivity variations associated with temperature and structural relaxation are seen to be in good agreement with the model. Because of the very short electronic mean free path in glassy metals, electronic interactions leading to pairing are of an atomic nature. The superconducting temperature of glassy alloys is thus essentially determined by the strength of atomic-based electron–phonon coupling. The superconducting behaviour of intertransition-metal glassy alloys as well as many amorphous transition-metal-based superconductors is found to agree with the BCS theory in the weak-coupling limit. This contrasts to the result with amorphous non-transition metals which is often characterised by a strong electron–phonon coupling. Whether the structural disorder alone would significantly alter the electron–phonon interaction remains to be answered.

At very low temperatures ($\leqslant 1$ K) there has been found for many metallic glasses a logarithmic increase in sound velocity, and for a superconducting glassy $Zr_{70}Pd_{30}$ ($T_c = 2{\cdot}53$ K), a linear temperature term in specific heat and a $T^{1{\cdot}9}$ dependence of thermal conductivity. These low-temperature anomalies are regularly observed for all non-metallic glasses and are supposed to arise from the two-level configurational system of intrinsic defects characteristic of disordered structure. Despite the distinct difference in structural packing between the dense-packed glassy metals and loose-packed non-metallic glasses, the estimated density of states and the strength of coupling constants are strikingly similar for metallic and other insulating glassy materials.

Although there is no actual large-scale industrial use of glassy metals, considering their combined technologically interesting properties, e.g. high strength with toughness, low acoustic loss, excellent soft magnetic behaviour, corrosion resistance to chloride and sulphuric solutions, and above all, inexpensive processing into ribbons or strips, one may expect that glassy metals will play an important role in a number of applications in the near future. Potential applications in both electronic and power devices have been discussed extensively by Luborsky *et al* (1978), Graham and Egami (1978) and Murakami (1978). Based on combinations of excellent mechanical, magnetic and chemical properties which are otherwise unattainable in crystalline metals, potential uses of metallic glasses in specific area such as audio tape-recorder heads, magnetic shields, brazing metals, magnetic filters for water processing, etc, would be envisioned.

Acknowledgments

The author is indebted to present colleagues, particularly L R Testardi and B G Bagley for critical comments on the manuscript, and K A Jackson and H J Leamy for valuable discussions. The author is also grateful to D Turnbull at Harvard, and T Masumoto and Tohoku University.

References

Adam G and Gibbs J H 1965 *J. Chem. Phys.* **43** 139–46
Adams D J and Matheson A J 1972 *J. Chem. Phys.* **56** 1989–94
Ali A, Grant W A and Grandy P J 1978 *Phil. Mag.* B **37** 353
Andonov P 1976 *J. Non-Cryst. Solids* **22** 145–58
Anderson P W 1961 *Phys. Rev.* **124** 41–53
Anderson P W, Halperin B I and Varma C M 1972 *Phil. Mag.* **25** 1–9
Andrews R, Grant W A, Grundy P J and Williams J S 1976 *Nature* **262** 380–1
Angell C A 1968 *J. Am. Ceram. Soc.* **51** 117–24
Arai K I and Tsuya N 1978 *J. Appl. Phys.* **49** 1918–20
Arai K I, Tsuya N, Yamada N and Masumoto T 1976a *IEEE Trans. Magn.* **MAG-12** 936–8
Arai K I, Tsuya N, Yamada N, Shirae H, Fujimori H, Saito H and Masumoto T 1976b *Rapidly Quenched Metals* (Cambridge, Mass: MIT Press) pp489–94
Argon A S and Salama M 1976 *Mater. Sci. Engng* **23** 219–30
Asami K, Hashimoto K, Masumoto T and Shimodaira S 1976 *Corrosion Sci.* **16** 909–1014
Ashby M F and Logan J 1973 *Scr. Metall.* **7** 513
Ast D G and Krenitsky D 1976 *Mater. Sci. Engng* **23** 241–6
Axe J D, Passell L and Tsuei C C 1974 *AIP Conf. Proc.* **24** 119–20
Axe J D, Shirane G, Mizoguchi T and Yamauchi K 1977 *Phys. Rev.* B **15** 2763–70
Babic E, Girt E, Krsnik R and Leontic B 1970 *J. Phys. E: Sci. Instrum.* **3** 1014
Bagley B G 1974 *Amorphous and Liquid Semiconductors* (New York: Plenum) pp1–43
Bagley B G, Chen H S and Turnbull D 1968 *Mater. Res. Bull.* **3** 159–68
Bagley B G and DiSalvo F J 1973 *Amorphous Magnetism* ed H O Hooper and A M deGraaf (New York: Plenum) pp143–8
Bagley B G and Turnbull D 1965 *Bull. Am. Phys. Soc.* **10** 1101
—— 1970 *Acta Metall.* **18** 857–62
Bagley B G and Vogel E M 1975 *J. Non-Cryst. Solids* **28** 29–32
Barfield R N and Kitchener J A 1955 *J. Iron Steel Inst.* **180** 324–9
Barmatz M and Chen H S 1974 *Phys. Rev.* B **9** 4073–83
Barmatz M, Wyatt K W and Chen H S 1976 *Rapidly Quenched Metals* (Cambridge, Mass. MIT Press) pp431–9
Barrett C S and Massalski T B 1966 *Structure of Metals* (New York: McGraw-Hill)
Basak S, Clarke R and Nagel S R 1979 *Phys. Rev.* B **10** 4278–86
Bauhofer W and Simon A 1978 *Phys. Rev. Lett.* **40** 1730–3
Bedell J R 1975 *US Patent No* 3862658
Bellessa G 1977 *J. Phys. C: Solid St. Phys.* **10** L285–7
—— 1978 *Phys. Rev. Lett.* **40** 1456–9
Bellessa G and Bethoux O 1977 *Phys. Lett.* **62A** 125–6
Bellessa G, Doussineau P and Levelut A 1977 *J. Phyique Lett.* **38** L65–6
Bennett C H 1972 *J. Appl. Phys.* **43** 2727–34
Bennett C H, Polk D E and Turnbull D 1971 *Acta Metall.* **19** 1295–8
Bergman G 1973 *Phys. Rev.* B **7** 4850–60
—— 1976 *Phys. Rep. Phys. Lett.* **27** 159–85
Bernal J D 1960 *Nature* **185** 68–70
Berry B S 1978 *Metallic Glasses* (Metals Park, Ohio: ASM) pp161–89
Berry B S and Pritchet W C 1973 *J. Appl. Phys.* **44** 3122–6
—— 1975 *Phys. Rev. Lett.* **34** 1022–5
—— 1976a *J. Appl. Phys.* **47** 3295–301
—— 1976b *AIP Conf. Proc.* **34** 292–7
Berry B S, Pritchet W C and Tsuei C C 1978 *Phys. Rev. Lett.* **41** 410–3
Bestul A B and Chang S S 1964 *J. Chem. Phys.* **40** 3731–3
Birac C and Lesueur D 1976 *Phys. Stat. Solidi* a **36** 247–51
Birgeneau R J, Tarvin J A, Shirane G, Gyorgy E M, Sherwood R C, Chen H S and Chien C L 1978 *Phys. Rev.* B **18** 2192–5
Bockrie J, O'M Mackenzie J D and Kitchner J A 1955 *Trans. Faraday Soc.* **51** 1734
Boswell P G 1977 *Scr. Metall.* **11** 701–7
Boswell P G and Chadwick G A 1976 *J. Mater. Sci.* **11** 2287

Boucher B Y 1972 *J. Non-Cryst. Solids* **7** 277–84
Boudreaux B S and Gregor J M 1976 *Rapidly Quenched Metals* (Cambridge, Mass.: MIT Press) pp323–7
Bozorth R M 1951 *Ferromagnetism* (New York: Van Nostrand) pp684–9
Brenner S S 1956 *J. Appl. Phys.* **27** 1484–91
Brooks H A 1976 *J. Appl. Phys.* **47** 344–5
Brooks H A and Chen H S 1977 *J. Appl. Phys.* **48** 4837–8
Brown G S, Testardi L R and Wernick J H 1977 *Solid St. Commun.* **23** 895–8
Buckel W and Hilsch R 1954 *Z. Phys.* **138** 109–20
Burton J J and Ray R P 1971 *J. Non-Cryst. Solids* **6** 393–6
Busch G and Güntherodt H J 1974 *Solid St. Phys.* **29** 235–313
Buschow K H J and Beekmans N M 1978 *Rapidly Quenched Metals III* vol 2 (London: Metals Society) pp133–6
Buschow K H J, van Diepen A M, Beekmans N M and Biesterbos J W M 1978 *Solid St. Commun.* **28** 181–5
Cahn R W 1970 *Fizika 2 Suppl. 2* Paper 25
—— 1976 *Nature* **259** 271–2
Calka A, Matyja H, Polk D E, Giessen B C, Sande J V and Madhava M 1977 *Scr. Metall.* **11** 65–70
Cargill G S 1970 *J. Appl. Phys.* **41** 12–29
—— 1974 *AIP Conf. Proc.* **18** 631–5
—— 1975a *Solid St. Phys.* **30** 227–321
—— 1975b *AIP Conf. Proc.* **24** 138–44
Chadwick G A 1965 *Liquids: Structure, Properties, Solid Interactions* (New York: Elsevier) pp326–45
Chattopadhyay K, Ramachandrarao P, Lele S and Anantharaman T R 1976 *Rapidly Quenched Metals* (Cambridge, Mass.: MIT Press) pp157–61
Chaudhari P, Graczyk J F, Henderson D and Steinhardt 1975 *Phil. Mag.* **31** 727–37
Chaudhari P and Turnbull D 1978 *Science* **199** 11–21
Chen H S 1973 *Scr. Metall.* **7** 931–5
—— 1974a *Acta Metall.* **22** 1505–11
—— 1974b *Acta Metall.* **22** 897–900
—— 1976a *Mater. Sci. Engng* **25** 59–69
—— 1976b *Mater. Sci. Engng* **23** 151–4
—— 1976c *Acta Metall.* **24** 153–8
—— 1976d *Phys. Stat. Solidi* a **34** K127–9
—— 1976e *Appl. Phys. Lett.* **29** 12–4
—— 1976f *Appl. Phys. Lett.* **29** 328–30
—— 1976g *Mater. Sci. Engng* **26** 79–82
—— 1977a *The Structure of Non-Crystalline Materials* ed P H Gaskell (London: Taylor and Francis) pp79–84
—— 1977b *Scr. Metall.* **11** 367–70
—— 1978a *J. Non-Cryst. Solids* **27** 257–63
—— 1978b *J. Appl. Phys.* **49** 3289–91
—— 1978c *J. Non-Cryst. Solids* **29** 223–9
—— 1978d *J. Appl. Phys.* **49** 462–3
—— 1978e *J. Appl. Phys.* **49** 4595–7
Chen H S and Chuang S Y 1975a *J. Electron.Mater.* **4** 783–9
—— 1975b *Appl. Phys. Lett.* **27** 316–7
—— 1977 *Appl. Phys. Lett.* **31** 255–6
Chen H S and Coleman E 1976 *Appl. Phys. Lett.* **28** 245–7
Chen H S and Goldstein M 1972 *J. Appl. Phys.* **43** 1642–8
Chen H S and Haemmerle W H 1972 *J. Non-Cryst. Solids* **11** 161–9
Chen H S and Jackson K A 1978 *Metallic Glasses* (Metals Park, Ohio: ASM) pp75–96
Chen H S and Krause J T 1977 *Scr. Metall.* **11** 761–4
Chen H S and Miller C E 1970 *Rev. Sci. Instrum.* **41** 1237–8
—— 1975 *Mater. Res. Bull.* **11** 49–54
Chen H S and Park B K 1973 *Acta Metall.* **21** 395–400
Chen H S and Polk D E 1974 *J. Non-Cryst. Solids* **15** 174–8

Chen H S and Turnbull D 1967 *Appl. Phys. Lett.* **10** 284–6
—— 1968 *J. Chem. Phys.* **48** 2560–71
—— 1969 *Acta Metall.* **17** 1021–31
Chen H S, Kimerling L C, Poate J M and Brown W L 1978 *Appl. Phys. Lett.* **32** 461–3
Chen H S, Ferris S D, Gyorgy E M, Leamy H J and Sherwood R C 1975a *Appl. Phys. Lett.* **26** 405–6
Chen H S, Krause J T and Sigety E A 1973/74 *J. Non-Cryst. Solids* **13** 321–7
Chen H S, Krause J T and Coleman E 1975b *J. Non-Cryst. Solids* **18** 157–71
—— 1975c *Scr. Metall.* **9** 787–9
Chen H S, Leamy H J and Barmatz M 1971 *J. Non-Cryst. Solids* **5** 444–8
Chen H S, Leamy H J and O'Brien M J 1973 *Scr. Metall.* **7** 115–20
Chen H S, Sherwood R C, Leamy H J and Gyorgy E M 1976 *IEEE Trans. Magn.* **MAG-12** 933–5
Chen H S, Sherwood R C and Gyorgy E M 1977 *IEEE Trans. Magn.* **MAG-13** 1538–40
Chen H S and Wang T T 1970 *J. Appl. Phys.* **41** 5338–9
Chen H S and Waseda Y 1979 *Phys. Stat. Solidi* a **51** 593–9
Chi G C and Cargill G S 1976a *AIP Conf. Proc.* **31** 359–65
—— 1976b *Mater. Sci. Engng* **23** 155–9
Chi G C, Chen H S and Miller C E 1978 *J. Appl. Phys.* **49** 1915–7
Chien C L and Hasegawa R 1977 *Phys. Rev.* B **16** 2115–23
Chikazumi S and Graham C D 1969 *Magnetism and Metallurgy* (New York: Academic) pp577–619
Chopra K L 1969 *Thin Film Phenomena* (New York: McGraw-Hill) pp195–214
Chou C P 1976 *Phys. Rev. Lett.* **37** 1004–7
Chou C P and Turnbull D 1975 *J. Non-Cryst. Solids* **17** 168–88
Christian J W 1965 *The Theory of Transformations in Metals and Alloys* (Oxford: Pergamon) pp525–48
Chuang S Y, Tao S J and Chen H S 1975 *J. Phys. F: Metal Phys.* **5** 1681–6
Clements W G and Cantor B 1976 *Proc. 2nd Int. Conf. on Rapidly Quenched Metals* (Cambridge, Mass.: MIT Press) pp267–72
Cochrane R W and Cargill G S 1974 *Phys. Rev. Lett.* **32** 476–8
Cochrane R W, Harris R, Strom-Olsen J O and Zuckerman M J 1975 *Phys. Rev. Lett.* **35** 676–9
Coleman E 1976 *Mater. Sci. Engng* **23** 161–7
Collver M M and Hammond R H 1973 *Phys. Rev. Lett.* **30** 92–5
—— 1977 *Solid St. Commun.* **22** 55–7
Connell G A N 1975 *Solid St. Commun.* **16** 109–12
Cote P J and Meisel L V 1977 *Phys. Rev. Lett.* **39** 102–5
Cote P J, Capsimalis G P and Meisel L V 1977a *Phys. Rev.* B **16** 4651–4
Cote P J, Capsimalis G P and Salinger G L 1977b *Amorphous Magnetism* (New York: Plenum) pp499–511
Cullis A G, Poate J M and Borders J A 1976 *Appl. Phys. Lett.* **28** 314–6
Davies H A 1976 *Phys. Chem. Glasses* **17** 159–73
Davies H A, Aucote J and Hull J B 1973 *Nature Phys. Sci.* **246** 13–4
Davies H A and Hull J B 1974 *J. Mater. Sci.* **9** 707–17
Davis L A 1975 *J. Mater. Sci.* **10** 1557–64
—— 1976 *J. Mater. Sci.* **11** 711–7
—— 1978 *Metallic Glasses* (Metal Parks, Ohio: ASM) pp191–223
Davis L A and Kavesh S 1975 *J. Mater. Sci.* **10** 453–9
Davis L A, Ray R, Chou C P and O'Hanley R C 1976 *Scr. Metall.* **10** 541–6
Dienes G J 1953 *Phys. Rev.* **91** 1283–4
Dietz G and Klett K 1978 *J. Magnet. Magn. Mater.* **8** 57–60
Dixmier J and Duwez P 1973 *J. Appl. Phys.* **44** 1189–93
Doi K, Kayano H and Masumoto T 1977 *Appl. Phys. Lett.* **31** 421–2
Douglas R W and Isard J O 1951 *J. Soc. Glass Tech.* **35** 206–25
Doyama M, Tanigawa S, Kuribayashi K, Fukushima H, Hinode K and Saito F 1975 *J. Phys. F: Metal Phys.* **5** L230–2
Dragomir I 1973 *The Properties of Liquid Metals* (London: Taylor and Francis) pp507–12
Dreirach O, Evans R, Güntherodt H J and Künzi H A 1972 *J. Phys. F: Metal Phys.* **2** 709–25

Dubinin E L, Esin O A, Vatolin N A and Kuranov A A 1967 *Russian J. Inorganic Chem.* **12** 1670–1
Duhaj P, Barancok D and Ondreijka A 1976 *J. Non-Cryst. Solids* **21** 411–28
Durand J 1976 *IEEE Trans. Magn.* **MAG-12** 945–7
Dutoit M 1974 *Phys. Lett.* **50A** 221–3
Dutoit M and Chen H S 1973 *Appl. Phys. Lett.* **23** 357–8
Duwez P 1967 *Trans. Am. Soc. Metals* **60** 607–33
—— 1976 *Ann. Rev. Mater. Sci.* **6** 83–117
Duwez P and Lin S C H 1967 *J. Appl. Phys.* **38** 4096–7
Egami T and Dahlgren S D 1978 *J. Appl. Phys.* **49** 1703–5
Egami T and Flanders P J 1975 *AIP Conf. Proc.* **29** 220–1
Egami T, Flanders P J and Graham C D 1974 *AIP Conf. Proc.* **24** 697–701
Egami T and Ichikawa T 1978 *Mater. Sci. Engng* **32** 293–5
Elliot J F and Gleiser M 1960 *Thermochemistry of Steelmaking* (Reading, Mass: Addison-Wesley)
Emmes W C, Vrijen J and Radelaar S 1975 *J. Non-Cryst. Solids* **18** 299–302
Evans R, Greenwood D A and Lloyd P 1971 *Phys. Lett.* **35A** 57–8
Farges J, DeFerrady M F, Rooult B and Torchet G 1975 *J. Physique* **36** C2
Felsch W 1969 *Z. Phys.* **219** 280–99
—— 1970a *Z. Angew. Phys.* **29** 217–24
—— 1970b *Z. Angew. Phys.* **30** 275–7
Finney J L 1970 *Proc. R. Soc.* A **319** 479–93
—— 1977 *Nature* **266** 309–14
Fisher H J and Phillips A 1954 *J. Metals Trans. AIME* 1060–70
Frank F C 1952 *Proc. R. Soc.* A **215** 43–6
Freed R L and Vander Sande 1978 *J. Non-Cryst. Solids* **27** 9–28
Fujimori H, Arai K I, Shirae H, Saito H, Masumoto T and Tsuya N 1976a *Jap. J. Appl. Phys.* **15** 705–6
Fujimori H, Kikuchi M, Obi Y and Masumoto T 1976b *J. Jap. Inst. Metals* **41** 111–6
Fujimori H and Masumoto T 1978 *Suppl. Sci. Rep. RITU* A 181–97
Fujimori H, Masumoto T, Chi Y and Kikuchi M 1974 *Jap. J. Appl. Phys.* **13** 1889–90
Fujimori H, Morita H, Obi Y and Ohta S 1977 *Amorphous Magnetism II* (New York: Plenum) pp393–402
Fujimori H, Obi Y, Masumoto T and Saito H 1976c *Mater. Sci. Engng.* **23** 281–4
Fujita F E, Masumoto T, Kitaguch M and Ura M 1977 *Jap. J. Appl. Phys.* **16** 1731
Fukamichi K, Kikuchi M, Arakawa S and Masumoto T 1977a *Solid St. Commun.* **23** 955–8
Fukamichi K, Kikuchi M and Masumoto T 1977b *Sci. Rep. Res. Inst. Tohoku Univ.* A **26** 225–31
Fukamichi K, Kikuchi M, Hiroyoshi H and Masumoto T 1978 *Suppl. Sci. Rep. RITU* A 199–214
Fukunaga T, Ichikawa T and Suzuki K 1977 *Proc. 2nd Int. Symp. on Amorphous Magnetism II* (New York: Plenum) pp521–8
Fukunaga T, Misawa M, Fukamichi K, Masumoto T and Suzuki K 1978 *Rapidly Quenched Metals III* vol 2 (London: Metals Society) pp325–32
Funakoshi N, Kanamori P and Manabe T 1977 *Jap. J. Appl. Phys.* **16** 515–6
Furrer P and Warlimont H 1977 *Mater. Sci. Engng* **28** 127–37
Gambino R J, Chandhari P and Cuomo J J 1974 *AIP Conf. Proc.* **18** 578–92
Gel'd P V and Gertman Yu M 1961a *Fiz. Metal. Metalloved.* **10** 793–4
—— 1961b *Fiz. Metal. Metalloved.* **12** 47–50
Gibbs J H and DiMarzio E A 1958 *J. Chem Phys.* **28** 373–83
Giessen B C and Elliott R O 1978 *Rapidly Quenched Metals III* vol 1 (London: Metals Society) pp406–11
Giessen B C, Hong J, Kabacoff L, Polk D E, Raman R and Amand S 1978 *Rapidly Quenched Metals III* vol 1 (London: Metals Society) pp249–60
Giessen B C and Wagner C N J 1972 *Liquid Metals* ed S Z Beer (New York: Dekker) pp633–95
Gilman J J 1973 *J. Appl. Phys.* **44** 675–99
—— 1975a *Phys. Today* **28** 46–53
—— 1975b *J. Appl. Phys.* **46** 1625–33
Golding B, Bagley B G and Hsu F S L 1972 *Phys. Rev. Lett.* **29** 68–70

Golding B, Graebner J E and Hammerle W H 1977 *Proc. Int. Conf. on Lattice Dynamics* (Paris: Flammarion Science) pp348–50
Golding B, Graebner J E, Korn A B and Black J L 1978 *Phys. Rev. Lett.* **41** 1487–91
Graebner J E, Golding B, Schultz R J, Hsu F S L and Chen H S 1977 *Phys. Rev. Lett.* **39** 1480–3
Graham C D and Egami T 1978 *Ann. Rev. Mater. Sci.* **8** 423–57
Grant W A 1978 *J. Vac. Sci. Technol.* **15** 1644–8
Gudmundsson H, Aström H U, New D, Rao K V and Chen H S 1978 *J. Physique Colloq.* C6–943
Gubanov A I 1960 *Sov. Phys.–Solid St.* **2** 468
Güntherodt H J and Künzi H U 1978 *Metallic Glasses* (Metals Park, Ohio: ASM) pp247–74
Gupta D, Tu K N and Asai K W 1975 *Phys. Rev. Lett.* **35** 796–9
Gyorgy E M 1978 *Metallic Glasses* (Metals Park, Ohio: ASM) pp275–303
Gyorgy E M, Leamy H J, Sherwood R C and Chen H S 1975 *AIP Conf. Proc.* **29** 198–203
Halperin B I 1976 *Ann. NY Acad. Sci.* **279** 173–9
Hansen M 1958 *Constitution of Binary Alloys* (New York: McGraw-Hill)
Hasegawa R 1972 *Phys. Lett.* **38A** 5–7
Hasegawa R and Tanner L E 1977 *Phys. Rev.* B **16** 3925–8
—— 1978 *J. Appl. Phys.* **49** 1196–9
Hasegawa R and Tsuei C C 1970 *Phys. Rev.* B **2** 1631–43
—— 1971 *Phys. Rev.* B **3** 214–9
Hashimoto K, Naka M, Asami K and Masumoto T 1979 *Corrosion Sci.* **19** 165–70
Hashimoto K, Naka M and Masumoto T 1976a *Sci. Rep. Res. Inst. Tohoku Univ.* **26A** 48–54
Hashimoto K, Osada K, Masumoto T and Shimodaira S 1976b *Corrosion Sci.* **16** 71–6
Hatta S, Egami T and Graham C D 1978 *Rapidly Quenched Metals III* vol 2 (London: Metals Society) pp183–7
Hausch G and Török E 1978 *Phys. Stat. Solidi* a **50** 159–64
Hauser J J and Tauc J 1978 *Phys. Rev.* B **17** 3371–80
Hauser E, Zirke R J, Tauc J, Hauser J J and Nagel S R 1978 *Phys. Rev. Lett.* **40** 1733–6
Hayes T M, Allen J W, Tauc J, Giessen B C and Hauser J J 1978 *Phys. Rev. Lett.* **40** 1282–5
Heeger A J 1975 *Solid St. Phys.* **23** 283–441
Heiman N, Hempstead R D and Kazama N 1978 *J. Appl. Phys.* **49** 5663–7
Heimendahl L V 1975 *J. Phys. F: Metal Phys.* **5** L141–4
Herd S R and Chaudhari P 1974 *Phys. Stat. Solidi* a **26** 627–42
Herold U and Köster U 1978 *Rapidly Quenched Metals III* vol 1 (London: Metals Society) pp281–90
Hines W A, Kabacoff L T, Hasegawa R and Duwez P 1978 *J. Appl. Phys.* **49** 1724–6
Hiraki A, Shimizu A, Iwami M, Narusawa T and Komiya S 1975 *Appl. Phys. Lett.* **26** 57–60
Hiroyoshi H, Fukamichi K, Kikuchi M, Hoshi A and Masumoto T 1978 *Phys. Lett.* **65A** 163–5
Hiwatari Y, Matsuta H, Ogawa T, Igita N and Ueda A 1974 *Prog. Theor. Phys.* **52** 1105–23
Ho P S, Lewis J E and Howard J K 1977 *J. Vac. Sci. Technol.* **14** 322–5
Ho P S, Lewis J E, Wildman H S and Howard J K 1976 *Surf. Sci.* **57** 393–405
Hoare M R and Pal P 1975 *Adv. Phys.* **24** 645–78
Hultgren R, Desai P D, Hawkins D T, Gleiser M and Kelley K K 1973 *Selected Values of the Thermodynamic Properties of Binary Alloys* (Metals Park, Ohio: ASM)
Hume-Rothery W and Anderson E 1960 *Phil. Mag.* **5** 383–405
Ichikawa T 1973 *Phys. Stat. Solidi* a **19** 707–15
—— 1975 *Phys. Stat. Solidi* a **29** 293–302
Imura T, Doi M and Kosaki H 1978 *Suppl. Sci. Rep. RITU* A 47–62
Inoue A, Masumoto T, Arakawa S and Iwadachi T 1978a *Rapidly Quenched Metals III* vol 1 (London: Metals Society) pp265–72
Inoue A, Masumoto T and Kimura H 1978b *J. Jap. Inst. Met.* **42** 303–9
Iwasaki H and Masumoto T 1978 *J. Mater. Sci.* **13** 2171–6
Jäckle J 1972 *Z. Phys.* **257** 212–23
Jackson K A 1958 *Growth and Perfection of Crystal* (New York: Wiley) pp319–23
—— 1969 *Progress in Solid State Chemistry* vol 4 (Oxford: Pergamon) pp229–47
Jagielinski T, Arai K I, Tsuya N, Ohmuma S and Masumoto T 1977 *IEEE Trans. Magn.* **MAG-13** 1553–5
Jensen J, Kristensen W D and Cotterill R M J 1973 *Phil. Mag.* **27** 623–32

Johnson W L and Poon S J 1975 *J. Appl. Phys.* **46** 1787–92
Johnson W L, Poon S J, Durand J and Duwez P 1978 *Phys. Rev.* B **18** 206–17
Johnson W L, Poon S J and Duwez P 1975 *Phys. Rev.* B **11** 150–4
Jones H 1973 *Rep. Prog. Phys.* **36** 1425–97
Kauzeman W 1948 *Chem. Rev.* **43** 219–56
Kavesh S 1978 *Metallic Glasses* (Metals Park, Ohio: ASM) pp36–73
Kawashima A, Hashimoto K and Masumoto 1976 *Corrosion Sci.* **34** 307–9
Kayano H, Masumoto T, Tomizawa S and Yajima S 1977 *Sci. Rep. Res. Inst. Tohoku Univ.* **26A** 240–5
Kazama N and Kameda M 1976 *AIP Conf. Proc.* **34** 307–9
Kazama N S, Mitera M and Masumoto T 1978 *Rapidly Quenched Metals III* vol 2 (London: Metals Society) pp164–71
Kemeny T, Vineze I, Fogarassy B and Arajs 1979 *Phys. Rev.* B **20** 476–88
Ketter F 1966 *Handb. Phys.* **18** part 2, p1
Kikuchi M, Fukamichi K and Masumoto T 1977 *Sci. Rep. Res. Inst. Tohoku Univ.* **26A** 232–9
Kimura H and Masumoto T 1975 *Scr. Metall.* **9** 211–22
Kimura H, Murata T and Masumoto T 1977 *Sci. Rep. RITU* A **26** 270–82
Klement W, Willens R H and Duwez P 1960 *Nature* **187** 869–70
Kobliska R J, Aboat J A, Grangulee A, Cuomo J J and Klokholm E 1978 *Appl. Phys. Lett.* **33** 473–5
Kondo J 1975 *Solid St. Phys.* **23** 183–281
Korn D, Mürer W and Zilbold G 1973 *Z. Phys.* **260** 351–60
Korn D, Pfeifle H and Zilbold G 1974 *Z. Phys.* **270** 195–202
Kovacs A J 1963 *Fort. Hochpolym.-Forsch.* **3** 394–507
Krause J T and Chen H S 1976 *Proc. 2nd Int. Conf. on Rapidly Quenched Metals* (Cambridge, Mass.: MIT Press) pp425–30
Krishnanand K D and Cahn R W 1975 *Scr. Metall.* **9** 1259–61
Laridjani M, Ramachandrarao P and Cahn R W 1972 *J. Mater. Sci.* **7** 627–30
Lasjaunias J C, Ravex A and Thoulouze D 1978 *J. Phys. F: Metal Phys.* **9** 803–14
Leamy H J, Chen H S and Wang T T 1972 *Metal. Trans.* **3** 699–708
Leamy H J and Dirks A G 1977 *J. Phys. D: Appl. Phys.* **10** L95–8
Leamy H J, Ferris S D, Joy D C, Sherwood R C, Gyorgy E M and Chen H S 1976 *Proc. 2nd Int. Conf. on Rapidly Quenched Metals* (Cambridge, Mass.: MIT Press) pp511–8
Leamy H J, Ferris S D, Norman G, Joy D C, Sherwood R C, Gyorgy E M and Chen H S 1975a *Appl. Phys. Lett.* **26** 259–60
Leamy H J, Gyorgy E M, Sherwood R C, Wakiyama T and Chen H S 1975b *AIP Conf. Proc.* **29** 211–3
Lee D and Devine T M 1976 *Proc. 2nd Int. Conf. on Rapidly Quenched Metals* (Cambridge, Mass.: MIT Press) pp393–9
Lewis B G and Davies H A 1976 *Mater. Sci. Engng* **23** 179–82
Li J C M 1976 *Frontier in Material Science* (New York: Marcel Dekker) p527
—— 1978 *Metallic Glasses* (Metals Park, Ohio: ASM) pp224–46
Liang V K C and Tsuei C 1973 *Phys. Rev.* B **7** 3215–25
Liou Z L, Brown W L, Homer R and Poate J M 1977 *Appl. Phys. Lett.* **30** 626–8
Liebermann H H and Graham C D 1976 *IEEE Trans. Magn.* **MAG-13** 921–3
Liebermann H H, Graham C D and Flanders P J 1977 *IEEE Trans. Magn.* **MAG-13** 1541–3
Lin S C H 1969 *J. Appl. Phys.* **2** 173–5
Lo K, Bevk J and Turnbull D 1977 *J. Appl. Phys.* **48** 2597–600
Logan J 1975a *Phys. Stat. Solidi* a **32** 361–8
—— 1975b *Scr. Metall.* **9** 379–82
Logan J and Ashby M F 1974 *Acta Metall.* **22** 1047–54
Luborsky F E 1976 *AIP Conf. Proc.* **29** 209–10
—— 1977 *Mater. Sci. Engng* **28** 139–44
Luborsky F E, Becker J J, Frischmann P G and Johnson L A 1978 *J. Appl. Phys.* **49** 1769–74
Luborsky F E, Becker J J and McCary R O 1975 *IEEE Trans. Magn.* **MAG-11** 1644–9
Luborsky F E and Walter J L 1977a *IEEE Trans. Magn.* **MAG-13** 953–6
—— 1977b *IEEE Trans. Magn.* **MAG-13** 1635–8
—— 1978 *Mater. Sci. Engng* **35** 255–61
Luborsky F E, Walter J L and Le Grand D G 1976 *IEEE Trans. Magn.* **MAG-12** 730–2

Lynn J W, Shirane G, Birgeneau R J and Chen H S 1976 *AIP Conf. Proc.* **34** 313–5
Maddin R and Masumoto T 1972 *Mater. Sci. Engng* **9** 153–62
Mader S 1966 *Recrystallisation Grain Growth and Textures* (Cleveland, Ohio: ASM) pp523–37
Mader S and Nowick A S 1965 *Appl. Phys. Lett.* **7** 57–9
Mader S, Nowick A S and Widmer H 1967 *Acta Metall.* **15** 203–14
Maeda K and Takeuchi 1978 *Suppl. Sci. Rep. Res. Inst. Tohoku Univ.* A 87–94
Maitrepierre P 1970 *J. Appl. Phys.* **41** 498–503
Mangin Ph, Marchal G, Rodmacq B and Janot Chr 1977 *Phil. Mag.* **36** 643–56
Mangin G, Margin Ph and Janot Chr 1975 *Phil. Mag.* **32** 1007–21
Maringer R E and Mobley C E 1974 *J. Vac. Sci. Technol.* **11** 1067–71
Masumoto T 1977 *Sci. Rep. Res. Inst. Tohoku Univ.* A **26** 246–62
Masumoto T, Hashimoto K and Fujimori H 1975 *Sci. Rep. Res. Inst. Tohoku Univ.* A **25** 232–44
Masumoto T, Inoue A and Kimura H 1977 *J. Jap. Inst. Met.* **41** 730–7
Masumoto T and Kimura H 1975a *Jap. J. Metals* **39** 273–80
—— 1975b *Jap. J. Metals* **39** 133–41
Masumoto T, Kimura H, Inoue A and Waseda Y 1976a *Mater. Sci. Engng* **23** 141–4
Masumoto T and Maddin R 1971 *Acta Metall.* **19** 725–41
—— 1975 *Mater. Sci. Engng* **29** 1–24
Masumoto T, Waseda Y, Kimura H and Inoue A 1976b *Sci. Rep. Res. Inst. Tohoku Univ.* A **26** 21–35
Matey J R and Anderson A C 1977 *J. Non-Cryst. Solids* **23** 129–37
Matthias B T 1955 *Phys. Rev.* **97** 74–6
Miedema A R, Boom R and De Boer F R 1975 *J. Less Common Metals* **41** 283–98
Miyazaki T and Takahashi M 1978 *Jap. J. Appl. Phys.* **17** 1755–63
Mizoguchi T, McGuire T R, Kirkpatrick S and Gambino R J 1977 *Phys. Rev. Lett.* **38** 89–92
Mizoguchi T, Kudo T, Irisawa T, Watanabe N, Niimura N, Mizawa M and Suzuki K 1978 *Rapidly Quenched Metals III* vol 2 (London: Metals Society) pp384–91
Mizoguchi T and Yamauchi K 1974 *J. Physique* **35** C4 287–9
Mizoguchi T, Yamauchi K and Miyajima H 1973 *Amorphous Magnetism* (New York: Plenum) pp325–30
Mizutani U, Hartwig K T, Massalski T B and Hopper R W 1978 *Phys. Rev. Lett.* **41** 661–4
Mook H A, Wakabayashi N and Pan D 1974 *Phys. Rev. Lett.* **34** 1029–33
Moss M, Smith D L and Lefever R A 1964 *Appl. Phys. Lett.* **5** 120–1
Mott N F 1972 *Phil. Mag.* **26** 1249–61
Mott N F and Gurney R W 1938 *Rep. Prog. Phys.* **5** 46–63
Murakami K 1978 *Suppl. Sci. Rep. RITU* A 221–31
Murata T, Kimura H and Masumoto T 1976a *Scr. Metall.* **10** 705–9
Murata T, Tomizawa S, Fukase T and Masumoto T 1976b *Scr. Metall.* **10** 181–4
Nagel S R, Fisher G B, Tauc J and Bagley B G 1976 *Phys. Rev.* B **13** 3284–9
Nagel S R and Tauc J 1975 *Phys. Rev. Lett.* **35** 380–3
Nagel S R, Tauc J and Giessen B C 1977 *Solid St. Commun.* **22** 471–4
Nagel S R, Vassiliou J, Horn P M and Giessen B C 1978 *Phys. Rev.* B **17** 462–7
Nagumo M and Takahashi T 1976 *Mater. Sci. Engng* **23** 257–9
Naka M, Hashimoto K and Masumoto T 1974 *J. Jap. Inst. Met.* **38** 835–41
—— 1976a *Corrosion* **32** 146–52
—— 1978a *J. Non-Cryst. Solids* **28** 403–13
—— 1978b *J. Non-Cryst. Solids* **30** 29–36
—— 1978c *J. Non-Cryst. Solids* **29** 61–5
Naka M, Nishi Y and Masumoto T 1978d *Rapidly Quenched Metals III* vol 1 (London: Metals Society) pp231–8
Naka M, Tomizawa S, Masumoto T and Watanabe T 1976b *Proc. 2nd Int. Conf. on Rapidly Quenched Metals* (Cambridge, Mass.: MIT Press) pp273–7
Narita K, Yamasaki J and Fukunaga H 1978 *IEEE Trans. Magn.* **MAG-14** 1016–8
Ninomiya T 1977 *Proc. Symp. on Structure of Non-Crystalline Materials* (London: Taylor and Francis) pp45–7
Oberle R, Künzi H U and Güntherodt H J 1976 *Phys. Lett.* **58A** 272–4
Ogura T, Fukushima K and Masumoto T 1976 *Mater. Sci. Engng* **23** 231–5
Ogura T, Masumoto T and Fukushima K 1975 *Scr. Metall.* **9** 109–14

O'Handley R C 1975 *AIP Conf. Proc.* **29** 206–8
O'Handley R C, Hasegawa R, Ray R and Chou C P 1976 *Appl. Phys. Lett.* **29** 330–2
Ohnuma S and Masumoto T 1978 *Rapidly Quenched Metals III* vol 2 (London: Metals Society) pp197–204
Ohring M and Haldipur A 1971 *Rev. Sci. Instrum.* **42** 530–1
O'Leary W P 1975 *J. Phys. F: Metal Phys.* **5** L175–80
Omori S and Hashimoto Y 1973 *J. Jap. Soc. Powder and Powder Metall.* **20** 80–6
Onn D G, Antoniuk T H, Donnelley T A, Johnson W D, Egami T, Prater J T and Durand J 1978 *J. Appl. Phys.* **49** 1730–2
Onn D G, Johnson W D, Gleeson P F, Donnelly T A, Egami T and Liebermann H H 1977 *J. Phys. C: Solid St. Phys.* **10** L639–42
Onorato P I K and Uhlmann D R 1976 *J. Non-Cryst. Solids* **22** 367–78
Orowan E 1952 *Proc. 1st National Congress of Applied Mechanics* (New York: ASME) p453
Osamura K, Shibue K, Shingu P H and Murakami Y 1979 *J. Mater. Sci.* **14** 945
Pampillo C A 1975 *J. Mater. Sci.* **10** 1194–227
Pampillo C A and Chen H S 1974 *Mater. Sci. Engng* **13** 181–8
Phillips W A 1972 *J. Low Temp. Phys.* **7** 351–60
Piché L, Maynard R, Hunklinger S and Täckle J 1974 *Phys. Rev. Lett.* **32** 1426–9
Pickart S J, Rhyne J J and Alperin H A 1974 *Phys. Rev. Lett.* **33** 424–7
Pietrowsky P 1963 *Rev. Sci. Instrum.* **34** 455–6
Poate J M, Borders J A, Cullis A G and Hirvonen J K 1977 *Appl. Phys. Lett.* **30** 365–8
Poate J M, Turner P A, DeBonte W J and Yabalom J 1975 *J. Appl. Phys.* **46** 4275
Pohl R O and Salinger G L 1976 *Ann. NY Acad. Sci.* **279** 150–72
Polk D E 1972 *Acta Metall.* **20** 485–91
Polk D E and Turnbull D 1972 *Acta Metall.* **20** 493–8
Pond R and Maddin R 1967 *Trans. Metall. Soc. AIME* **245** 407–12
Pratten N A and Scott M G 1978 *Scr. Metall.* **12** 137–42
Predecki P, Giessen B C and Grant N J 1965a *Trans. Metall. Soc. AIME* **233** 1438–9
Predecki P, Mullendore A W and Grant N J 1965b *Trans. Metall. Soc. AIME* **233** 1581–6
Rahman A 1972 *Interatomic Potentials and Simulation of Lattice Defect* (New York: Plenum) pp233–48
Rahman A, Mandel M J and McTague J P 1976 *J. Chem Phys.* **64** 1564–8
Raj K, Budnick J L, Alben R, Chi G C and Cargill G S 1976 *AIP Conf. Proc.* **31** 390–5
Ramachandrarao P, Lavidjani M and Cahn R W 1972 *Z. Metall.* **63** 43–9
Räpp O, Grindberg J E and Rao K V 1978a *J. Appl. Phys.* **49** 1733–4
Räpp O, Lindberg B, Chen H S and Rao K V 1978b *J. Less Common Metals* **62** 221–4
Rostogi P K 1973 *J. Mater. Sci.* **8** 140–3
Rawson H 1967 *Inorganic Glass-Forming System* (New York: Academic)
Ray R, Giessen B C and Grant N J 1968 *Scr. Metall.* **2** 357–9
Ray R, Hasegawa R, Chou C P and Davis L A 1977 *Scr. Metall.* **11** 973–8
Ray R and Musso E 1976 *US Patent No* 3981722
Rhyne J J, Pichart S and Alperin H A 1974 *AIP Conf. Proc.* **18** 563–77
Roberge R and Herman H 1968 *Mater. Sci. Engng* **3** 62–3
Robinson A L 1973 *Science* **182** 908–10
Romanov A A and Kochegarov V G 1964 *Fiz. Metal. Metalloved.* **19** 67–73
Roy R 1970 *J. Non-Cryst. Solids* **3** 33–40
Ruby S L, Love J C, Flinn P A and Zabransky B J 1975 *Appl. Phys. Lett.* **27** 320–2
Ruhl R C 1967 *Mater. Sci. Engng.* **1** 313–20
Sadoc J F and Dixmier J 1976 *Mater. Sci. Engng* **23** 187–92
Sadoc J F, Dixmier J and Guinier A 1973 *J. Non-Cryst. Solids* **12** 46–60
Sadoc J F and Lienard A 1978 *Rapidly Quenched Metals III* vol 2 (London: Metals Society) pp405–9
Savage H I, Clark A E and Powers J M 1975 *IEEE Trans. Magn.* **MAG-11** 1355–7
Schroeder G, Schäfer R and Kronmüller H 1978 *Phys. Stat. Solidi* a **50** 475–81
Scott G D 1962 *Nature* **194** 956–8
Scott G D and Kilgour D M 1969 *J. Phys. D: Appl. Phys.* **2** 863
Scott M G and Maddin R 1976 *Proc. 2nd Int. Conf. on Rapidly Quenched Metals* (Cambridge, Mass.: MIT Press) pp249–58
Scott M G and Ramachandrarao P 1977 *Mater. Sci. Engng* **29** 137–44

Scott W W and MacCrone R K 1970 *Phys. Rev.* B **1** 3515–24
Shen L Y L, Chen H S, Dynes R C and Gurno J P 1978 *J. Phys. Chem. Solids* **39** 33–8
Sherwood R C, Gyorgy E M, Chen H S, Ferris S D, Norman G and Leamy H J 1974 *AIP Conf. Proc.* **24** 745–6
Sherwood R C, Gyorgy E M, Leamy H J and Chen H S 1976 *AIP Conf. Proc.* **34** 325–7
Shingu P H, Shimomura K, Kobayashi K and Ozaki R 1976a *Mater. Sci. Engng* **23** 183
Shingu P H, Shimomura K, Kobayashi K and Ozaki R 1976b *Proc. 2nd Int. Conf. on Rapidly Quenched Metals* (Cambridge, Mass.: MIT Press) pp45–50
Shingu P H, Shimomura K, Ozaki R, Osamura K and Murakami Y 1978 *Rapidly Quenched Metals III* vol 1 (London: Metals Society) pp315–24
Shull W H and Naugle D G 1977 *Phys Rev. Lett.* **39** 1580–3
Simpson A W and Brambley D R 1971 *Phys. Stat. Solidi* **43** 291–300
Simpson A W and Hodkinson P H 1972 *Nature* **237** 320–2
Singhal S P, Herman H and Hirvonen J K 1978 *Appl. Phys. Lett.* **32** 25–6
Sinha A K 1970 *Phys. Rev.* B **1** 4541–6
—— 1971 *J. Appl. Phys.* **42** 338–42
Sinha A K and Duwez P 1971 *J. Phys. Chem. Solids* **32** 267–77
Sinha A K, Giessen B C and Polk D E 1976 *Treatise on Solid State Chemistry* vol 3, ed N B Hanney (New York: Plenum) pp1–88
Soshiroda T, Koiwa M and Masumoto T 1976 *J. Non-Cryst. Solids* **22** 173–87
Spaepan F 1975 *Acta Metall.* **23** 615–20
Spaepan F and Turnbull D 1974 *Scr. Metall.* **8** 563–8
—— 1978 *Metallic Glasses* (Metals Park, Ohio: ASM) pp118–27
Srivastava P K, Giessen B C and Grant N J 1972 *Metall. Trans.* **3** 977–82
Staudinger A and Nakahara S 1977 *Thin Solid Films* **45** 125–33
Stephens R B 1976 *Phys. Rev.* B **13** 852–65
Stewart A M and Phillips W A 1978 *Phil. Mag.* B **37** 561–7
Strange E H and Pim C A 1908 *US Patent No* 905758
Street W B, Raveche J H and Mountain R D 1974 *J. Chem. Phys.* **61** 1960–9
Sumiyama K, Shiga M and Nakamura Y 1976 *J. Phys. Soc. Japan* **40** 996–1001
Suzuki K, Fukunaga T, Misawa M and Masumoto T 1976 *Sci. Rep. Res. Inst. Tohoku Univ.* A **26** 1–11
Szofran F R, Gruzalski G R, Weymouth J W, Sellmyer D J and Giessen B C 1976 *Phys. Rev.* B **14** 2160–70
Takahashi T, Fujimori H and Masumoto T 1977 *80th Annual Meeting at the Japanese Institute of Metals No* 393
Takayama S 1976 *J. Mater. Sci.* **11** 164–85
Tanaka K, Matsumoto M, Maruno S and Hiraki A 1975 *Appl. Phys. Lett.* **27** 529–31
Tangonan G L 1975 *Phys. Lett.* **54A** 307–8
Tanner L E and Ray R 1977 *Scr. Metall.* **11** 783–9
Tarvin J A, Shirane G, Birgeneau R J and Chen H S 1978 *Phys. Rev.* B **17** 241–6
Taub A I and Spaepen F 1979 *Scr. Metall.* **13** 195–8
Taylor G I 1950 *Proc. R. Soc.* A **201** 192–6
Testardi L R, Krause J T and Chen H S 1973 *Phys. Rev.* B **8** 4464–9
Togano K and Tachikawa K 1975 *J. Appl. Phys.* **46** 3609–13
Tsuei C C 1977 *Amorphous Magnetism II* (New York: Plenum) pp181–94
Tsuei C C and Duwez P 1966 *J. Appl. Phys.* **37** 435
Tsuei C C and Hasegawa R 1969 *Solid St. Commun.* **7** 1581–5
Tsuei C C, Johnson W L, Laibowitz R B and Viggiano J M 1977 *Solid St. Commun.* **24** 615–8
Tsuei C C and Lilienthal H 1976 *Phys. Rev.* B **13** 4899–906
Tsuei C C, Longworth G and Lin S C H 1968 *Phys. Rev.* **170** 603–5
Tsuya N, Arai K I, Shiraga Y and Masumoto T 1975a *Phys. Lett.* **51A** 121–2
Tsyua N, Arai K I, Shiraga Y, Yamada M and Masumoto T 1975b *Phys. Stat. Solidi* a **21** 557–61
Turnbull D 1956 *Solid St. Phys.* **3** 225–306
—— 1969 *Contemp. Phys.* **10** 473–88
—— 1977 *Scr. Metall.* **11** 1131–6
Turnbull D and Bagley B G 1975 *Treatise on Solid State Chemistry* vol 5 (New York: Plenum) pp513–54

Turnbull D and Cohen M H 1958 *J. Chem. Phys.* **29** 1049–54
—— 1960 *Modern Aspects of the Vitreous State* vol 1, ed J D Mackenzie (London: Butterworths) pp36–62
—— 1961 *J. Chem. Phys.* **34** 120–5
Uhlmann D R 1971 *J. Non-Cryst. Solids* **7** 337–48
Ukhov V F, Dubinin E L, Esin O A and Vatolin N A 1968 *Russian J. Phys. Chem.* **42** 1391
Valenkov N and Porai-Koshits E 1937 *Z. Krist.* **95** 195
Vitek J M, Vander Sande J B and Grant N J 1975 *Acta Metall.* **23** 165–76
Vostryakov A A, Vatolin N A and Yesin O A 1963 *Fiz. Metal. Metalloved.* **16** 675–80
Wagner C N J 1976 *Proc. 2nd Int. Conf. On Rapidly Quenched Metals* (Cambridge, Mass.: MIT Press) pp359–67
Walter J L, Bacon F and Luborsky F E 1976 *Mater. Sci. Engng* **24** 239–45
Wang R and Merz M D 1976 *Nature* **260** 35–6
Warren B E 1937 *J. Appl. Phys.* **8** 645–54
Waseda Y 1977 *J. Solid St. Phys.* **12** 181
Waseda Y, Aust K T and Masumoto T 1979 *Scr. Metall.* **13** 187–90
Waseda Y and Chen H S 1978a *Phys. Stat. Solidi* a **49** 387–92
—— 1978b *Rapidly Quenched Metals III* vol 2 (London: Metals Society) pp415–8
—— 1978c *Phys. Stat. Solidi* b **87** 777–82
Waseda Y and Masumoto T 1975 *Z. Phys.* B **22** 121–6
Waseda Y, Masumoto T and Tamaki S 1977b *Liquid Crystals 1976. Inst. Phys. Conf. Ser. No 30* ed R Evans and D A Greenwood (Bristol: The Institute of Physics) pp268–73
Waseda Y and Ohtani M 1974 *Phys. Stat. Solidi* b **62** 535–46
Waseda Y, Okazaki H, Naka M and Masumoto T 1976 *Sci. Rep. Res. Inst. Tohoku Univ* A **26** 12–20
—— 1977a *Sci. Rep. Res. Inst. Tokohu Univ.* A **26** 202–7
Watanabe T and Tanabe Y 1976 *Mater. Sci. Engng* **23** 97–100
Weaire D, Ashby M F, Logan J and Weins M J 1971 *Acta Metall.* **19** 779–88
Weeks J 1977 *Phil. Mag.* **35** 1345–63
Wiesner H and Schneider J 1974 *Phys. Stat. Solidi* a **26** 71–5
Willens R H 1962 *J. Appl. Phys.* **38** 405–6
Williams E and Angell C A 1973 *Polymer Lett.* **11** 383–7
Williams R S and Egami T 1976 *IEEE Trans. Mag.* **MAG-12** 927–9
Wong J, Lytle F W, Greeger R B, Liebermann H H, Walter J L and Luborsky F E 1978 *Rapidly Quenched Metals III* vol 2 (London: Metals Society) pp345–51
Woodcock C A, Angell C A and Chesseman P 1976 *J. Chem. Phys.* **65** 1665
Yamamoto R, Mihara T, Taira K and Doyama M 1979 *Phys. Lett.* **70A** 41–3
Yamauchi K and Mizoguchi T 1975 *J. Phys. Soc. Japan* **39** 541–2
Yamauchi K and Nakagawa Y 1971 *Jap. J. Appl. Phys.* **10** 1730
Yamauchi K and Narita K 1978 *Appl. Phys. Lett.* **33** 468–70
Yeh H L 1976 *PhD Thesis* University of Pennsylvania
Yeh H L and Maddin R 1976 *Proc. 2nd Int. Conf. on Rapidly Quenched Metals* (Cambridge, Mass.: MIT Press) pp281–91
Zachariasen W H 1932 *J. Am. Chem. Soc.* **54** 3841–51
Zentko A, Kuhaj P, Potocky L, Tima T and Bansky J 1975 *Phys. Stat. Solidi* a **31** K41–2
Ziman J M 1961 *Phil. Mag.* **6** 1013–34